THE EFFECTS OF *IN UTERO* THYROXINE EXPOSURE ON MANDIBULAR SHAPE IN MICE

by

Matthew J. Kesterke

B.A., Anthropology, University of Wyoming, 2003

M.A., Anthropology, University of Wyoming 2008

Submitted to the Graduate Faculty of the

Kenneth P. Dietrich School of Arts and Sciences in partial fulfillment

of the requirements for the degree of

Doctor of Philosophy in Anthropology

University of Pittsburgh

2016

UNIVERSITY OF PITTSBURGH

DIETRICH SCHOOL OF ARTS AND SCIENCES

This dissertation was presented

by

Matthew J. Kesterke

It was defended on

October 21st, 2016

and approved by

James M. Cray, PhD, Assistant Professor

Mark P. Mooney, PhD, Professor

Michael I. Siegel, PhD, Professor

Co-Chair: Seth M. Weinberg, PhD, Associate Professor

Dissertation Advisor: Margaret M. Judd, PhD, Associate Professor

THE EFFECTS OF *IN* UTERO THYROXINE EXPOSURE ON MANDIBULAR SHAPE IN MICE

Matthew J. Kesterke, PhD

University of Pittsburgh, 2016

An estimated 3% of U.S. pregnancies are affected by maternal thyroid dysfunction, with between one and three of every 1,000 pregnancies being complicated by overactive maternal thyroid levels. Overactive maternal thyroid hormones have been linked to neurological impairment and craniofacial development dysmorphogenesis, affecting both endochondral and intramembranous bone. Using both Euclidean Distance Matrix Analysis (EDMA) and geometric morphometric approach, this study evaluates the role of *in utero* thyroxine overexposure on the growth of offspring mandibles in a sample of 241 mice. Principle component analysis (PCA) and canonical variate analysis (CVA) utilized 16 unilateral mandibular landmarks obtained from 3D microCT to assess shape changes between unexposed controls (n=63) and exposed mice (n=178). By evaluating shape changes in the mandible between different age groups (15, 20, and 25 days postnatal) and different dosage levels (low, medium, and high), this study found that maternal thyroxine alters offspring mandibular shape in both age- and dosage-dependent manners, particularly within the high dosage individuals in the oldest age group. The EDMA results demonstrate marked shape changes throughout the mandible, with the gonial angle and alveolus undergoing significant ($p < 0.10$) changes. Geometric morphometric analysis revealed that group differences in overall shape were significant ($p < 0.001$ for both PCA and CVA) and showed major changes in regions of the mandible associated with muscle attachment (coronoid process, gonial angle) and regions of growth largely governed by articulation with the cranial base (condyle) and occlusion (alveolus). These results compliment recent studies demonstrating that maternal thyroxine levels can alter the cranial base and cranial vault of offspring, contributing to a better understanding of both normal and abnormal mandibular development and facilitating a fuller understanding of evolutionary and medical implications of craniofacial growth and development.

TABLE OF CONTENTS

LIST OF TABLES

LIST OF FIGURES

PREFACE

Many people have been crucial to my graduate studies and success. I must thank my committee members - Margaret Judd, Seth Weinberg, Mark Mooney, Michael Siegel, and Jim Cray – for their encouragement, feedback, and support. Though not on my committee, many members of the department have helped with my professional development: Bryan Hanks, Elizabeth Arkush, David Montgomery, Loukas Barton, and Jack Schumann. Many of my colleagues have provided invaluable comments and challenges to my research, all of which have made me a better researcher: Allison Gremba, Patrick Mullins, Camilla Sturm, and Jessica Walker. I would also like to thank Todd Surovell, Jim Ahern, and George Gill for their continued support and friendship from afar. Finally, I want to thank my wonderful wife Nerissa for her encouragement, patience, and love for the last four years.

This research was funded in part from an American Cleft Palate/Craniofacial Anomalies Grant Award and grants from NIH/NIDCR (R03DE02335A), NIH/NIGM (P30GM103331), and NIH/NIA (1P01AG036675). The University of Pittsburgh Anthropology Department and the University of Pittsburgh Graduate Student Organization also provided additional funding for this project.

1.0 INTRODUCTION

An estimated 3% of U.S. pregnancies are affected by maternal thyroid dysfunction, with between one and three of every 1,000 pregnancies being complicated by overactive maternal thyroid levels (Casey and Leveno 2006; Negro and Mestman 2011; Mestman 2009). Overactive maternal thyroid hormones have been linked to neurological impairment, bowel and urogenital malformation, and craniofacial development and dysmorphogenesis, particularly in regards to the development of both endochondral and intramembranous bone (Casey and Leveno 2006; Hershman 2009). These issues of human skeletal growth have long been an interest of human biologists and clinicians, and forays in to the field from anthropologists are increasingly more common. Biological anthropology provides a unique lens with which to review existing and new data regarding developmental skeletal biology, providing much needed population and cultural perspectives regarding human growth anomalies. Much of the existing research delves in to the role of genetic and physiological influences on developmental anomalies; contributing maternal factors are often overlooked in clinical and academic scholarship, especially in regards to the role of maternal endocrine factors during embryological and early human growth and development. In particular, the role of maternal thyroid levels and their influence on growth and development has yet to be linked from clinical settings and animal models to the anthropological literature.

1.1 RESEARCH RATIONALE

This dissertation aims to understand the role of aberrant maternal thyroid levels in offspring craniofacial development. By focusing on the mandible, a region that develops and grows largely in response to extrinsic factors such as cranial base growth and occlusal properties, this research will aid in understanding the role of maternal environment on the craniofacial growth and development of offspring. Characterizing the role of maternal thyroid on offspring mandibular shape has far-reaching implications for anthropology, clinical medicine, and corrective and aesthetic practitioners. This dissertation fills a substantial gap in research regarding the role of maternal environment on craniofacial growth and development.

1.2 LITERATURE REVIEW

1.2.1 Normal Bone Growth

The musculoskeletal system originates early in embryonic development as the mesoderm gives rise to two rows, called the paraxial mesoderm, on either side of the neural tube, which then give rise to segmented blocks called *somites* (Moore, Persaud, and Torchia 2013). Bones in different parts of the body form from different regions. Many of the craniofacial bones form from the mesenchymal cells of neural crest origins: the other bones in the body arise from mesenchyme of somite origin or mesenchyme in the head mesoderm or lateral plate mesoderm during the third through fifth weeks of embryonic development (Resnick et al. 2002; Moore, Persaud, and Torchia

2013). The majority of the musculoskeletal system is formed by week seven in utero, though the biomechanical and habitual forces exerted on the individual play a large role in the further development of the skeleton (Carter, van der Meulen, and Beaupré 1996). At the cellular level, osteoblasts arise from pluripotent mesenchymal cells, whereas osteoclasts are derived from hematopoietic cells; the interaction between such cells and the other organic and inorganic aspects of bone result in overall skeletal growth seen at a macroscopic level (Donahue, Siedlecki, and Vogler 2005).

An understanding of bone embryogenesis is essential to the study of bone development, as the process of embryogenesis is very similar to the processes of bone remodeling and bone repair (Bruder, Fink, and Caplan 1994; Gerstenfeld et al. 2003). This is not to say that the process is simple or well studied. The process of bone embryogenesis illustrates that the role of mesenchymal cells is remarkably similar between these apparently disparate processes. Mesenchymal cells give rise to new bone during development, but also to osteogenic cells present during bone remodeling and repair after trauma and during illness affecting the bone (Bruder, Fink, and Caplan 1994). These mesenchymal cells can proliferate and differentiate in to various tissues, including osteoblasts, chondrocytes, myoblasts, stromal cells, fibroblasts, and various other cells responsible for the growth and development of connective tissues (Bruder, Fink, and Caplan 1994; Moore, Persaud, and Torchia 2013; Adler 2000). This proliferation results in the cartilaginous precursors of long bones that provide the models for the future ossification of long bones and the membranous boundaries found in intramembranous ossification (described below).

The transition of these mesenchymal cells into osteoprogenitor cells (sometimes called pre-osteoblasts), then in to osteoblasts, and finally in some cases in to osteocytes, is a complex process involving multiple cytokines and growth factors. This transition also differs slightly depending on

both the method of ossification and local epigenetic influences (Caplan and Boyan 1994; Ballock and O'Keefe 2003). In fact, this sequence is almost the same seen in fracture repair. The initial phase, be it embryological or the inflammatory period directly after a fracture, begins with the accumulation of mesenchymal stem cells; these cells then differentiate in to cartilage and/or bone cells that begin forming stabilizing structure around the fracture, or a growth collar in the case of embryological growth (Linkhart, Mohan, and Baylink 1996). The cartilage begins to atrophy as the bone cells begin more extensive osteogenesis, and the now woven bone undergoes remodeling and further ossification until healthy bone is achieved (Bruder, Fink, and Caplan 1994; Caplan and Boyan 1994; White, Black, and Folkens 2012). Both chemical signaling and biomechanical influences affect the processes of bone growth and remodeling, and these influences can be seen in a review of the two forms of bone formation.

Growth factors play key roles in the development of both endochondral and intramembranous bones, namely insulin-like growth factors, transforming growth factors, and fibroblast growth factors, but biomechanical stressors and forces also play a crucial role (Croucher and Russel 1999; Doll 2005). For example, the growth of the fetal brain dictates much of the growth patterns of the cranial intramembranous bones, but *Fgf* and *Twist* receptors play an important role in the development of the flat bones of the skull, specifically in the sutural regions of the parietal and frontal bones (Doll 2005). Bone morphogenic proteins (BMP's) and fibroblastic growth factors (FGF's) also play a key role in the development of the bones of the midface and cranial vault as they help regulate tissue induction and the proliferation of osteogenic cells (Sperber 2002; Leboy 2006). The bones of the cranial vault are not uniform in their origins, or in the timing of their development, suggesting multiple genetic pathways are responsible for their development. Bone growth in the cranial vault, midface, and mandible is of primary interest to craniofacial

researchers, and the complex growth process has been debated for well over 40 years (see Enlow 1982; Moss and Salentijn 1969a; Latham 1970; Siegel et al. 1990). The timing and completion of osteogenesis of intramembranous bone is of utmost importance to clinicians, specifically those manipulating the growth and development of the face for medical or aesthetic purposes. Once the bones have fused and completed their growth, they are no longer as pliable as developing bones and must be altered surgically.

The various genes coding for proteins during the normal development of bone result in a complex interaction of cell differentiation and migration. While certain genes affect the differentiation of bone cells in localized areas, other genes are responsible for the regulation of the positional orientation of the embryo in all vertebrates (Argiropoulos and Humphries 2007). These genes, called *Hox* genes, are an (estimated) 39 genes located on various chromosomes in humans that regulate the segmental differentiation and growth of the embryo (Krumlauf 1994). Simply put, *Hox* genes organize the developing body of all vertebrates along the axis, conferring the axial identity of the body from head to tail without actually forming the limbs themselves (McGinnis and Krumlauf 1992). *Hox* genes alone do not affect the formation of bone tissue; rather they affect body plan and organization, thereby affecting the *pattern* of body and limb development (Sperber 2002). Just as mutations in various genes responsible for the normal growth of bone can cause abnormalities (FGFR-3 mutations and achondroplasia and endochondral dysplasia, for example), mutations in *Hox* genes can result in changes ranging from relatively minor abnormalities (e.g., polydactyly, synpolydactly) to much more serious developmental abnormalities (e.g., dysgenesis disorders), cancers, and intrauterine death (Goodman and Scrambler 2001; Quinonez and Innis 2014; Horton, Hall, and Hecht 2007; Deng et al. 1996). Furthermore, investigations in to the role of *Hox* genes in the regulation of hematopoietic stem cell, and possibly even leukemogenic stem

cell production suggests that the pathways involved with *Hox* genes play a significant role in bone osteogenesis and development (see Argiropoulos and Humphries 2007).

The complex interaction between patterning *Hox* genes and the aforementioned regulatory genes result in the development of human bone, and are thus key to the understanding of normal skeletal growth (Argiropoulos and Humphries 2007). However, bone is not a static tissue once it has completed development, as it changes throughout an individual's life. Once bone has attained adult size and orientation, it still undergoes the complex process of bone remodeling. Broadly defined, remodeling refers to the alteration of existing bone. This process occurs throughout an individual's life, and is integral in an organism's ability to adapt to mechanical and environmental stresses exhibited on the body (Boskey 1999). The process of bone remodeling was poorly understood until the late 19th century, when researchers sought to better understand the process of mechanical loading on the skeleton and the body's subsequent response (Aldersey-Williams 2013; Grob 2014). Bone remodeling involves the same basic histological structures as growth and development, though it is regulated by different factors and results in a myriad of outcomes.

The remodeling process relies heavily on the interaction of osteoblasts and osteoclasts. As mentioned above, osteoclasts continually resorb longitudinal cavities in cortical bone that will become *osteons*, the basic unit of healthy bone facilitating communication and repair between disparate areas of the bone. As osteoblasts migrate to the area and deposit osteoid that will later become ossified. As the osteoid is deposited in the developing osteon, it becomes calcified and the osteon becomes progressively narrower (White, Black, and Folkens 2012). The central canal remains open, and a series of enlargements by osteoclasts followed by deposition of new osteoid by osteoblasts follows, leaving telltale markers (reversal lines) between the new osseous material and the material deposited earlier in the process (Doll and Koch 2005). Osteoblasts may also

deposit osteoid in trabecular bone, and the deposited fibular matrix is structurally similar despite not being laid down in the same layered manner as in lamellar bone (Marotti 1990). This ever-present process of new osteon formation is vital for the healthy turnover of bone and the tissue's ability to respond to biomechanical stress, the environment, and the metabolic demands of the body. As the primary store of the body's calcium, necessary for normal cell function, muscle contraction, and healthy nerve function, the mammalian skeleton provides a reservoir of calcium essential to the organism's survival (Costanzo 2014). The main hormone responsible for the resorption of bone, which initiates a release of free calcium ions in to the body, is parathyroid hormone (Vogl et al. 1993). The release of parathyroid hormone initiates formation of hematopoietic stem cells that differentiate in to osteoclasts, which in turn resorb bone; this process is typically followed by osteoblastic activity at the site, which deposits new bone at the areas of resorption (Doll and Koch 2005). In times of metabolic stress, however, this balance may not be maintained and can result in an imbalance of osteoblastic and osteoclastic activity and an overall deformation of bone (Ooi and Fraser 1997; Resnick et al. 2002; Roberts et al. 2006).

Osteoblastic activity in healthy individuals is regulated by the hormone calcitonin, released by the thyroid, during times of calcium excess in the body (Murphy and Williams 2004). As stressed above, the balance between osteoblasts and osteoclasts is integral in the healthy maintenance of the human skeleton, and numerous diseases can cause issues with the chemical signaling of either type of bone cell (Cole and Cohen 1990; Resnick et al. 2002). These cellular imbalances can cause overactivity of the osteoclasts, such as Paget's disease of bone, which in turn causes the body to signal for the production of osteoblasts. This imbalance causes a rapid increase of poorly formed bone as the osteoblasts and osteoclasts both increase in activity (Delmas and Meunier 1997). While Paget's disease of bone is a relative rare disease linked to a genetic mutation

in SQSTM1, a gene involved in the binding of ubiquitin, it demonstrates the body's attempts to continually balance the activity of bone cells (Ooi and Fraser 1997; Ortner 2003). There are numerous diseases that affect the activity of these bone cells, any of which can lead to a cascade of cellular activity that leads to a cellular imbalance and ultimately affects the skeletal system. Other pathogenic processes can affect the substances necessary for the production and maintenance of bone, such as calcium (e.g., osteoporosis), vitamin C (e.g., scurvy), vitamin D (e.g., rickets), or numerous less common diseases affecting problems with collagen production, such as osteopetrosis, osteogenesis imperfecta (Ortner 2003; Grob 2014). The recognition of the balance between the deposition and resorption of bone is essential in an understanding of how bone responds to biomechanical stress and environment. The exact stimulus initiating bone resorption is not fully understood, though it is likely a combination of paracrine factors of osteocytes, piezoelectric response, and mechanical stimuli (Murphy and Williams 2004).

Bone response to biomechanical loads and stress was poorly understood well in to the 19th century. A comprehensive explanation for the role of biomechanical loads on bone was finally postulated in 1892 by Julius Wolff (Wolff 1892; Murray 1936). Now called Wolff's Law, Wolff's hypothesis was indispensable in the overall understanding of how bones gain and maintain their shape as a result of biomechanical stress. Multiple translations of Wolff's original manuscript exist, but the core argument of his argument is:

> "Every change in the form and function of bone or of their function alone is followed by certain definite changes in their internal architecture and equally definite secondary alteration in their external conformation, in accordance with mathematical laws." (Ethier and Simmons 2007: 11)

Simply put, Wolff's law states that biomechanical forces exerted on bone, such as habitual movement through locomotion, can change that bone's shape. Wolff's law was the first definitive argument that external forces can alter and affect bone, but does not provide evidence as to how these changes may occur (Frost 1990). Wolff's original proposition that bone remodels interstitially by deposition bone between existing layers was novel in its time, opposing existing viewpoints that bone only remodeled by resorbing old bone and depositing new bone in its place (Prendergast and Huiskes 1995). Wolff correctly hypothesized that bone responded to some sort of external signal, be it chemical or electrical, and responded to these stimuli by depositing or resorbing bone until the stress was reduced and the signaling ceased. It has since been shown that stress response in bone is largely due to the activity of osteocytes and their associated lacunae and trabeculae (Frost 1994). Building upon the principles of Wolff's work, more recent studies have shown that it is indeed stress that plays the integral role in the shaping of bones, and that human bones can almost be described as self-designing structures (Carter, van der Meulen, and Beaupré 1996). As stress is applied or removed to bone, biochemical responses within the structure respond to the stimuli, either depositing new bone or resorbing existing bone to adapt to the external environment (Figure 6; Frost 1994). The relatively recent development of human genome mapping and better methods for identifying the nuanced roles of the endocrine system have furthered the understanding of Wolff's Law in recent years, and allowed researchers to apply these concepts beyond cortical bone to trabecular bone and other regions of the body, such as the mandible (Roberts et al. 2006a; Roberts et al. 2006b).

Trabecular bone still remodels at similar rates as cortical bone, though the basic multicellular unit (BMU) of the remodeling system involves surface resorptive cavities and subsequent bone deposition rather than the cutting methods with subsequent lamellae observed in

cortical bone (Roberts et al. 2006). The pioneers in this development utilized bone research at the molecular level, a realm that was not well understood by early researchers. Recent histological research has shown that this remodeling process takes similar amounts of time for both cortical and trabecular bone. In humans, it takes roughly one month to create a resorptive cavity one quarter of a millimeter in diameter, and nearly four times as long to fill the cavity (Vanderoost and van Lenthe 2014; Roberts, Epker, et al. 2006). Using this model, microdamage as a result of stress is the driving factor behind bone remodeling. Microdamage causes the release of inflammatory cytokines, which causes T cells to migrate to the area and release RANK ligand (RANKL), inducing osteoclast production (Boyle, Simonet, and Lacey 2003). As bone is resorbed, growth factors are released that deactivate the osteoclasts and new osteogenic cells move in to the resorption cavity is eventually filled with new bone (Boyle, Simonet, and Lacey 2003; Roberts, Epker, et al. 2006). Biomechanical stress is not the only factor regulating bone resorption, however, as the endocrine system regulates the body's calcium levels primarily through the resorption of trabecular bone (Roberts, Epker, et al. 2006). It is through this complex interaction that bone is not only remodeled, but calcium levels remain in homeostasis.

The overarching process of bone remodeling can best be envisioned using a model, first proposed in the 1980's by Harold M. Frost (Stout and Crowder 2012; Frost 1983). Called the 'mechanostat', this system takes in to account longitudinal bone growth, microstructural bone remodeling, and biomechanical stress to predict BMU remodeling in human bone (Figure 1). Using a household thermostat as a model, the mechanostat model argues that bone that is strained at a level *below* the minimum effective strain level is kept in a sort of 'conservative' mode, much like a furnace that only turns on once a minimum temperature is met; if this threshold is not met, however, bone will not remodel and will instead go in to a 'disuse' mode (resulting in osteopenia

and/or osteoporosis; Frost 1983; Stout and Crowder 2012; Webster 2005). Loading during the conserve mode leads to overall bone remodeling. Conversely, *overloading* the bone during the conserve mode, or that above the minimum level of effective strain, can lead to microfractures; if these levels of strain continue and the bone cannot remodel at a sufficient rate to repair the microfractures, the bone will fail (Stout and Crowder 2012; Frost 1983). Simply put, the mechanostat model argues that levels of strain necessary for stress are lower than those for remodeling, which are in turn lower than those for pathology, which are in turn lower than those leading to fracture (Figure 1; Frost 1983; Webster 2005). The mechanostat model does a fine job of evaluating bone remodeling, though it does little to effectively describe the process of bone remodeling from a cellular level.

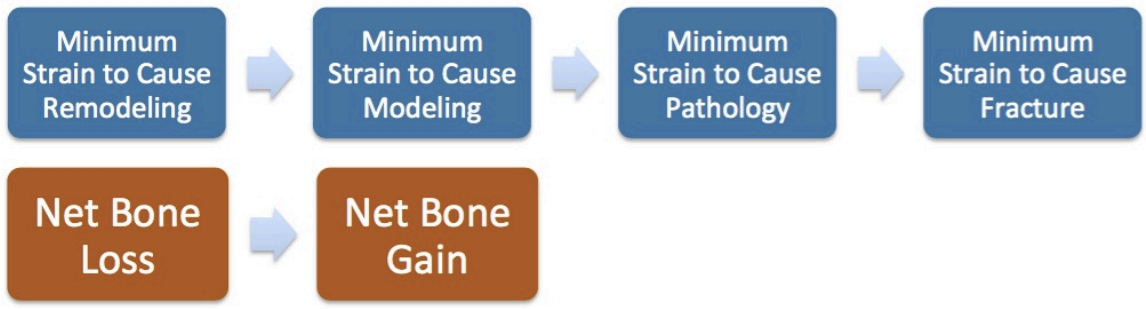

Figure 1. Frost's 'mechanostat' feedback loop explaining BMU remodeling of human bone. ***Modified from Webster (2005): 7.***

A new paradigm, stemming from multiple theorists and workshops seeking to integrate various fields of skeletal research, arose in the 1990's in an attempt to incorporate Frost's model and that of other fields (Stout and Crowder 2012; Webster 2005). This new model, dubbed the 'Utah Paradigm', is an extensive feedback loop that builds upon the mechanostat model (Figure 2; Webster 2005). Incorporating the fact that continual strain from natural biomechanical loading leads to microfractures in bone, which leads to bone repair under pathological and non-fracturing

levels of strain, the Utah paradigm is being continually modified to incorporate contemporary studies in the molecular and genetic factors of bone remodeling (osteocyte apoptosis and subsequent osteoblastic activity). In this updated model, biomechanical forces and strain are still the main cause of skeletal remodeling, though hormones, diet, sexual dimorphism, and other nonmechanical factors play an important role in the process (Figure 2; Stout and Crowder 2012; Webster 2005). As described above, it should be readily apparent that hormones, especially growth factors, play an important role in both growth and development (Table 1). Key among these hormones are calcitonin and parathyroid hormone, which regulate osteoblasts and osteoclasts, but there are numerous other hormones that affect the growth and development of bone; estrogen and testosterone play crucial roles in osteogenic and chondrogenic processes, especially later in life, while vitamin D and even insulin (both produced by the body in conjunction with dietary intake) play a role in bone remodeling (Lieberman 2011; Moore, Persaud, and Torchia 2013). It then stands to reason that hormones and other factors gained from diet (minerals, vitamins, dietary hormones) affect other aspects of the body that are also regulated by the same inputs, and that skeletal physiology and biology will be altered disparately depending on environmental factors. This loop is not a replacement of Frost's mechanostat model, though it has shaped Frost's approach to the factors affecting bone growth (Roberts et al. 2006; Frost 1998; Frost 2000).This feedback model allows for all perceivable contributing factors to bone remodeling, and provides the foundation for most contemporary theories regarding bone remodeling and biomechanical loading of bone (Stout and Crowder 2012; Webster 2005).

Table 1. Major hormones/growth factors affecting skeletal growth throughout life (*from* Lieberman 2011).

Hormone	Major Effects on Skeletal Growth
Estrogen	Up-regulates osteoblasts Up-regulates chondrocytes at moderate levels Down-regulates chondrocytes at high levels Down-regulates osteoclasts
Testosterone	Up-regulates chondrocytes and osteoblasts at moderate levels
Vitamin D	Up-regulates osteoblast and chondrocytes
Thyroid Hormone	Up-regulates osteoblasts and chondrocytes at normal levels Up-regulates osteoclasts at high levels
Parathyroid Hormone	Up-regulates osteoclasts
Growth Hormone	Up-regulates osteoblast, chondrocyte, and osteoclast activity
IGF-I	Up-regulates osteoblasts and chondrocytes
Calcitonin	Down-regulates osteoclasts Up-regulates osteoblasts
Cortisol	Down-regulates osteoblasts and chondrocytes Up-regulates osteoclasts
Insulin	Up-regulates osteoblasts and chondrocytes

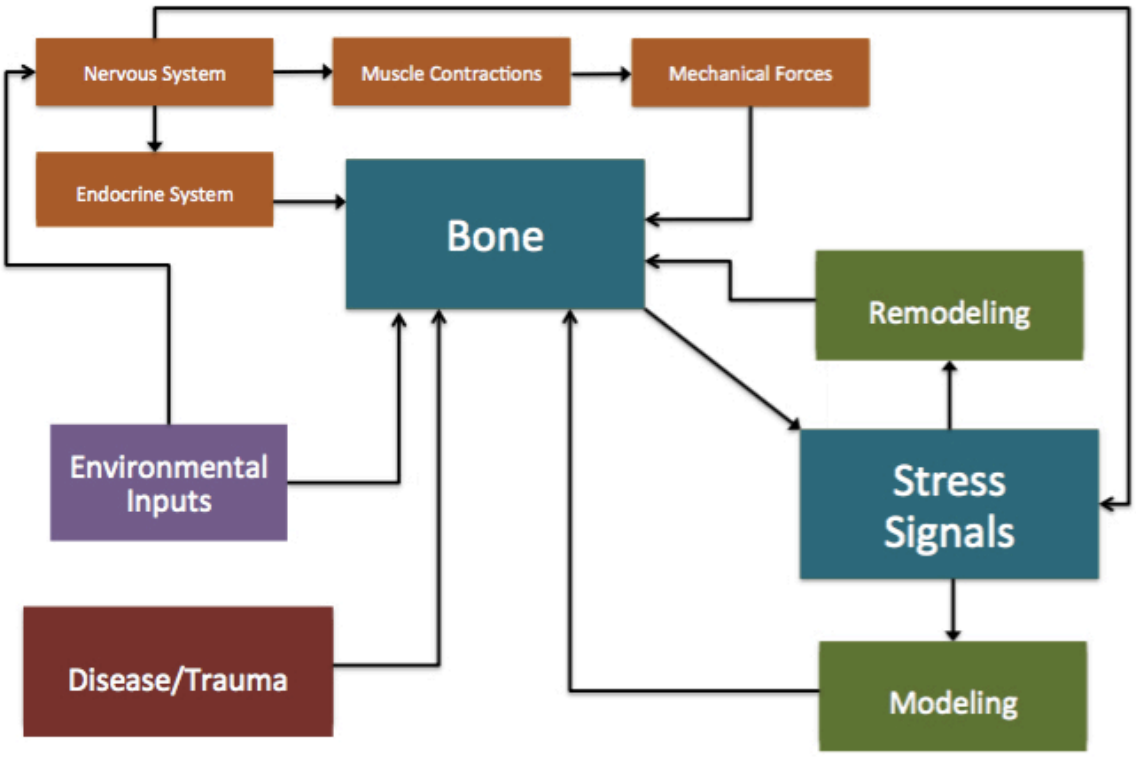

Figure 2. The 'Utah paradigm', which incorporates input from environmental (e.g., diet, minerals), biomechanical, and local epigenetic factors in to Frost's mechanostat model. ***Modified from Webster (2005): 8.***

1.2.2 Role of the Thyroid

The thyroid plays a substantial role in human growth, from embryological development through senescence. In particular, thyroid hormone, growth hormone, insulin-like growth factors, and glucocorticoids play an important part in linear development during childhood (Figure 3). Thyroid hormone deficiencies in childhood can lead to shortened bones due to osteoblast and osteoclast imbalance, as well as inhibited chondrocyte activity in growth plates and premature suture closure in the skull (Harvey et al. 2002; Hershman 2009; Singer 2009; Browne et al. 2009;

Cray et al. 2013). Skeletal changes seen in the craniofacial complex make it an ideal anatomical region to study the effects of maternal thyroid levels on skeletal growth and development, as both endochondral and intramembranous ossification are involved during growth and development in the region.

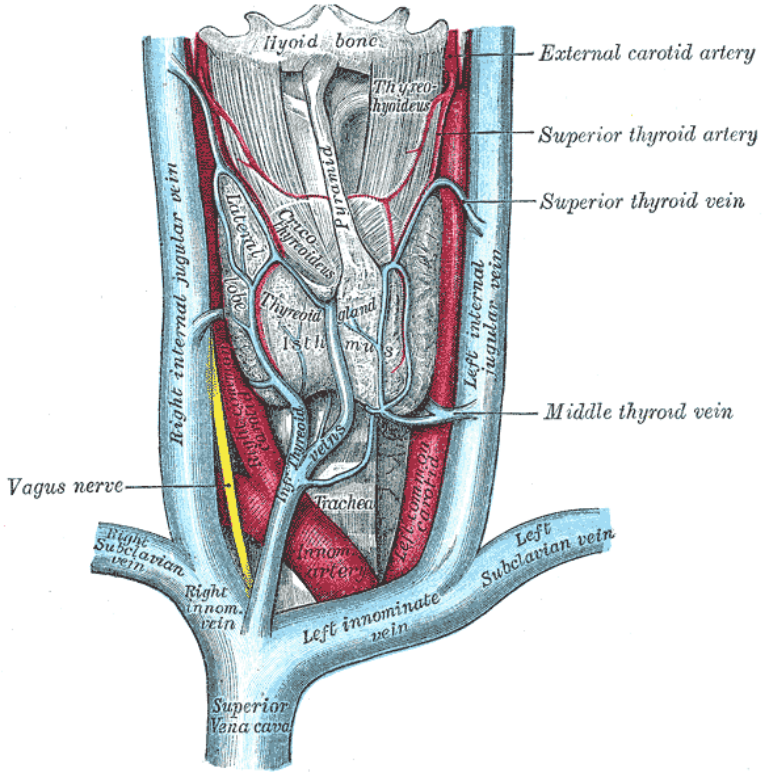

Figure 3. Location and blood supply of the human thyroid hormone. ***From Gray's Anatomy, Plate 1174 (1918).***

The thyroid is responsible for the secretion of hormones that act on almost every major system in the human body (Costanzo 2014). The active hormones produced by the thyroid are triiodothyronine (T_3) and thyroxine (T_4, also called I-thyroxine). The release of these hormones is stimulated by the release of thyroid-stimulating hormone (TSH) from the anterior pituitary gland, which is itself signaled by the release of thyrotropin-releasing hormone (TRH) from the hypothalamus (Singer 2009; Costanzo 2014). Once secreted, both T_3 and T_4 circulate via the

bloodstream, where they inhibit thyroid-releasing hormones in healthy individuals; this acts as a feedback loop to maintain normal levels of thyroid hormones in the body (Figure 4). While T_3 is the more active of the two hormones, the epithelial cells of the thyroid produce substantially more T_4, which is then converted to the more active T_3 form by target tissues. Due to naturally increased levels of T_3 and T_4 during normal pregnancy, the role of maternal thyroid levels is difficult to study. The increased secretion of thyroid hormones by the mother arises due to increased secretion of human chorionic gonadotropin hormone (hCG) during pregnancy (Mestman 2009; Drake, Vogl, and Mitchell 2010). Since T_3 and T_4 significantly affect growth and development, the central nervous system, basal metabolic rate, overall metabolism, as well as the cardiovascular and respiratory systems (*see* Figure 4), any alterations, excesses, deficiencies, or abnormalities can have substantial effects on the human body (Singer 2009; Hershman 2009; Mestman 2009).

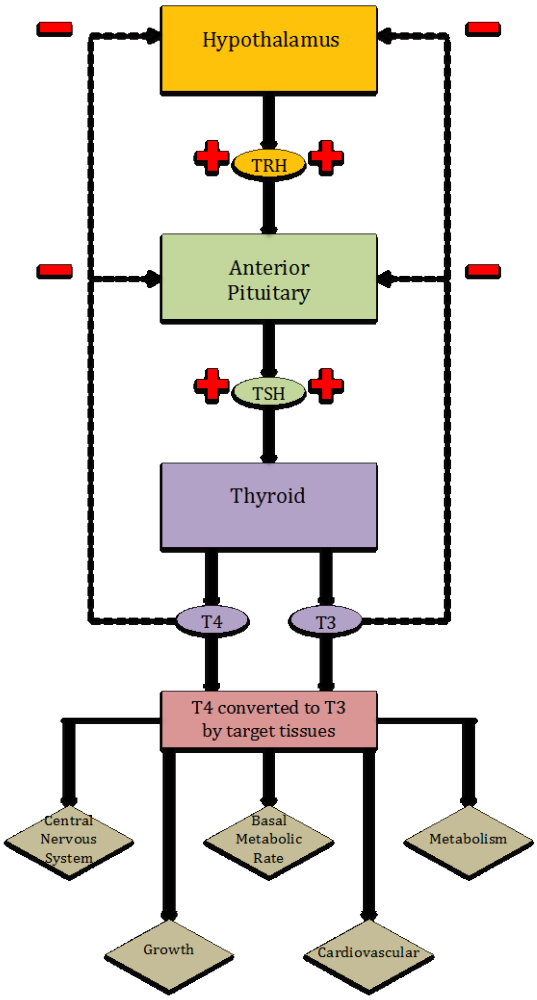

Figure 4. The role of thyroid hormones in the human body.

The first scientific review of the relationship of the thyroid and the skeleton dates to the late 19th century, and focused on increased fracture rates in a patient with excess thyroid production, or hyperthyroidism (Von Recklinghausen 1891). This case study involving a young woman with thyrotoxicosis relied more on gross clinical observations than microbiological analyses of thyroid dysfunction, yet it represents the first serious foray in to the impact of the

thyroid on the skeleton. Von Recklinghausen's notion of thyroid dysfunction causing bone demineralization would remain the dominant paradigm for decades to come. The concept of endogenous thyrotoxicosis causing bone loss, especially in old age, remains today in both clinical and research data (Cooper 1988; Grob 2014). Key research in the United States focused on the role of the thyroid dysfunction and overall metabolism, with side forays in to questions regarding diet (primarily iodine; Grob 2014). By the 1920's, clinicians began to notice skeletal changes in hyperthyroidism patients, namely in the hips and the skull.

This change towards studies of hormone levels in senescence, namely the higher prevalence rate of fractures and overall bone thinning and demineralization, was noted in multiple cases and linked to thyroid dysfunction (Judd 1920). With the advent of antithyroid hormone therapy treatment in the 1940's, it appeared that thyroid-related mineral loss in bone was on the decline (Dhanwal 2011; Grob 2014). Again, research was concerned primarily with adult patients suffering from thyroid dysfunction, through research continued on the impact of exogenous thyroid hormone function. Most research was focused on parathyroid disorders due to their link with osteoclastic disruption, though continued research on the thyroid was essential due to its roll in overall metabolism and the prevalence of hormone treatments (Seeman et al. 1982; Hershman 2009; Grob 2014). Levothyroxine (L-thyroxine), a commonly-prescribed synthetic mimic of thyroxine, has been shown to cause bone mineral loss in post-menopausal women (Paul et al. 1988). Other studies show that thyrotoxicosis leads to increased osteoclastic activity in the adult skeleton, leading to increased mineral resorption of bone, and eventually a negative calcium balance (Cooper 1988). The advent of histomorphometric studies allows further researcher of bone mineral loss at the molecular level, demonstrating that excess thyroid leads to increases of bone

remodeling through interaction with both bone deposition and resorption (Murphy and Williams 2004; Dhanwal 2011).

Studies of this sort of hormonal imbalance are common in geriatric medicine, as the hormone imbalance largely affects elderly individuals, especially post-menopausal women (Grob 2014). The role of thyroid dysfunction on young children accelerates growth and bone maturation, leading to premature bone fusion and shortened stature (Wojcicka, Bassett, and Williams 2013). However, studies of maternal thyroid levels on the skeleton of offspring are comparatively rare. The majority of studies concerning maternal thyroid levels focus primarily on the role of the disorder on the mother, citing the developing fetus only as a target of healthy birth (Talbert et al. 1970). Even contemporary literature on the topic focuses more on diagnosis, management, and treatment of the mother and subsequent testing of the neonate.

1.2.3 Thyroid and Craniofacial Studies

Despite our contemporary understanding of maternal hyperthyroidism and its effects on offspring, little research is directed on its role in the long-term development of the offspring (Hershman 2009; Mestman 2009; Negro and Mestman 2011). Fetal thyroid hormone is active by ten weeks post-conception, so studies of the role of thyroid hormones, be they maternal or of the embryo, necessitate further evaluation (Burrow, Fisher, and Larsen 1994). The few in vivo studies of thyroid levels on bones conducted in animal models show that thyroid dysfunction leads to offspring cranial malformation, low birth weight, and mental deficiencies, though these changes have not been precisely quantified (Khoury, Becerra, and D'Almada 1989; Haddow et al. 1999). Maternal hyperthyroidism and the resulting thyrotoxicosis have also been linked to

craniosynostosis and cerebral developmental impairment in human populations (Daneman and Howard 1980; Rasmussen et al. 2007; Browne et al. 2009), as well as fetal hypertension and fetal growth restriction (Luewan, Chakkabut, and Tongsong 2011). The above studies demonstrate a marked moved towards maternal studies of thyroid levels on offspring growth and development, but do not specifically address the issues.

In light of the lack of human studies, animal models are the obvious choice for research regarding the role of maternal thyroid levels on offspring growth and development. The earliest of these studies suggests that increased thyroxine exposure in rat fetuses may delay the appearance of ossification centers, though the actual timing of the delay has not been quantified (Weiss and Noback 1949). Embryonic chick long bone cultures exposed to excess thyroxine showed increased maturation rate of cartilage, with overall growth retardation at higher levels of thyroxine exposure, especially during later stages of bone development (Fell and Mellanby 1955). Further studies along this line show that this growth retardation in culture-grown long bones was a result of cartilage cell hypertrophy leading to premature growth cessation (Fell and Mellanby 1956). Exogenous exposure to thyroxine in developing chicks embryos showed similar results; embryos exposed to the hormone for eight days of incubation had shorter and lighter tibia than those of control groups, with specific deficiencies in the articular cartilage (Hall 1973). Mice have even been bred completely devoid of thyroid function (via lack of thyroid receptors) and are still viable, though they exhibit numerous deficiencies in bone histogenesis (Göthe et al. 1999; Harvey et al. 2002).

Studies of the role of thyroxine in amphibians are prevalent, as the hormone is essential in determining whether long bones ossify before or after tadpole metamorphosis in amphibian taxa (Kemp and Hoyt 1969a; Kemp and Hoyt 1969b). Further studies in amphibians also demonstrate that exogenous thyroxine can affect the bone growth of the cranial vault by stimulating

chondrogenesis, though it has no effect on the onset of osteogenesis (Hall 2015). The broad applicability of these studies to mammal models, and eventually humans, are somewhat limited, through the tissue- and molecular-level implications provide promising avenues for future research.

At the molecular level, the role of maternal thyroxine on the developing fetus itself is also poorly understood, though recent studies show that maternal thyroid hormones do in fact act on offspring thyroid receptors (Nucera et al. 2010). The role of in vivo thyroxine on osteogenesis has seen recent research demonstrating that excess thyroid hormone exposure results in increased gene product markers for osteogenesis (Cray et al. 2013). Further studies have also shown that, in mouse models, excess maternal thyroxine significantly alters offspring cranial base dimensions and shape (Cray, *unpublished*). Yet again, the existing studies regarding the role on maternal thyroxine levels on offspring development focus more on anomalies and birth defects rather than its role in normal variation. The cranium and especially the mandible, due to its complex growth process, represent a promising avenue of research regarding the role of maternal environment on offspring ontogeny.

1.2.4 History of Mandibular Research

1.2.3.1 History of Embryonic Mandibular Development

The development of the craniofacial complex, and the mandible in particular, has a long and storied history spread across multiple fields, beginning with late-18th and early-19th century work in the budding field of embryological development. Formulated independently by Goethe and Oken and known at the time as the "vertebral theory of the skull", the first dominant paradigm of embryological craniofacial development posited that the skull essentially developed as a set of

vertebrae and differentiated in segments similar to the rest of the trunk, and that all craniofacial cells arose exclusively from the mesoderm (Kingsbury 1926; Depew, Tucker, and Sharpe 2002). This theory dominated the study of craniofacial development in the 19th century, dictating the head be studied in the same manner as the segmentation of the trunk:

> "The upper arch is formed by the walls of the cavity containing the brain, and stands in the same relation to it, as does the neural arch of a vertebra to the spinal cord, with which that brain is continuous. The lower arch encloses the other viscera of the head, in the same way the ribs embrace those of the thorax" (Huxley 1859: 382).

In viewing the skull as such, adult crania were compared and discussions of dissimilarity formed the basis of scientific endeavor, omitting the review of embryological origins of the skull (Huxley 1859). In his eloquent dismantling of the vertebral theory, Huxley again and again stressed the importance of embryological study of craniofacial development, frowning upon the gradation approach of classification:

> "…the study of the mode in which skulls of vertebrate animals are developed, demonstrates the great truth which is foreshadowed by a careful and comprehensive examination of the gradations of form which they present in their adult state; namely, that they are all constructed upon one plan; that they differ, indeed, in the extent to which this plan is modified, but that all these modifications are foreshadowed in the series of conditions through which the skull of any one higher *Vertebrata* passes" (Huxley 1859: 424).

The earliest of these embryological studies focused primarily on the differentiation of the various craniofacial structures from other body tissues. In particular, zoologist William King Gregory focused his research on the origins of craniofacial structures in both sea and land vertebrates.

Gregory's work synthesized the previous insights of Huxley, Wiedersheim, Smith Woodward, and other prominent zoologists on the evolutionary relationship between autostylic (jaws directly attached to the cranium, as seen in tetrapods), hyostylic (jaws not attached directly the cranium, as seen in most fish), and amphystylic (upper jaw braced against the cranium, as seen in sharks), arguing that we must study the embryology differentiation of the first two branchial arches to adequately describe mandibular development (Gregory 1904). Though incorrect in his theoretical assumptions that all aspects of the craniofacial complex originated solely from mesodermal derivatives (Depew, Tucker, and Sharpe 2002), Gregory was pivotal in developing a better understanding of branchial arch differentiation, the role of evolutionary principles on this process, and the treatment of the mandible as an independent craniofacial region. In line with Gregory's work is that of B.F. Kingsbury, a prominent zoologist and pioneer of histology at Cornell, who argued that the differentiation of the head did not follow segmentation similar to the rest of the body. Kingsbury used histological evidence to show the cephalocaudal progression of branchial arches, which remains the dominant paradigm of branchial arch development to this day (Kingsbury 1926). Of particular interest is Kingsbury's argument that all aspects of the branchial arches are not, in fact, formed solely from the dorsal somites; after a lengthy comparison between the branchial arches in various other vertebrates, he proceeded to number the branchial arches cephalocaudally, and concluded calling on further study of the complex differentiation of craniofacial tissues (Kingsbury 1926).

The swing from vertebral theory to that of Kingsbury marked a pivotal shift in the study of craniofacial development. Research now focused on more nuanced developmental models that more precisely described the complex transformation present in embryological development of the skull and mandible. Later studies would follow in Kingsbury's footsteps to develop the

contemporary understanding of craniofacial growth and development, specifically the integration of the growth of the mandible, palate, and maxilla (Björk 1951; Moss and Young 1960; Frost 1964; Enlow 1968).

1.2.3.1 History of Postnatal Mandibular Development

Research on the postnatal growth of the mandible in anthropology is particularly interesting, as the skeletal element preserves well in the archaeological record and represents some of the first paleoanthropological finds in the 18th and 19th centuries. These early studies began to understand that the mandible and maxilla were jointly formed as a result of the interaction between mastication and other biomechanical needs upon the facial region. The earliest studies showed that occlusion and the biomechanical forces involved therein were key contributors to overall craniofacial and mandibular shape. These studies, largely carried out by removing muscles of mastication (Walkhoff 1902) or removal of teeth (Baker 1922) in animal models, demonstrated that teeth and occlusion affected mandibular growth. However, it could not be determined if these changes were a result of occlusion itself or the development and eruption of the teeth (Thoma 1938). Key to the resolution of this debate was the concept that the mandible and maxilla are solitary objects, instead consisting of multiple regions under competing biomechanical and functional purposes (Scott 1938; Thoma 1938). This led researchers to recognize that the mandible has some basic genetic predetermination, though its growth and development are largely determined by environmental and functional demands on various regions of the skeletal anatomy (Lifshitz 1976). By using this model of mandibular development, further studies were conducted studying the role of alteration and/or removal of biomechanical loads on craniofacial shape in an

attempt to better understand the shape and function of the mandible in past hominin populations (Watt and Williams 1951; Lifshitz 1976).

Orthodontic and dental literature regarding the growth and development of the mandible boomed in the late 1950's and early 1960's as researchers grasped the concept of varying inputs on different regions of the bone itself (Massler and Frankel 1951; Begg 1954; Ricketts 1960; Graber 1963). Researchers recognized that different areas of the skull can be considered 'growth centers', though the locations of these were hotly debated (Carlson 2005). The concept of genetic determinism crept in to craniofacial biology, arguing that growth was predetermined by an individual's genetics (harkening back to racially-determined patterns of growth popular in the 1800's), and debate moved to *where* craniofacial growth was occurring. Some argued that it occurred at the sutures (creatively named the Sutural Theory), where skeletal growth occurred first as cartilaginous expansion at the sutures due to genetic signaling (Weinmann and Sicher 1947). Others argued that soft tissue drove the expansion of the face, such as the nasal septum "driving" the midface forward, and sutures simply "play catch up" to the main engine of facial growth (Nasal Septum Theory; Scott 1956). These theories of craniofacial growth would soon be dismantled and restructured by the work of multiple scientists proposing a more functional approach to the anatomy of the head and face (Carlson 2005). Key among these works are the concepts of and theories of three clinicians and scientists, all of whom built upon each others work to set the foundations for our current understanding of craniofacial growth and development.

Some of the earliest work utilizing this more functional theory was that of Arne Björk, a Swedish dentist who looked at human subjects using longitudinal studies and radiographic techniques. Björk's early work demonstrated an understanding of the dynamic process of mandibular development, primarily in regards to orthodontic treatment (Björk 1951), with key

insights in to the contribution of overall body size in the in craniofacial growth (Björk 1953). However, Björk is best remembered for his pivotal longitudinal study of mandibular and maxillary growth in adolescents. Recognizing the need for a holistic picture of craniofacial development, Björk and colleagues hammered small metallic implants in to various regions of the mandible and maxilla of young Scandinavian children; these children were then subjected to numerous cephalometric x-rays to establish not only which regions were growing at which ages, but also the magnitude of these growth changes (Björk 1955; Björk 1963; Björk 1968). The longitudinal nature of these studies was unprecedented, and for both logistical and ethical reasons today, this research has not been matched. Overall, Björk and colleagues established that postnatal mandibular growth is a result of the posterior and superior growth of the ascending ramus, growth of the alveolus with subsequent drifting of the dental arcade, the relative lack of growth along the inferior border of the mandible, and the overall forward and downward position of the mandible in relation to the rest of the head due to growth in the cranial base (Björk 1968; Björk and Vibeke Skieller 1983). These studies did not identify the factors causing the differential growth of the various regions of the mandible, but did set the stage for our current understanding of how - and more importantly why - these changes happen.

While Björk and colleagues made enormous strides in understanding changes in the size and shape of the human mandible from birth to adulthood, they never adequately described *why* these changes were taking place. The key researcher in this realm was Melvin Moss, an American dentist best known for his Functional Matrix Theory. The Functional Matrix Theory began in 1960, and states that the form of all cranial skeletal elements is a direct result of their function (Moss and Young 1960). As such, it is often easier to summarize Moss' model by stating that the craniofacial skeleton does not *grow*, but rather *is grown*. This concept argues that cranial growth is a result of

not just genetic predisposition, but the sum of all internal and external factors acting on the cranium as a result of its function (Moss and Young 1960; Moss 1968; Moss and Rankow 1968). What would now likely be termed as 'epigenetics' was to Moss and his colleagues the sum total of all functions on the skull necessitated by the sum of its functions: house and protect the brain and other organs of the head, provide leverage for mastication and movement, and the incorporation of all other soft-tissues of the cranium (Moss and Salentijn 1969b; Moss and Salentijn 1969a). Moss divided the skull in to two functional areas: the 'neural' and the 'facial' components, and within each of these components were the total of all regions related to the organs, such as the brain, the eyes, the ears, and so on (Moss and Young 1960). These can be further divided in to their constituent skeletal units: macroskeletal units, such as the mandible or maxilla, and microskeletal units, such as the coronoid process or the chin. Finally, Moss identified either capsular matrices (eye, nasal, oral) or periosteal matrices (areas of active growth and transformation). Therefore, the overall growth of the larger macroskeletal units is dictated by the growth of the smaller microskeletal units such as processes and muscle attachments, which are in turn dictated by the type of matrix at the site (Moss and Young 1960; Moss 1968).

Moss' Functional Matrix Theory has held up remarkably well in the decades since its inception (Moss 1997a; Moss 1997b). The main debate against the theory revolves around the concept of open spaces within the face and how 'nothing', or the lack of soft tissue, can cause growth of the face. To compliment his Functional Matrix Theory, which relies on periosteal growth, Moss proposed a capsular matrix aspect to account for the growth of patent areas of the face, namely the vomernasal organ. In the absence of soft tissue and the corresponding functional matrices, Moss argued that patency of the airway and translational growth of other functional matrices resulted in the open aspect of humans' nasal complex (Moss and Salentijn 1969b; Moss

and Salentijn 1969a). This concept, often termed “spaces grow faces”, stood in stark contrast to the Nasal Septum Theory and the Sutural Theory of craniofacial growth (Weinmann and Sicher 1947; Scott 1956). These theories adequately explained the patency of the nasopharynx, either through growth at the sutures causing expansion of the open space, or by the growth of the cartilageof nasal septum, which has a growth vector; it would take some time before these two theories were entirely disproven (*see* Siegel et al. 1990), and Moss’ concept of the functional matrix and capsular matrix remain the dominant paradigm in craniofacial biology.

This cascade of growth processes, the lynchpin of modern craniofacial growth theory, is easily demonstrated with the example of the eye. As the eyeball itself grows (in a capsular matrix), it exerts function demands on the surrounding bone of the eye orbit; these demands cause periosteal reaction in some regions of the orbit, resulting in bone deposition, and resorption in other regions. As a result, the eye grows larger, resulting in the growth of the eye orbit of the skull, which is constrained by the growth demands of the surrounding regions, namely the vomernasal complex below and the brain above and behind. The functional matrix here, the eyeball, dictates the skeletal growth in the region.

This interaction between different functional needs in different regions, the functional matrices, results in the overall growth pattern of the human skull (Moss and Young 1960; Moss and Rankow 1968). The same principle can then be applied to any functional matrix of the skull, for example the masseter, which comprises one functional matrix associated with a single function: to elevate the mandible during mastication. This results in two skeletal aspects of the matrix (skeletal matrices), the angle of the mandible and the inferior aspect of the zygomatic arch, where the superior aspect of the masseter muscle attaches. As the masseter fulfills its function, contracting and thus elevating the mandible, it dictates that the zygomatic arch and the angle of

the mandible serve as attachments points for the biomechanical loading, and thus take the recognizable shape over the course of growth and development. In sum, the bones of the skull are grown as a result of the functional needs placed upon them, and do not grow by some predetermined design.

The third key researcher in the area of postnatal growth and development is orthodontist Donald Enlow, who sought to better understand exactly *how* the adult midface and mandible come to its final shape from birth to adulthood. Building upon the work of Björk and Moss, as well as numerous studies in the 1960's and 1970's utilizing removal or paralysis of certain musculature of the face, Enlow geared his work primarily towards orthodontics students and practitioners. While he recognized the dearth of research regarding the intricacies of how the human mandible developed from birth to adult form from a clinical perspective, he applied his research towards a more theoretical understanding of craniofacial growth. Enlow also incorporated various advances in histology to look at specific regions of the mandible to establish exactly where bone deposition and resorption were occurring during the growth process. Key amongst these ideas are the concepts of remodeling, drift, and displacement. As the human craniofacial complex grows, primarily in an anterior and inferior direction in response to the growing brain, the face is displaced anterior and inferior in relation to the cranial base (Enlow 1968). The displacement of the mandible, therefore, occurs at the temporomandibular joint, while the mandible is simultaneously remodeling, with bone deposition occurring and the posterior and superior aspects of the ramus and bone resorption occurring on the anterior margin (Enlow 1982; Enlow 1990). Bone remodeling is also occurring at anterior and inferior margins of the endocranium and the posterior and superior margins of the vomernasal region, thus maintaining occlusion (Enlow 1982). Arguably the most influential aspect of Enlow's work was the concept of the V-principle, wherein bone deposition occurs along the

inner side of a "V" shaped region (e.g., the hard palate) and resorption occurs on the outer side of the "V"; as a result, the region grows and expands at the same time (Figure 5; Enlow 1982; Enlow 1990; Enlow and Hans 1996). Enlow's work incorporates Moss's Functional Matrix theory, namely the maxilla and mandible, to better understand the variations in occlusion seen by clinicians. The combination of the work of Björk, Moss, Enlow, and the research that they use to build their growth models led to our current understanding of facial growth (see section 1.2.5).

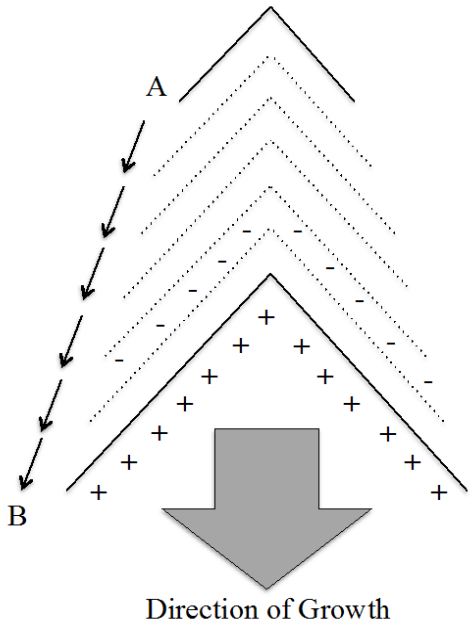

Figure 5. Enlow's "V" Principle. The earliest stage of development (A) grows through the "V" principle to the later stage (B) through deposition (+) and resorption (-). ***Adapted from Enlow 1982: 41.***

1.2.3.2 History of Anthropological Mandibular Research

Björk, Enlow, and Moss certainly were not the only researchers concerned with the topic of mandibular growth and development. Whereas these scientists found a captive audience

primarily in dentistry and orthodontics, anthropologists were particularly interested in questions related to paleoanthropological specimens. Mandibles, such as the Mauer mandible of Germany and Peking Man of China, were common among paleoanthropological finds in Europe, Asia, and Africa during the 19th and 20th centuries. In fact, due to their high preservation rates, mandibles have always represented some of the most common finds of extinct hominin species (Smith and Ahern 2013). The evolutionary trajectory of the mandible has long been a focal point for paleoanthropological research, dating back to some of the earliest hominin discoveries (Huxley 1859). Key amongst these more anthropologically leaning works are those of DuBrul and Sicher (1954), who sought to explain the overall function of the hominin mandible and chin as an adaptive feature. Their extensive survey of primate, fossil, and modern chin morphology remains a cornerstone in anthropological literature as an explanatory model for the chin (and lack thereof) in all primates except for modern humans, tracing our chins in part to the vertical nature to bipedality and the upright nature of human posture and compensatory changes as a result of the more vertical orientation of the human head (DuBrul and Sicher 1954). This anthropological fascination with the human chin is not new, and presence of the trait has been used since the beginning of the field to debate the inclusion of specimens from our taxa, leading Arthur Keith and others to use the mandible and chin as an exclusionary feature in human phylogenetic debates revolving around the Piltdown hoax in the early 20th century (Hrdlička and Pearson 1911; Robinson 1913; Keith 1916; Wallis 1917; Keith 1928). This "membership" within our species has not faded from contemporary debates, either, as the chin has played a role in debates regarding hominin speech, diet, and overall morphology and variation (Lieberman and Crelin 1971; Carlisle and Siegel 1974; Schwartz and Tattersall 2000; Antón 2002; Lieberman 2011; Pampush and Daegling 2016).

The staying power of the "chin debate" is largely due to the focus of many anthropologists on the uniqueness of the chin and its ability to predict "humanness"; in the lack of large samples of paleoanthropological material, the mandible often represents the best source of data for phylogenetic reconstructions (*see* Dobson and Trinkaus 2002; Kesterke and Ahern 2007; Lieberman 2011). The roles of the chin and the mandible itself have been evaluated using biomechanical and electromyographic data, which suggests that the primate mandible shape, specifically fusion of the mandibular symphysis, also develops in response to torsion caused by mastication (Hylander 1975; Hylander 1979). Evidence also suggests that the primate mandible developed in part to counteract shear caused in unilateral loading (Hylander 1984), and is allometrically scaled with body size and masticatory habits (Hylander 1985). The works of Hylander demonstrate the dominant assumption underlying the enigma of the human chin: biomechanical adaptation.

The chin as an adaptation to loading has been supported by both microscopic and macroscopic studies, as well (Riesenfeld 1969; Daegling 2001; Dobson and Trinkaus 2002). The advent of geometric morphometrics allows more detailed modeling of load vectors in the human chin, further supporting the theory that the primate mandible and human chin have adapted to the nuanced loading resulting from unilateral mastication (Ichim, Swain, and Kieser 2006; Gröning, Fagan, and O'Higgins 2011; Gröning, Fagan, and O'Higgins 2012). This strong evidence for the chin as an adaptive feature has led many anthropologists to use it as a defining feature for the inclusion or exclusion in phylogenetic reconstructions based solely on mandibular form (Thayer and Dobson 2010; Garvin and Ruff 2012; Bejdová et al. 2013). The outcomes of these studies demonstrate the importance of a better understanding of mandibular growth and development in the study of anthropology and human evolution.

The review above brings about the contemporary understanding of mandibular development. Dysfunction and dysmorphology of the craniofacial complex is relatively common compared to other aspects of human anatomy, and are therefore beyond the scope of this dissertation. As such, this chapter focuses on the normal growth and development of the human mandible in an attempt to display the standard patterns of growth observed through centuries of research on the human mandible.

1.2.5 Normal Prenatal Growth and Development of the Mandible

Key to the study of mandibular development is an understanding of the first pharyngeal arch formation and its interaction with Meckel's cartilage. Meckel's cartilage has a long evolutionary history, being present in most vertebrates in some form or another (Hall 2015). In mammals, this tubular cartilaginous structure arises primarily from neural crest cells in the mandibular prominences and eventually ossifies to form the mandible, though it is not through traditional endochondral formation seen in other long bones. The role of Meckel's cartilage in animal models has long been studied as a viable analog to human mandible growth and development (Bhaskar, Weinmann, and Schour 1952; Frommer and Margolies 1970). Correlating the fetal development of the mouse and human mandibles, particularly Meckel's cartilage, was an integral aspect of developmental biology through the later part of the 20th century (Bhaskar, Weinmann, and Schour 1952; Frommer and Margolies 1970; Siegel and Mooney 1990), and the use of mouse models for the study of craniofacial ontogeny is now recognized as a valuable window in to growth and development (Miettinen et al. 1999; Hill, Reeves, and Richtsmeier 2007; Feng et al. 2009). Within these mouse models of growth and development, common correlations

between mouse developmental stages and human developmental stages have been established, called Carnegie Stages. For example, the first Carnegie Stage (C1) represents a fertilized oocyte shortly after conception, whereas Carnegie Stage 3 (C3) represents the formation of the blastocyst cavity. Due to the more rapid development of mice compared to humans, these stages occur on different temporal scales, but the Carnegie Stages between the two species are comparable (*see* Table 2).

Normal mandibular development begins early after conception around the 4th week post-conception. This period of embryological development is key to the normal form and function of the human craniofacial development, and corresponds to the 8th day of mouse craniofacial development (Table 2). Mouth development begins with the stomodaeum, a depression in the ectoderm surrounding the primordial face that will eventually form the oral cavity (Depew, Tucker, and Sharpe 2002). A period of cell rearrangement and death occurs in the region, eroding the barrier between the surface ectoderm and the endoderm of the foregut at 22 days (E9.5 in mice; Sperber 2002; Schoenwolf et al. 2009). The formation of the first pharyngeal arch is apparent by 24 days post-conception (E10.0 in mice), shortly after the stomodaeum is established, and the rapid growth of these structures marks the beginning of mandibular development. The first pharyngeal arch will eventually give rise to Meckel's cartilage, leading to the development of the mandible, incus, and malleus; the second pharyngeal arch gives rise to Reichert's cartilage and the stapes; the third pharyngeal arch gives rise to the hyoid (Sperber 2002; Depew, Tucker, and Sharpe 2002; Jiang, Bush, and Lidral 2006; Hall 2015).

Table 2. Stages of mandibular development in both humans and mice.

Carnegie Stage	Human Age[a]	Mouse Age[a]	Description of craniofacial and mandibular development
9	20	9.0	The neural plate is expanding and begins to fold as gastrulation continues in the primitive streak. Neural crest cells migrating towards the facial region. Somite segmentation begins as stomodaeum appears.
10	22	9.5	Neural fold fuses and begins to close. Paraxial mesoderm continues to segment in to somites. Stomodaeum deepens.
11	24	10.0	Neural tube closure continues. Paraxial mesoderm continues segmentation, otic placodes being sinking, first and second pharyngeal arches form caudally to the frontonasal prominence. Stomodaeum is widens as prominences swell.
12	26	10.5	Brain growth causes lateral facial expanse. Paraxial mesoderm continues segmentation, third pharyngeal arch becomes apparent, and stomodaeum deepens. Mandibular prominences merge in the first pharyngeal arch, forming a continuous structure.
13	28	11.0	Paraxial mesoderm continues segmentation as nasal pits form from olfactory placodes, and fourth pharyngeal arch becomes apparent.
14	33	11.5	Optic placodes and nasal pits readily apparent. Paraxial mesoderm continues segmentation. Medial and lateral prominences are apparent around nasal pits.
15	36	12.0	Lens pits close and stomodaeum deepens as medial and lateral prominences begin growing towards each other, coming in contact.
16	40	12.5	Nasal pits move ventrally, auricular ridges appear. Medial and lateral nasal prominences contact and epithelial fin forms.
17	42	13.0	Nasal pits continue ventral movement and auricular ridges become more prominent. The medial nasal prominences merge, forming the upper lip and nose. Meckel's cartilage appears in the first pharyngeal arch.
18	44	13.5	Nasal pits continue ventral movement and medial and maxillary prominences come in contact above the mandibular prominence. Epithelial fin dissolves and maxillary prominences begin to fuse.
19	48	14.0	Nasal pits continue ventral movement as medial and maxillary prominences fuse, forming a continuous upper lip. Ossification begins.
20	52	14.5	Nasal pits continue ventral movement and ossification continues.
21	54	15.0	Nasal pits continue ventral movement, eyelids, eyes, nose, and external acoustic meatus all apparent.
22	55	15.5	Nose becomes recognizable, and eye pigmentation is apparent.
23	58	16.0	Ossification continues, differentiation of cranial structures complete.

[a]Days post-conception (adapted from Sperber 2002; Depew, Tucker, and Sharpe 2002)

As the brain continues to grow, it forces the nasal and maxillary prominences ventrally to accommodate the growing forebrain, and the rapid expanse of these swellings leads to eventual contact around 40 days post-conception (E12.5 in mice; Sperber 2002; Jiang, Bush, and Lidral

2006). The medial upper lip and nose are formed by 42 days post-conception (E13.0 in mice), and the eyelids, eyes, nose, and external acoustic meatus are all readily apparent by 54 days post-conception (E15.0 in mice). This complex process (Table 2) is responsible for the recognizable human face, and any interruptions, teratogenic response, or cellular dysfunction or shortage during this time of development can result in any number of facial deformities (Radlanski and Renz 2006; Schoenwolf et al. 2009).

The human embryo consists of five pairs of pharyngeal arches, numbered Arches 1-6. Arch 5 rarely develops in humans, and even then it results in a negligible contribution to craniofacial growth and development (Sadler 2012). Arising from the mesoderm of the first pharyngeal arch, Meckel's cartilage first appears around 42 days post-conception (Table 2) as solid hyaline cartilage surrounded by a fibrocellular capsule (Schoenwolf et al. 2009). Nested within the pharyngeal arch, the structures run from the midline of the fused mandibular process to the otic capsule (Figure 6 and Figure 7). Both the right and left sides of the first pharyngeal arch contain a single Meckel's cartilage, as the two structures are not fused on the midline and only contact each other through a thin mesenchymal sheet (Figure 6; Rodríguez-Vázquez et al. 1997). Integral to the development of this cartilage, and the eventual mandible, is the development of the lingual nerve of the mandibular branches of the trigeminal nerve; the lingual nerve develops along the medial aspect of each Meckel's cartilage, while the inferior alveolar nerve runs along the lateral aspect (Figure 7; Gray 1918; Drake, Vogl, and Mitchell 2010). By roughly 45 days post-conception, mesenchyme condenses anteriorly to the cartilage just lateral to the midline as the inferior alveolar nerve begins to branch in to the mental and incisive branches. The primary intramembranous ossification center of the mandible appears at this time, spreading both anteriorly and posteriorly, as well as inferiorly below the incisive nerve to form a groove (later becoming the incisive canal; Orliaguet et al. 1993).

Overall, the ossification of the fetal mandible displays a posterior spread of bone towards the ascending rami, forming a recognizable mandible by the 10th week post-conception (Frommer and Margolies 1970; Schoenwolf et al. 2009).

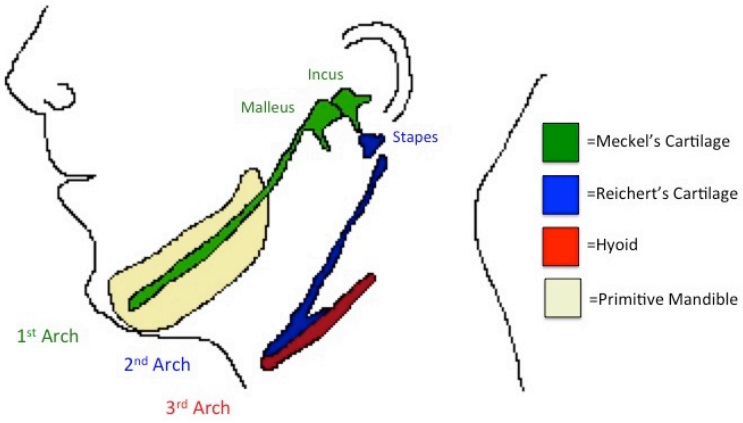

Figure 6. Meckel's cartilage within the pharyngeal arches (lateral view).

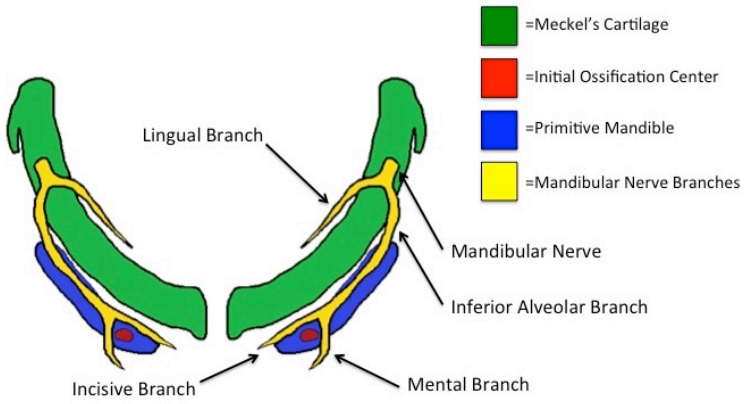

Figure 7. Development of the alveolar process of the mandible (superior view).

Chondrocytes are present throughout the developmental lifespan of Meckel's cartilage, and the complex interplay of ossification of the mandibular body and cell hypertrophy and death lead to the incorporation of the mandibular nerves and vessels within the developing bony

mandible (Figure 8-Figure 11). Chondrocytes are largely responsible for the eventual fate of Meckel's cartilage: in the distal region of Meckel's cartilage, chondrocytes atrophy and ossify endochondrally. Chondrocytes in the middle region become fibrous tissue, while chondrocytes from the posterior region differentiate in to two separate cartilages that will become the incus and the malleus (Figure 8; Orliaguet et al. 1993; Schoenwolf et al. 2009; Hall 2015). The lingual aspect is replaced by fibrous tissue to become the sphenomandibular ligament, while small patches of cartilage appear along the anterior edge of the coronoid and within the condylar processes (Radlanski, Renz, and Klarkowski 2003).

The alveolar process of the mandible forms shortly after the deciduous tooth buds appear, ossifying in bands of bone along the medial and lateral margins of the buds and eventually forming septa between each of the individual teeth (Radlanski, Renz, and Klarkowski 2003; Radlanski and Renz 2006). The mandibular canal forms deep to these newly formed crypts, separated from the rest of the alveolar process by a horizontal band of bone (Figure 10 and Figure 11). Once this primitive mandible is formed, the further growth of the mandible (both pre- and post-birth) is governed by growth in the condyles, coronoid processes, and at the mandibular symphysis (Enlow 1982; Enlow 1990; Enlow and Hans 1996). As such, Meckel's cartilage effectively disappears, leaving only the developing mandible, ear ossicles (which will begin ossification at 16 weeks post-conception), and various tissues surrounding the mandible itself (Schaefer, Black, and Scheuer 2009).

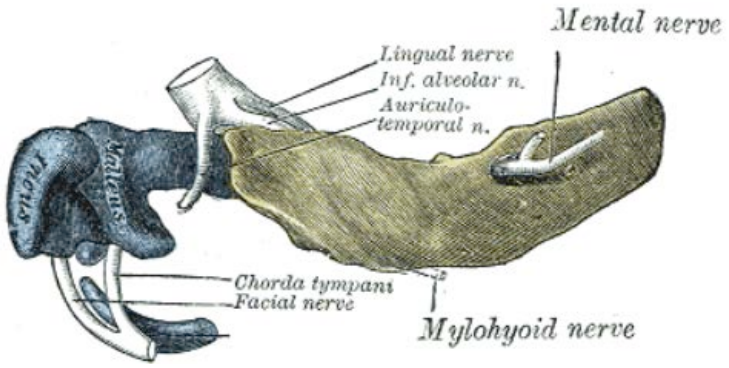

Figure 8. Development of Meckel's cartilage within the first pharyngeal arch (lateral view towards midline). From Gray's Anatomy, Plate 178 (1918).

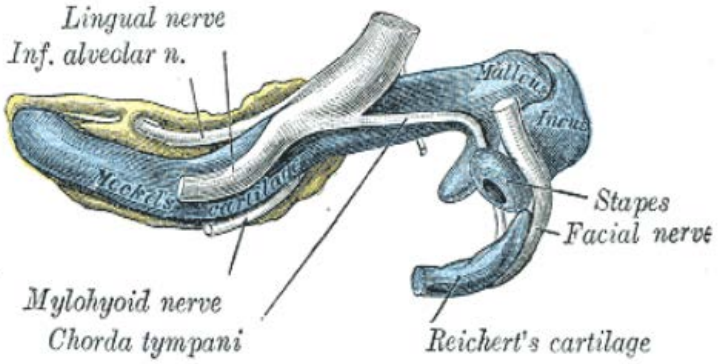

Figure 9. Development of Meckel's cartilage within the first pharyngeal arch (lingual view). *From Gray's Anatomy, Plate 179 (1918).*

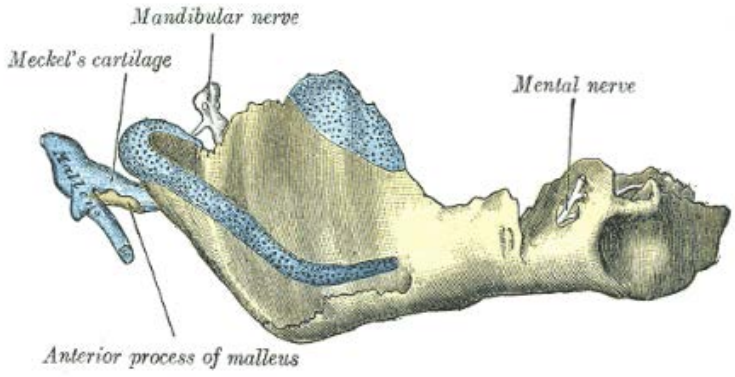

Figure 10. Development of Meckel's cartilage within the first pharyngeal arch (lateral view towards midline). *From Gray's Anatomy, Plate 180 (1918).*

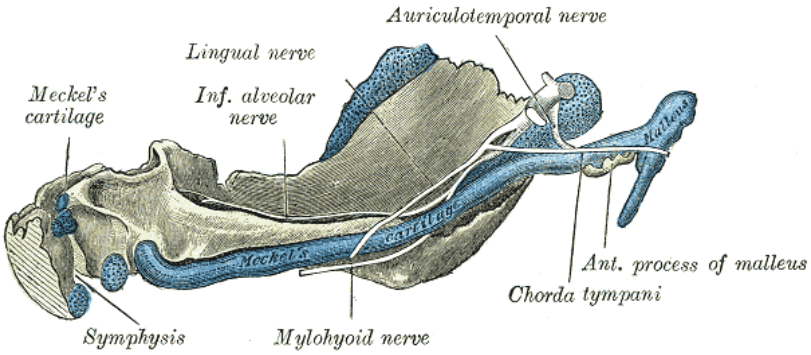

Figure 11. Development of Meckel's cartilage with the first pharyngeal arch (lingual view). *From Gray's Anatomy, Plate 181 (1918).*

1.2.6 Postnatal Mandibular Growth and Development.

The postnatal growth of the mandible has been extensively studied, particularly in light of its significance for both anthropological and orthodontic research. Anthropological research has focused on overall morphology of the bone, as implications of both size and shape have far-

reaching significance for paleoanthropology. Orthodontic research in particular has studied the growth of the subadult and adult mandible, as corrective intervention and the timing thereof are particularly important for correcting various malocclusions and eruption problems. Much of this research focuses on maxillary growth and development, as the ontogeny of the midface involves a complicated interplay of growth, transposition, and translation of the various cranial complex (Moss and Salentijn 1969b; Enlow 1982). The mandible, however, also develops from a complex interplay of the various musculature and other soft tissues contributing to the bone. A contemporary understanding of the postnatal growth and development of the human mandible, based largely on the work of Björk, Moss, and Enlow, is described here.

Early postnatal development of the mandible is best visualized as a set of individual functional matrices (Moss and Rankow 1968):

(1) the alveolar processes
(2) the coronoid processes
(3) the angular processes
(4) the mandibular bodies
(5) the condyles
(6) the chin

The functional matrix of the alveolar process is the teeth, meaning they dictate the growth and development of this area of the mandible (Moss and Rankow 1968; Moss and Salentijn 1969b). The temporalis muscle is the functional matrix of the coronoid process, being responsible for the growth and development of this aspect of the mandible (Moss and Rankow 1968). The functional matrix of the angle of the mandible are the masseter and medial pterygoid muscles, while the function matrix of the chin is the digastric muscles; similar resection/paralysis studies have shown that immobilization of these muscles leads to dysmorphology of that particular microskeletal unit (Moss 1968; Moss and Salentijn 1969a). The functional matrix of the mandibular body varies

slightly, though it adheres to the same principle of growth, where the nerves and vessels of the mandibular canal dictate the growth and development of the region.

The condyles of the mandible exhibit a more complicated growth pattern than those of the other microskeletal units of the mandible due to their origins as secondary cartilage. Secondary cartilage growth differs from that of primary cartilage growth in that it is largely dependent on biomechanical loads for proper formation (Sperber 2001). Whereas primary cartilage has its own growth vector, secondary cartilage does not form or forms improperly in the absence of mechanical pressure, resulting in ossification (Hall 1993). The basic concept of growth at the condyles is that of cartilaginous growth, though secondary cartilage undergoes metaplasia, where it is directly transformed in to osteoblasts and osteocytes (Moss and Rankow 1968; Enlow 1982). Condylectomy severely limits the growth of the condylar region in animal models, though it does not directly affect the overall growth and development of the all microskeletal units of the mandible (Moss and Rankow 1968; Hall 1993). The growth and development of the mandible therefore consists of a number of microskeletal units with a relationship to one another; these units develop independently of each other, and only drastic and massive changes in one unit can cause a cascade affecting the surround units (Moss and Rankow 1968; Moss and Salentijn 1969b).

The postnatal growth of the mandible occurs through the "V" principle, with the overarching appearance of the mandible growing anteriorly and inferiorly as appositional growth and condylar growth against the glenoid fossa of the cranial base (Figure 12; Enlow and Hans 1996). The anterior margin of the chin grows appositionally as bone is deposited and the anterior-inferior border with subsequent resorption on the posterior margin. Along the alveolus, growth occurs to accommodate the erupting teeth (both deciduous and adult) throughout ontogeny, with some resorption along the anterior margin just below the first and second incisors; this process

helps form the recognizable human chin (Enlow 1982; Enlow 1990). The mandibular body grows both medially and laterally as the angular process grows as a result of mechanical response to both the masseter and medial pterygoid muscles. The coronoid process grows superiorly in response to the temporalis muscle, and the condyle grows superiorly and posteriorly, effectively "pushing" the mandible forward and downward away from the cranial base (Figure 12; Enlow 1982; Björk and Vibeke Skieller 1983; Enlow and Hans 1996). The sum of all these interconnected processes results in the recognizable human mandible in adults.

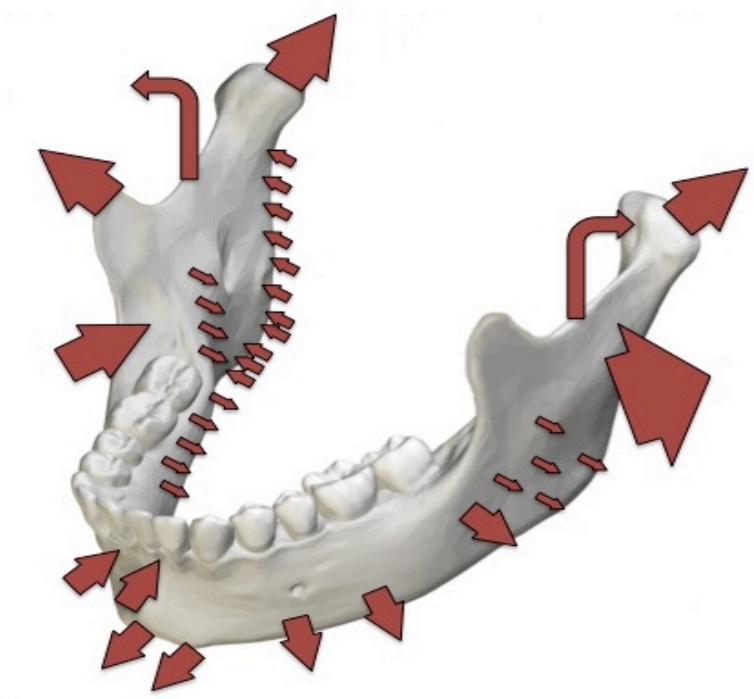

Figure 12. Postnatal growth of the human mandible. ***Adapted from Enlow (1982).***

1.3 RESEARCH GOALS AND DESIGN

This review highlights the complex nature of human mandibular growth and development. These processes demonstrate how the mandible can be envisioned as a set of microskeletal units with independent growth vectors and trajectories. It has also been shown that thyroid hormone has a direct effect on bone growth, particularly in the craniofacial complex. As such, this research proposes that alteration in maternal thyroxine levels will therefore have an effect on the ontogeny of the offspring mandible. It is expected that heightened levels of maternal thyroxine will result in shape changes of the offspring mandible in all areas of mandibular growth, particularly areas related to muscle attachments and areas of the mandible that grow in response to occlusion or the cranial base.

1.3.1 Hypotheses

The goal of this dissertation is to utilize isogenic mouse model data and micro-CT scanning of mandibles of mice exposed to exogenous thyroxine during fetal development, mimicking maternal hyperthyroidism. The primary hypothesis of this research is that mice exposed to excess exogenous thyroxine during fetal development will demonstrate altered shape compared to the unexposed control mice.

Secondary Predictions:

(1) The shape changes in exposed mice will be most pronounced in regions of the mandible associated with muscular attachment (mandibular angle, coronoid process).

(2) The shape changes in exposed mice will be more pronounced as age increases.

(3) The shape changes in exposed mice will be more pronounced as thyroxine dosage increases.

These hypotheses will be assessed using Euclidean Distance Matrix Analysis and geometric morphometric methodologies. The EDMA methodology will be used to address any size changes, as well as basic shape changes, associated with the increased maternal thyroxine levels. The GM methodology is used exclusively for shape analysis, and will adequately describe and evaluate any shape changes present in the sample. Under these hypotheses, any size and/or shape changes in the offspring mandibles are attributable to increased maternal thyroxine levels.

1.4 RESEARCH SIGNIFICANCE

The results of this research will advance anthropological and clinical studies in numerous ways. While postcranial skeletal studies have focused on the role of thyroid dysfunction in poor bone formation and suture fusion, cranial studies have addressed issues of suture homeostasis, craniosynostosis, and clefting (Hanken and Summers 1988; Göthe et al. 1999; Allan et al. 2000; Harvey et al. 2002; Luewan, Chakkabut, and Tongsong 2011). This study will add to the scant literature concerning the role of maternal thyroid function and the ontology of the mandible; in doing so, this research provides a framework for future studies regarding the role of the maternal endocrine system in relation to offspring growth and development. This research also adds to existing literature concerning the role of maternal environmental contribution to offspring

craniofacial growth and development (Daneman and Howard 1980; Johnston and Bronsky 1995; Talaeipour et al. 2005; Kau et al. 2006; Rasmussen et al. 2007; Cray et al. 2013; Šešelj, Duren, and Sherwood 2015). The complex gene-environment interaction during craniofacial ontogeny cannot be completely understood by any single study, though this research project adds to the mounting literature documenting the intricate interaction between body systems during growth and development.

The proposed research also contributes to research concerning the role of maternal health and wellness during pregnancy. Clinical research focuses on the etiology and pathology of endocrine disorders (Hershman 2009; Mestman 2009; Singer 2009), or on the disorders of the individuals affected (Brixen and Eriksen 1999; Adler 2000; Luewan, Chakkabut, and Tongsong 2011), but rarely addresses the implications of such maladies on developing embryos. The increasing prevalence of thyroid dysfunction in modern populations promises to have profound impacts in future medical and cultural studies regarding maternal health and wellness (Allan et al. 2000; Luewan, Chakkabut, and Tongsong 2011; Grob 2014).

More broadly, the results will be of interest to clinicians and other researchers interested in pregnancy care, be it prenatal planning, screening, or maternal care. While this study focuses primarily on biological aspects of maternal endocrine levels, its anthropological background showcases the potential for studies on maternal environment. Hyperthyroidism, either autoimmune- or pregnancy-induced, affects a large number of potential mothers both in the U.S. and abroad (Canaris et al. 2000; Hollowell et al. 2002; Murphy and Williams 2004), so the very nature of this research displays its broad applicability to biological anthropology research. Furthermore, the endocrine system plays a substantial role in the development of metabolic disease processes in the past and these endocrine dysfunctions (e.g., hypothyroidism, hyperthyroidism,

hyperparathyroidism, rickets, scurvy) have played important roles in shaping ancient and historical populations (Ortner and Mays 1998; Ortner 2003; Brickley and Ives 2006; Mays, Brickley, and Ives 2006; Mays, Brickley, and Ives 2007). Thus, the potential of this study to identify cranial and mandibular shape changes associated with maternal hyperthyroidism in modern populations provides a springboard for future studies utilizing shape analysis to evaluate endocrine disorders in the past.

Finally, this study will further demonstrate the overall efficacy of animal models in the study of human growth and development. Anthropologists have long been interested in variable growth rates and craniofacial morphology of the earliest hominin populations (Viòarsdóttir, O'Higgins, Paul, and Stringer 2002; Hennessy and Stringer 2002), and the large samples provided by animal models such as the one proposed here demonstrate the power of geometric-morphometric analyses as correlates for human ontogeny. Clinicians will benefit from the additional data produced regarding the teratogenic effects acting on developing embryos, as well as additional information relating to the chemical pathways of bone growth and development. This investigation therefore balances anthropological and clinic research to provide a framework for future studies in skeletal biology, human growth and development, pathology and paleopathology, and craniofacial biology.

2.0 MATERIALS AND METHODS

This dissertation utilizes an isogenic mouse model and micro-CT scanning of mice exposed to exogenous thyroxine during fetal development to mimic maternal thyrotoxicosis. This project is an extension of a larger, NIH-funded project being conducted by Dr. James Cray at Georgia Regents University and continued at the Medical University of South Carolina, who was responsible for the maintenance of the animal sample, the administration of thyroxine dosages, the sacrifice of the litters, the embedding of the animal bodies for later histological processing, and the CT scanning of the skulls. The Georgia Regents University Animal Care and Use Committee approved all data collection and care of the animal subjects, and much of the data from the sample are stored at the University of Pittsburgh

2.1 ANIMAL MODEL

The 241 mice used for this project are C57BL-6 background specimens (Timed Pregnant; Jackson Laboratories, Bar Harbor, ME), a strain of mice commonly used in animal model studies (Crawley et al. 1997). The thyroxine dosage was given as levothyroxine (a synthetic compound identical to thyroxine) to pregnant dams at 13 days post-conception through drinking water under normal consumption of 3-5 ml of water/day. This time period in embryological development corresponds to the period of cranial development prior to sutural closure, and therefore represents a crucial time for the effect of teratogens on overall craniofacial development (*see* Chapter 1;

Morriss-Kay and Wilkie 2005). The light cycles utilized were standard 12:12 cycles, and sacrifice of mice was conducted using CO_2 inhalation with concurrent cervical dislocation, in compliance with ARRIVE Guidelines.

Dams were separated in to a control group with no maternal thyroxine treatment (n=63 resulting pups), a low dosage group receiving ~0.25 mcg of thyroxine/day (n=67 resulting pups), a medium dosage group receiving ~0.50 mcg of thyroxine/day (n=46 resulting pups), and a high dosage group receiving ~1.0 mcg of thyroxine/day (n=65 resulting pups). Litters were serially selected for sacrifice at 15 days (49 mice), 20 days (74 mice), and 25 days (118 mice); seven litters were sacrificed for each time period (21 total litters), resulting in total dam numbers larger than 14 per group required by preliminary tests for most groups (α=0.05, β=80, n= 336; Cray, *pers. comm.*). The resulting litters within the 15-, 20-, and 25-day samples are adequate to establish parity between mothers, offspring, and variation within each of the selected age groups (Table 3). Control group mothers were bred multiple times, but any mothers receiving thyroxine were utilized only once. The age groups of the sacrificed offspring were selected due to their approximate correlation to juvenile and adolescence in humans; final brain development in mice is complete 12-14 days after birth, and mice are considered juvenile until 24 postnatal days (Depew, Tucker, and Sharpe 2002; Morriss-Kay and Wilkie 2005). The dosages of thyroxine were also chosen as correlates to therapeutic dosages (10-250 mcg/day) used in human clinical trials (Cray, *pers. comm.*). Due to sample constraints, namely the absence of data of 15-day old mice that received a medium developmental dose of levothyroxine, some age groups were underrepresented. Sex data for the sample was not available for parts of the 15-day old mice, precluding this sample from certain statistical tests (*see* Section 3.0), but available data are presented in Table 3. Sample sizes are still sufficient to address age- and dose-dependent shape variation (Table 3).

Table 3. Sample sizes of C57BL/6 individuals and associated age, sex, and thyroxine dosages utilized for this study.

Age	Dosage				TOTAL
	Control (sex)	Low Dose (sex)	Medium Dose (sex)	High Dose (sex)	
15 Days	21 (unknown)	19 (8M, 11F)	0 (unknown)	9 (4M, 5F)	**49**
20 Days	19 (10M, 9F)	11 (9M, 2F)	17 (13M, 4F)	21 (14M, 7F)	**74**
25 Days	23 (13M, 10F)	31 (13M, 18F)	29 (14M, 15F)	35 (20M, 15F)	**118**
TOTAL	**63**	**67**	**46**	**65**	**241**

2.2 MICRO-CT SCANNING

The skulls of all mice were separated from the bodies in Dr. Cray's lab and fixed for 3D micro-computed tomography (micro-CT) scanning utilizing a SkyScan 1172 (Kontich, Belgium) set at 19.36μm voxel resolution. To adequately visualize and later landmark the mandibles, the output images from the micro-CT scanner (saved as .bmp files) must be constructed as a stack of image files. This stacking was conducted using the Amira software program (http://www.fei.com/software/amira-3d-for-life-sciences/), a powerful tool for both compiling imaging outputs and visualizing these outputs for landmarking and analysis. The .bmp stacks were compiled in Amira by Dr. Trish E. Parsons, a postdoctoral fellow at the University of Pittsburgh's Center for Craniofacial and Dental Genetics (CCDG) and saved as Amira files (.am file format) on the Center's servers. The images were downsampled in ImageJ (*see* Schneider, Rasband, and

Eliceiri 2012) to improve rendering performance, and the minor loss of image resolution associated with resampling would not affect the landmarks selected for this project (Parsons et al. 2014). Once these images were imported in to Amira, a Gaussian smoothing filter was applied (σ= 0.3 in X, Y, and Z; isometric kernel size =3; Parsons et al. 2014). No hole-filing or smoothing algorithms were applied to the imported image.

The finalized Amira files were utilized for multiple projects within Dr. Cray's larger research project. These finalized Amira files marked the starting point for data collection on the present project, which began with mandible visualization and landmarking. For the current study, thresholds were first selected for optimal viewing of landmarks with the Amira package; thresholds within Amira refer to the opacity thresholds for the imported images, meaning a higher threshold setting results in clear reconstruction of denser, less lucent structures (e.g., teeth) are rendered without that addition of thinner, more lucent structures (e.g., suture edges, thinner cortical bone). For this project an image threshold of 42 was chosen, as it allowed both the accurate depiction of gross landmarks without loss of rendering at thinner aspects of the mouse mandibles (Appendix A).

2.2.1 Landmarking

Once saved as .am files, the reconstructed images of the mouse crania were visualized in Amira for landmarking and the export of landmark data sets; for a step-by-step guide of the landmarking process, see Appendix A. Landmarking refers to the placement of digital landmarks on a three-dimensional image, resulting in x, y, and z coordinates for each landmark on each mandible. Landmarks cannot be arbitrarily assigned, and must represent homologous points on

each individual shape, adequately cover the form, and be reliably found in consistently relative positions (Zelditch et al. 2004). The landmarks represent fixed points on the shape being analyzed, and are selected to represent accurate and replicable representation of the shape being studied (Bookstein 1991). Not all landmarks are necessarily useful; Bookstein (1991) identified three types of landmarks:

Type 1: discrete points such as intersections or foramina
Type 2: points located along maximal or minimal curvatures
Type 3: points along extremes defined by other points

For this project, only Type 1 and Type 2 landmarks were selected, as Type 3 landmarks are considered "deficient" due to their reliance on the placement of other landmarks (Bookstein 1991). Once identified on each subject, these landmarks can be exported to various software packages, allowing for the easy manipulation, visualization, and evaluation of both size and shape of each individual mandible.

A total of 32 landmarks were selected for this project, with 16 points being mirrored on both sides of the mandible (Figure 13). These landmarks represent a common set of mouse mandibular landmarks used in numerous other Euclidean Distance Matrix Analyses and geometric morphometric analyses (Klingenberg and Leamy 2001; Klingenberg et al. 2001; Hennessy and Stringer 2002; Klingenberg, Leamy, and Cheverud 2004), and are selected within Amira in the appropriate order (Table 4). Only the 16 landmarks from the left mandible of each sample were utilized for this dissertation. These landmarks adequately encapsulate the overall shape and size of each mandible to allow for the evaluating of any shape changes occurring due to maternal thyroxine levels.

Once landmarked, the file is saved in a new directory on the CCDG servers, and the landmark data were exported as .ascii files for import in to Microsoft Excel (Microsoft Excel for Mac 2011) as a .csv spreadsheet of uniform landmark data.

Table 4. Order of mandibular landmarks (left side). These landmarks are mirrored on the right side of each mandible and excluded from this study.

Side	Landmark Number	Landmark
Left	1	Anterior superior incisor alveolar rim (midline)
	2	Anterior edge of mental foramen
	3	Anterior edge molar alveolar rim (midline)
	4	Intersection molar alveolar rim and coronoid process
	5	Apex of coronoid process
	6	Posterior base of coronoid process (midline)
	7	Anterior edge of mandibular condyle (midline)
	8	Posterior edge mandibular condyle (midline)
	9	Most anterior point of subcondylar incisive
	10	Posterior tip of mandibular angle
	11	Most superior point of inferior border of mandibular angle
	12	Anterior edge of inferior border of masseteric ridge
	13	Most inferior point on mandibular symphysis
	14	Anterior inferior incisor alveolar rim (midline)
	15	Anterior edge of mandibular foramen
	16	Most posterior point along molar alveolar border

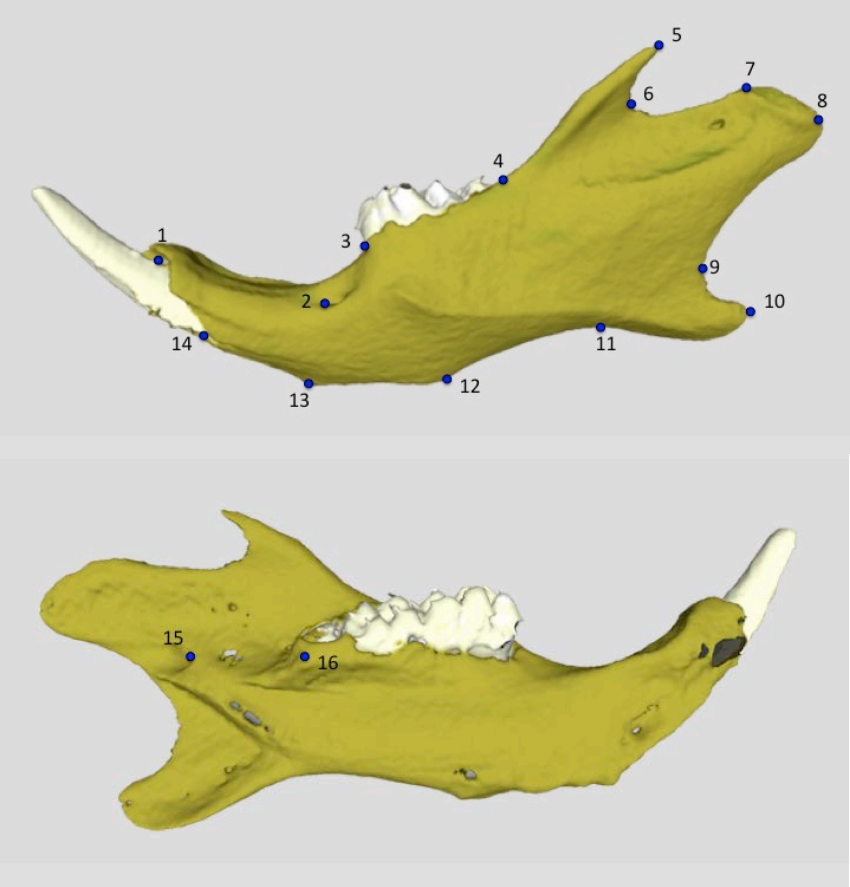

Figure 13. Landmarks utilized for this study (left mandible).

2.2.2 Observer Error

To ensure accuracy in landmark placement, observer error trials were conducted during data collection. Prior to data collection, 30 mandible images were selected and landmarked as a practice run. These same 30 mandibles were then landmarked a second time, and the landmark files (.ascii files) were saved in a separate directory. Finally, these same 30 mandibles were landmarked a third time for comparison with the second run. Each of the three runs was separated by at least a week to avoid memory bias in placing each landmark. By doing so, intraobserver error

could be calculated using a modified reliability analysis and intraclass correlation coefficient tests conducted in SPSS v23.0.0.0 (IBM SPSS Statistics for Macintosh 2015). Intraclass correlation (ICC) is a useful estimate of reliability of quantitative data, effectively measuring the reliability of the single researcher in placing the landmarks consistently across structures (Landers 2015). These calculations, similar to those of a Pearson's correlation coefficient, result in an intraclass correlation calculation (1.000 being perfect correlation between landmark placement between all 30 mandibles), a 95% confidence interval across each landmark across all 30 mandibles, and associated degrees of freedom (Landers 2015). For this study, a threshold of 0.90 was selected in accordance with most scientific publishing standards for research; as such, any values below 0.90 were highlighted and evaluated as instances of intraobserver error. No such errors were found in this study, suggesting that landmark placement was precise across all landmarking procedures conducted for this study (Table 5).

Table 5. Intra-observer error calculations.

		Intraclass Correlation Coefficients		
	Landmark	**x**	**y**	**z**
1	Anterior superior incisor alveolar rim (midline)	0.999	1.000	0.997
2	Anterior edge of mental foramen	1.000	1.000	0.999
3	Anterior edge molar alveolar rim (midline)	1.000	1.000	0.999
4	Intersection molar alveolar rim and coronoid process	1.000	1.000	0.998
5	Apex of coronoid process	1.000	1.000	1.000
6	Posterior base of coronoid process (midline)	0.999	0.999	0.999
7	Anterior edge of mandibular condyle (midline)	1.000	1.000	0.999
8	Posterior edge mandibular condyle (midline)	1.000	0.999	0.998
9	Most anterior point of subcondylar incisive	1.000	0.999	1.000
10	Posterior tip of mandibular angle	1.000	1.000	1.000
11	Most superior point of inferior border of mandibular angle	1.000	0.999	0.999
12	Anterior edge of inferior border of masseteric ridge	1.000	1.000	0.999
13	Most inferior point on mandibular symphysis	1.000	1.000	1.000
14	Anterior inferior incisor alveolar rim (midline)	1.000	1.000	0.990
15	Anterior edge of mandibular foramen	1.000	0.999	1.000
16	Most posterior point along molar alveolar border	0.999	1.000	0.997

2.3 EUCLIDEAN DISTANCE MATRIX ANALYSIS

The first method of statistical analysis utilized is Euclidean Distance Matrix Analysis (EDMA). The EDMA methodology arose out of more traditional morphometric studies utilizing linear distances between landmark points to evaluate the overall size differences and/or changes between two or more biological specimens. This method employs the same landmarks used for geometric morphometric analyses, and is used to compliment rather than compare any shape changes demonstrated by geometric morphometric approaches. This method does not require superimposition methods used by geometric morphometric approaches, as the selection of such a method can affect the landmarks and estimates (Rohlf and Marcus 1993). As such, EDMA provides a lens with which to evaluate form of an object without rotation and scaling associated with geometric morphometrics.

The EDMA method was pioneered in the 1990's as a method of evaluating form of an object by calculating mean distances between *all* landmarks within a sample (Lele and Richtsmeier 1991; Lele 1993; Lele and Richtsmeier 2001). The form of an object with K landmarks is thus defined by a matrix of distances between each landmark, with K rows and K columns, otherwise called a form matrix (FM). Since each landmark has a distance calculated between each other landmark, the total number of distances (K) is defined as:

$$K = \frac{n(n-1)}{2}$$

For each age and control group, the mean distance between each landmark will then be calculated and entered in to a form matrix, allowing for arithmetic and statistical comparisons of each form matrix between the groups (Lele and Richtsmeier 1991; Lele and Richtsmeier 2001).

For example, two separate groups (group *A* and group *B*) are entered in to form matrices FM(*A*) and FM(*B*). These two matrices are then compared, resulting in a form distance matrix (FDM) representing differences in mean distances between the two original matrices, resulting in FDM (*A*,*B*), or the difference FM(*A*) - FM(*B*). This new FDM results in size and shape differences between the two groups *A* and *B*, and can also be scaled to accounted for size differences between samples not of interest to the project (Lele and Richtsmeier 1991; Lele and Richtsmeier 2001).

Once the landmark data for each age and treatment are entered as form matrices, further statistical calculations can be conducted. Working from the null hypothesis that the forms of each age and treatment group are the same, EDMA uses a suite of standard parametric and nonparametric statistical tests to evaluate size and shape of each FM (Lele and Richtsmeier 1991; Lele 1993). Test statistics are calculated through bootstrap resampling of the data, allowing for the evaluation of differences between each of the samples, should they exist (Lele 1993). It should be noted that that a significance level of 0.90 is used due to the involvement of bootstrap resampling and scaling factors, which can affect the tails of each constructed distribution and to lead to errors in interpretation (Lele and Cole 1996). Alpha (α) levels for each test are noted both here and in the results section.

Further testing allows for identification of specific areas of differences between two or more groups using 90% confidence intervals for each distance within each group (Lele and Richtsmeier 1995). This method has been used successfully in past studies to calculate shape distance matrices (SDM) to generate a distribution of values for each calculated mean distance (Lele and Richtsmeier 1995; Lele and Cole 1996; Lele and Richtsmeier 2001). A simple identification of any statistically significant results in the form (shape) differences can be conducted by comparing of these SDM's and their associated upper and lower bounds and

identifying any that do not contain the null value (omnibus testing). Omnibus testing allows one to assume that the forms compared between the two samples are not the same (Lele and Cole 1996; Lele and Richtsmeier 2001). This comparison is done using a Monte Carlo bootstrapping method, which begins with the calculation of form matrices for each sample, FM(*A*) and FM(*B*), and a variance-covariance matrix for the samples. These matrices are then used to generate a new sample of observations for each sample using Gaussian perturbation models, which results in two new samples of observations for group A and group B, which are again used to create a new FDM; this process is repeated many times (typically 1,000; Lele and Richtsmeier 2001). The Monte Carlo method and a regular bootstrapping method are very similar, differing only in the fact that the Monte Carlo method utilizes a Gaussian model whereas the bootstrapping is random. Since both methods use randomized procedures and result in different estimates each time the analysis is conducted, though the high number of repetitions means the differences between each run will not confound any conclusions (Lele and Richtsmeier 2001). The 90% confidence intervals are then obtained, meaning that they are element-wise confidence intervals and are therefore computed for *each* linear distance and can only be used to identify form differences between linear distances; this method does not used to determine if forms are statistically different, and is instead used to determine *where* shape differences are occurring between the two samples (Lele and Richtsmeier 2001).

Hypothesis testing in EDMA is facilitated using the null-hypothesis that the two shapes being compared are the same. Once an empirical distribution is calculated using Monte Carlo resampling and confidence intervals have been computed, the upper and lower bounds of the distribution are evaluated. Using the accepted alpha level (α=0.90), any linear distance with upper and lower bounds that exclude the null value is considered significantly different between the two

groups (Lele and Cole 1996; Lele and Richtsmeier 2001). Finally, the upper and lower 5% of the bootstrapped samples (resulting in the necessary 90% interval) are removed, and the remaining sample is sorted low to high: if the 90% confidence interval for a distance does not contain the null-value (zero), then the null hypothesis that the two forms are the same is rejected.

2.3.1 Application of Euclidean Distance Matrix Analysis

For this project, the 16 landmarks collected on the left side of each mandible will first be represented as a set 120 linear distances. Outliers will first be evaluated for landmark placement error and removed if necessary. Due to the fact that EDMA is an older, unsupported beta software program, some planned analyses could not be conducted. The geometric mean was used to scale the data for this project, effectively removing size from the sample, by calculating the geometric mean of each of the 16 linear distances on the left side of the mandible. Any skulls within the sample that were not fit during the initial rendering process could not be evaluated, which removed the 15-day controls from the sample. The medium dose group was also excluded from analysis due to the lack of 15-day old samples within the sample. As such, a total of four form matrices (FM) will be calculated for this project to adequately quantify shape differences in relation to the project hypotheses: 20-day low dose, 20-day high dose, 25-day control, and 25-day high dose. The low dose groups are compared to the high dosage groups within each age. These groups were utilized for all calculations within WinEDMA, the program used for all aspects of EDMA for this project (Cole 2003).

A form matrix (FM) was first created for each sample being compared (e.g., 20-day low dose and 20-day high dose), and was then divided by the scaling factor (the geometric mean of the distances) to create a shape matrix (SM) for each sample. These SM's were then compared, and a new matrix was calculated for the shape differences between the two samples (Appendix B). A Z-statistic was calculated (alpha = 0.10), and resampled (1,000 resamples with replacement) to create a new shape-difference matrix (SDM). This SDM is then sorted, allowing easy identification of any linear distance that rejects the null hypotheses (the 90% confidence interval does NOT contain zero). This element-wise method allows for differentiation of regions of the mandible that are different between the two samples, which were then depicted on micro-CT scans and reconstructions for easy visualization of shape changes. Complete outputs for EDMA are presented in Appendix B.

2.4 GEOMETRIC MORPHOMETRIC ANALYSIS

The second method of statistical evaluation utilized is geometric morphometrics (GM). The field of GM arose throughout the 20th century, following numerous scholarly debates regarding the best method(s) of evaluating relationships between biological entities. Geometric morphometrics has become as staple method within the field of biology, and is used here to compliment the traditional morphometric analyses provided by the EDMA approach.

> *"The study of form may be descriptive merely, or it may become analytical. We begin by describing the shape of an object in the simple words of common speech: we end by defining it in the precise language of mathematics; and the one method tends to follow the other in strict scientific order and historical continuity."* (Thompson 1915)

The field of geometric morphometrics arose from traditional morphometric analyses, which sought to evaluate similarities and differences between biological entities, and stems from debate between two prominent biostatisticians in the early 20th century (Bookstein 1991). The two scientists, William Bateson and Karl Pearson, argued about continuous or discontinuous evolutionary processes and the best method of evaluating these processes (Bateson 1902; Pearson 1902; Bookstein 1991). Traditional morphometric analysis, like that utilized by Bateson and Pearson, relies on measures of size, namely length, width, height, and depth (Zelditch et al. 2004). These measurements result in data amicable to quantifying and analyzing size, but fail to adequately deal with the overall *shape* of the biological entity being investigated. Prominent Cambridge mathematician D.G. Kendall best demonstrates the value of shape studies: "If we are not interested in the location, orientation or scale of the resulting configuration, then we find ourselves working with a continuous stochastic process describing its change of shape" (Kendall 1977: 428). Therefore, the overall goal of geometric morphometrics is the analysis of shape once size has been removed, allowing geometric relationships between specimens to be evaluated without the potentially confounding elements of size (Adams, Rohlf, and Slice 2013a).

The pioneer of shape studies in the field of biology was D'Arcy Thompson, who worked during the early 20th century to define how shapes could be morphed (in his words, deformed) in to another (Thompson 1917; Zelditch et al. 2004). Thompson showed that change in shape could be described by using a Cartesian coordinate system; by overlying a coordinate system over a shape, then dividing this system in to a rectangular grid, Thompson could then study how the shape of one organism deformed in to another (Thompson 1917; Zelditch et al. 2004). The arguments put forth by Thompson went largely unappreciated until the 1980's and 1990's, when his worked

was resurrected and incorporated in to the developing field of geometric morphometrics. The term 'geometric morphometrics' was popularized in the late-1980's and early-1990's as biologists built upon the ideas of Thompson and the relatively new advances in computing to develop powerful new tools to evaluate shape (Corti 1993; Rohlf and Marcus 1993).

As studies of shape became more prominent, especially in anthropological and anatomical settings, the methodology associated with geometric morphometrics became increasingly complex. The foundation of geometric morphometrics, landmark analysis, was expanded to incorporate outlines, curves, and more elaborate surfaces (Adams, Rohlf, and Slice 2013a). The central tenet of geometric morphometrics became the "Procrustes Paradigm", or the statistical underpinnings and analytical analyses of landmark superimposition (Kendall 1981; Adams, Rohlf, and Slice 2013a). Contemporary trends in geometric morphometric analyses have moved towards three dimensional data, phylogenetic recreation, and inclusion of larger and more complex datasets thanks to advances in computing and imaging.

Geometric morphometric analysis begins with the identification of necessary landmarks of the shape of specimen of interest (*see* Table 4 and Figure 13). Next, these landmarks undergo a generalized Procrustes analysis, which superimposes the landmarks of every specimen in the study group in to a common coordinate system (Rohlf and Marcus 1993; Zelditch et al. 2004). The Procrustes analysis utilizes least-squares, a type of regression analysis of data fitting, wherein the observed landmark locations are centered, scaled, and rotated to the centroid size of the average configuration (Zelditch et al. 2004; Klingenberg 2011). The end result of this superimposition are Procrustes shape coordinates relating to each object in space, allowing for the comparison of the shape of each specimen regardless of size variables.

The next step in geometric morphometrics is the applications of multivariate statistical models, ranging from regression to multivariate analysis of variance (MANOVA) to principle component analysis (PCA) to discriminant function analysis (Rohlf and Marcus 1993; Rohlf and Corti 2000; Zelditch et al. 2004). Statistical tests are chosen based on the hypotheses of the study: covariation patterns can be established using partial least squares (PLS), while shape differences can be evaluated using multivariate regression (Rohlf and Corti 2000; Adams, Rohlf, and Slice 2013a). Of particular interest to anthropologists and anatomists are visualization and explanation of shape changes, typically achieved through the use of PCA and discriminant function analysis (Adams, Rohlf, and Slice 2013b). Harkening back to D'Arcy Thompson's "deformation" of shapes, these visualizations allow researchers to evaluate the direction and magnitude of shape changes in visual planes (Figure 14). The use of GM also allows for testing not available to conventional linear metric analysis (Hallgrimsson et al. 2015). Finally, GM analyses also showcase the vast range of inter- and intra-species variability of tissue shape, and the ontogeny of the mandible is of particular interest to paleoanthropologists and paleontologists alike (O'Higgins and Collard 2002; Viòarsdóttir, O'Higgins, Paul, and Stringer 2002; Viòarsdóttir and O'Higgins 2003).

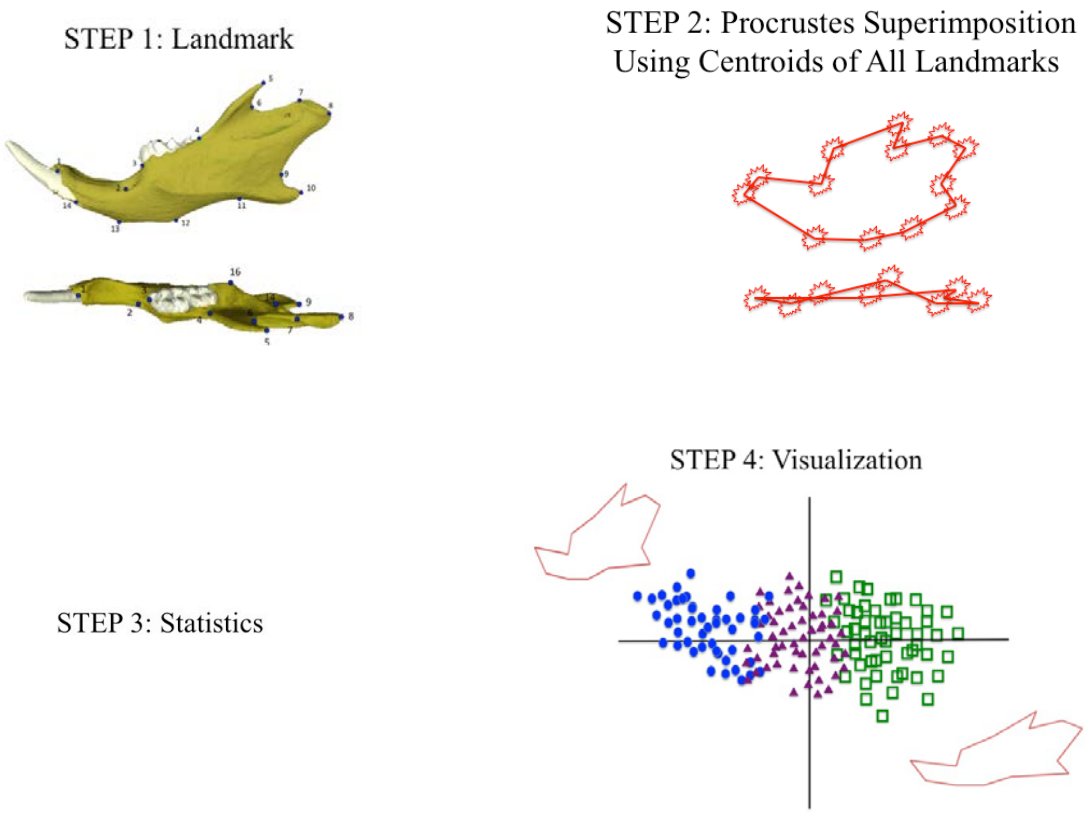

Figure 14. Visual explanation of the steps involved in geometric morphometric analysis.

2.4.1 Application of Geometric Morphometric Analysis

The landmarks defined in Amira were imported in to MorphoJ (Klingenberg 2011), a popular free program for geometric morphometric analysis. Only landmarks from the left side of the mandible were utilized for GM studies in this project, as some mandibles were misaligned during the embedding process, which could potentially introduce false interpretations of torsion between the two mandibular halves during shape analyses. Data points were evaluated first in Microsoft Excel to verify correct import of landmarks from Amira to .ascii file format. Once verified in Excel, all landmarks, qualifying variables (age, treatment, sex), and potential covariates (age) were exported as plain text (.txt) files for import in to MorphoJ. Landmarks were imported

as three-dimensional data with no object symmetry and subjected to a preliminary Procrustes fit for transformation in to tangent space (Klingenberg 2011). Preliminary transformation was conducted by aligning landmarks by principle axis for easy identification of outliers or any quality control issues with the landmark data (e.g., landmark transposition, missing landmarks: Figure 15). No data points for this project were excluded from the analysis based on outliers. Landmarks were then verified and again evaluated for outliers or potential data control issues (Figure 16). Finally, a covariance matrix was generated based on all landmarks, and qualifiers and covariates were imported for data grouping and later analysis of subsets of mandibles (see Section 3.0).

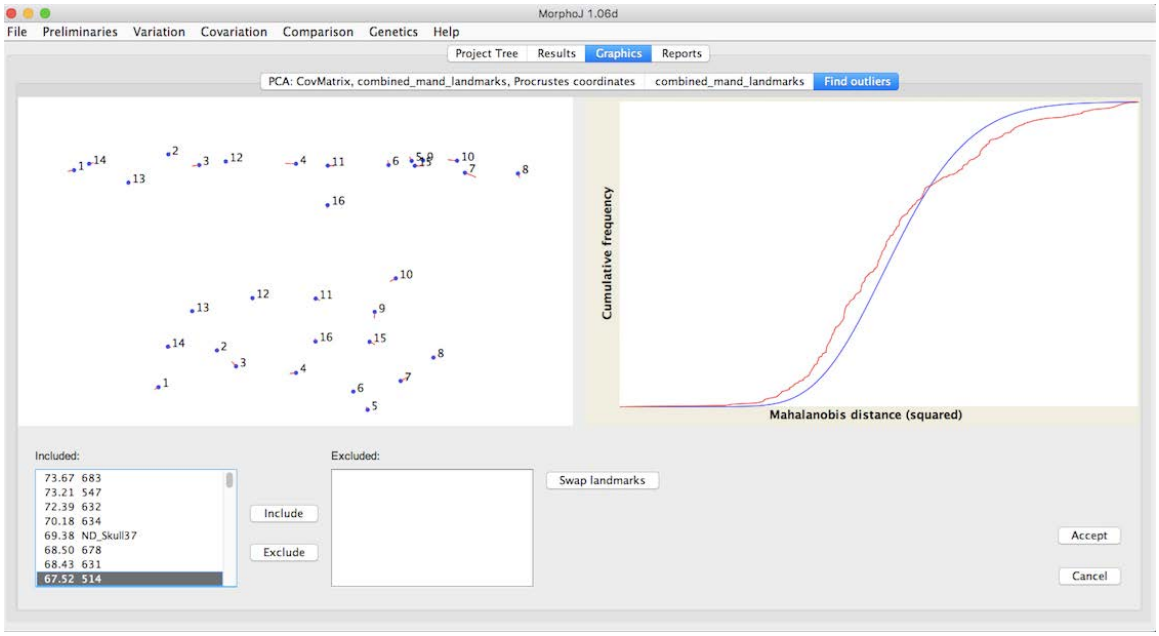

Figure 15. MorphoJ output for identification of outliers and quality control of landmark data.

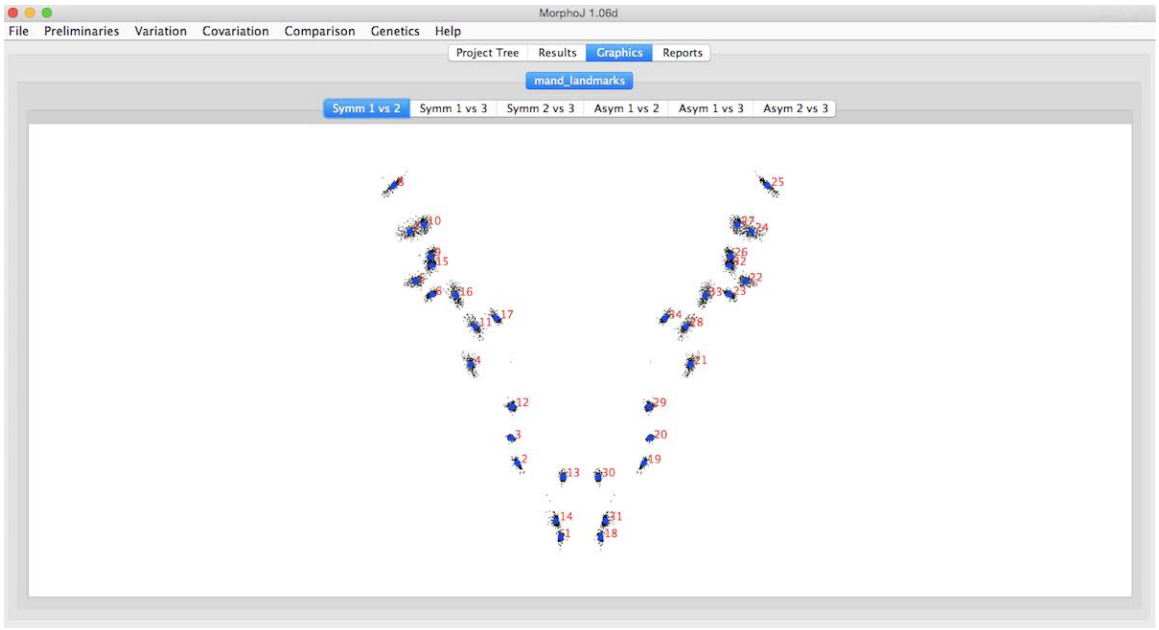

Figure 16. MorphoJ output of all landmarks (both sides of the mandible to double-check for swapped landmarks) prior to data grouping using qualifier variables of age and dosage.

Once all landmark data were imported and fit using Procrustes transformation, evaluation of shape differences between ages and doses began. Wireframes were created for each age and treatment group, allowing for easier visualization of any shape changes. MorphoJ allows for various analyses, ranging from principle component analysis (PCA), analysis of variance (ANOVA) based on the Procrustes fit, matrix correlation, partial least squares (PLS), canonical variate analysis, and discriminant function analysis (Klingenberg 2011). Due to sample sizes and hypotheses, not all analyses necessarily apply; this research utilizes PCA and discriminant function analysis to evaluate any shape changes occurring in the mouse mandibles based on age and/or treatment. The full MorphoJ protocol for this dissertation is presented in Appendix C.

2.5.1.1 Principle Component Analysis

Principle component analysis is a type of multivariate analysis pioneered in the early 20th century (Hotelling 1933). With principle component analysis (PCA), variables are plotted against one another and a directionality of the correlation, or the distance along the long axis of the scatterplot, represents the first principle component (PC). This PC can be said to explain the largest portion of variation between the two groups by summing the squared distances from the line (Figure 17). While this PC explains the most variation within the plotted sample, it does not explain *all* the variation. The variation that is not explained by the first PC can be captured using a second PC, which runs perpendicular to the first PC (Figure 17). This process of PCA can be used for both two- and three-dimension data, and is one of the hallmarks of GM analysis (Zelditch et al. 2004). In three-dimensional data, the third PC will again run perpendicular to both the first and second PC's. Additional PC's can be calculated until all variation within the sample is explained, and these PC's are then used to explain variation within the sample (Claude 2008).

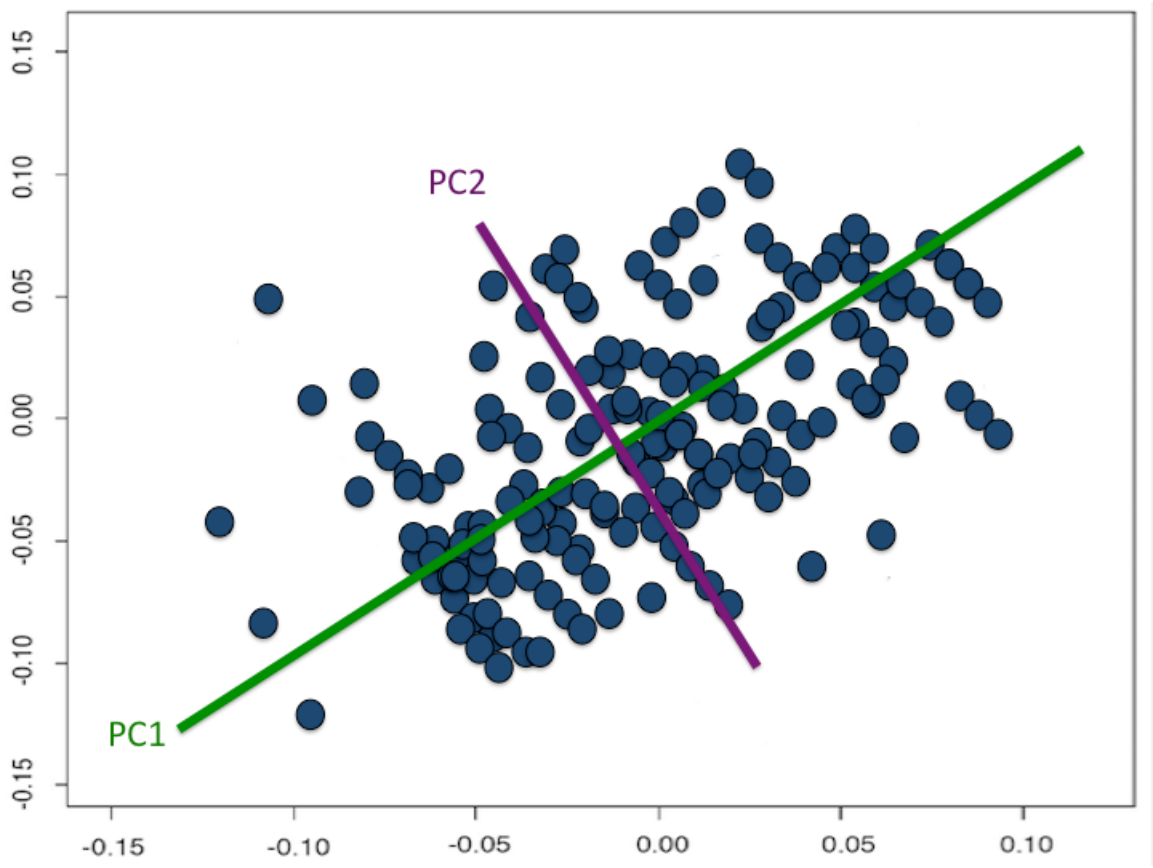

Figure 17. Visual depiction of principle component analysis, where PC1 explains the largest proportion of variation and PC2 explains the remaining variance within the population.

For this project, data were evaluated both across the whole group and within each treatment group. Eigenvalues, which are measures of the amount of variation explained by each PC, were calculated for each specimen. Principle components were then selected that explained ~90% of the variance within the group (Figure 18). These PC's can then be interpreted visually as wireframe figures, lollipop figures, or scatterplots with confidence ellipses around each group (Figure 19). This allows for interpretation of results by demonstrating the variation between PC's as an explanation of shaped changes between groups (Zelditch et al. 2004; Claude 2008; Klingenberg 2011).

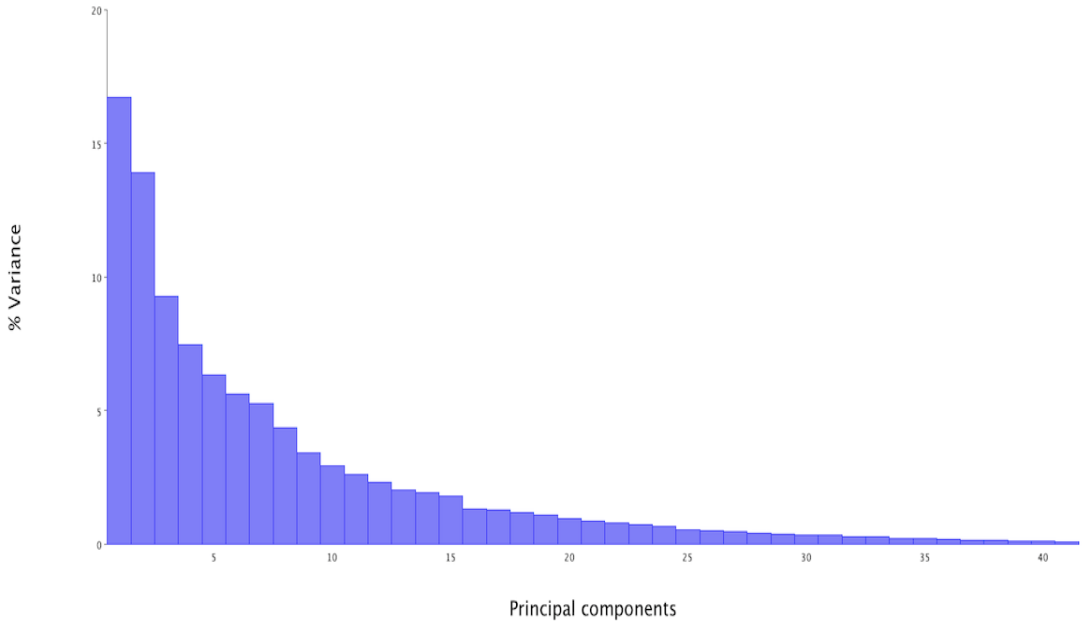

Figure 18. Sample eigenvalues showing the % of variation explained by a principle component.

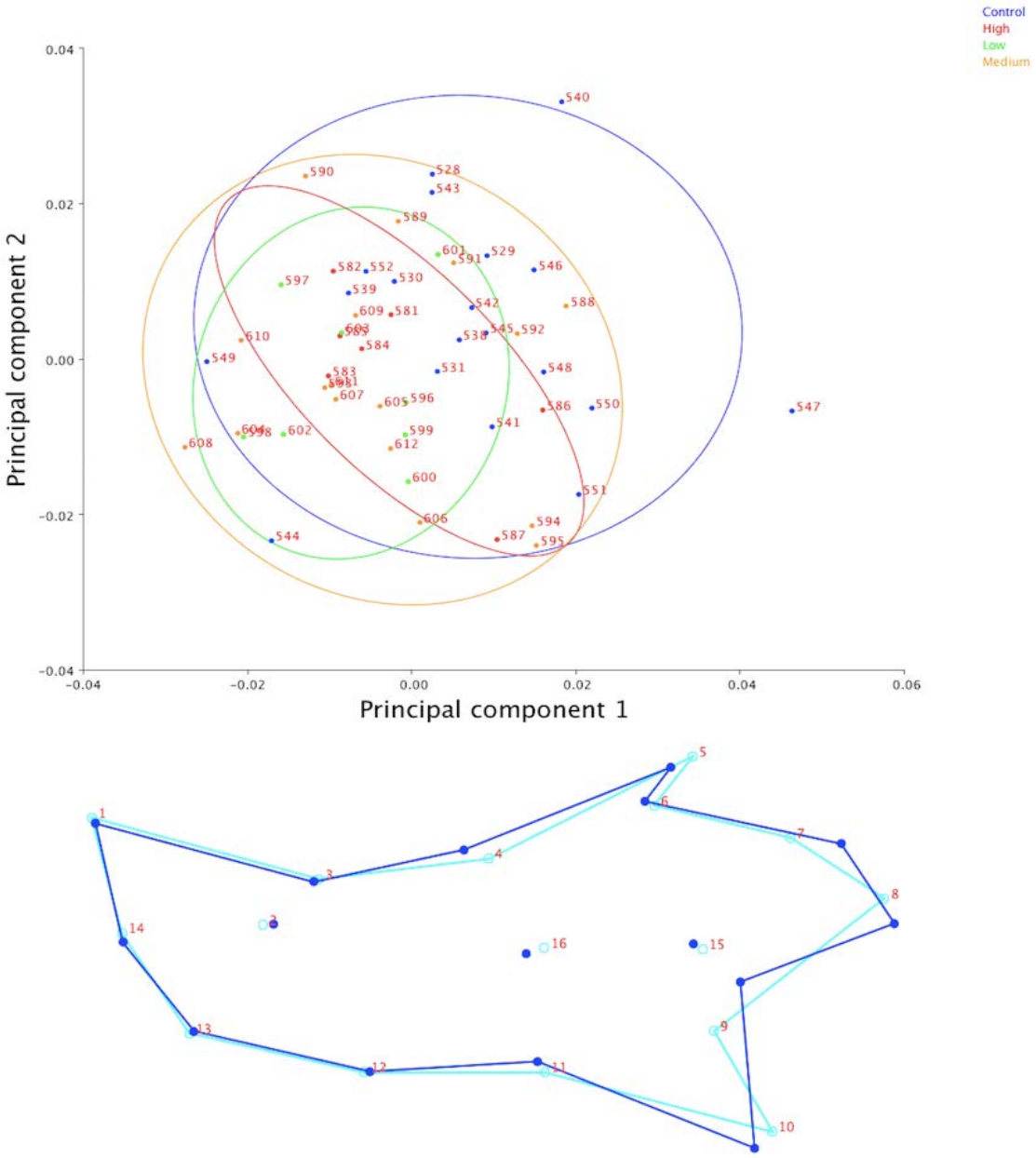

Figure 19. Sample visualizations of PCA from MorphoJ software.

2.5.1.2 Canonical Variate Analysis

Canonical variate analysis (CVA) is similar to discriminant function analysis, as it is attempts to differentiate samples in to known groups (Klingenberg 2011). Unlike discriminant function analysis, which can only be used to distinguish between two known groups, CVA allows regression in to multiple groups based on highest calculated correlation. With CVA, MorphoJ finds the axes that best discriminate between groups; these axes, called canonical variates (CV's), separate the groups based on maximum between-group variance in relation to with-in group variance in each dimension (Zelditch et al. 2004). This discrimination results in scores that are then used to differentiate between groups, including any individuals of unknown group affiliation (Zelditch et al. 2004; Claude 2008). The most intuitive aspect of CVA results are once again wireframe and scatter plots, both of which depict variation among the data in relation to the canonical variates (Figure 20). Furthermore, CV's can be used to separate the sample in to groups via scatterplots. For smaller samples such as the one used in the present study, CVA is an adequate substitute for tests predictive tests such as discriminant function analysis.

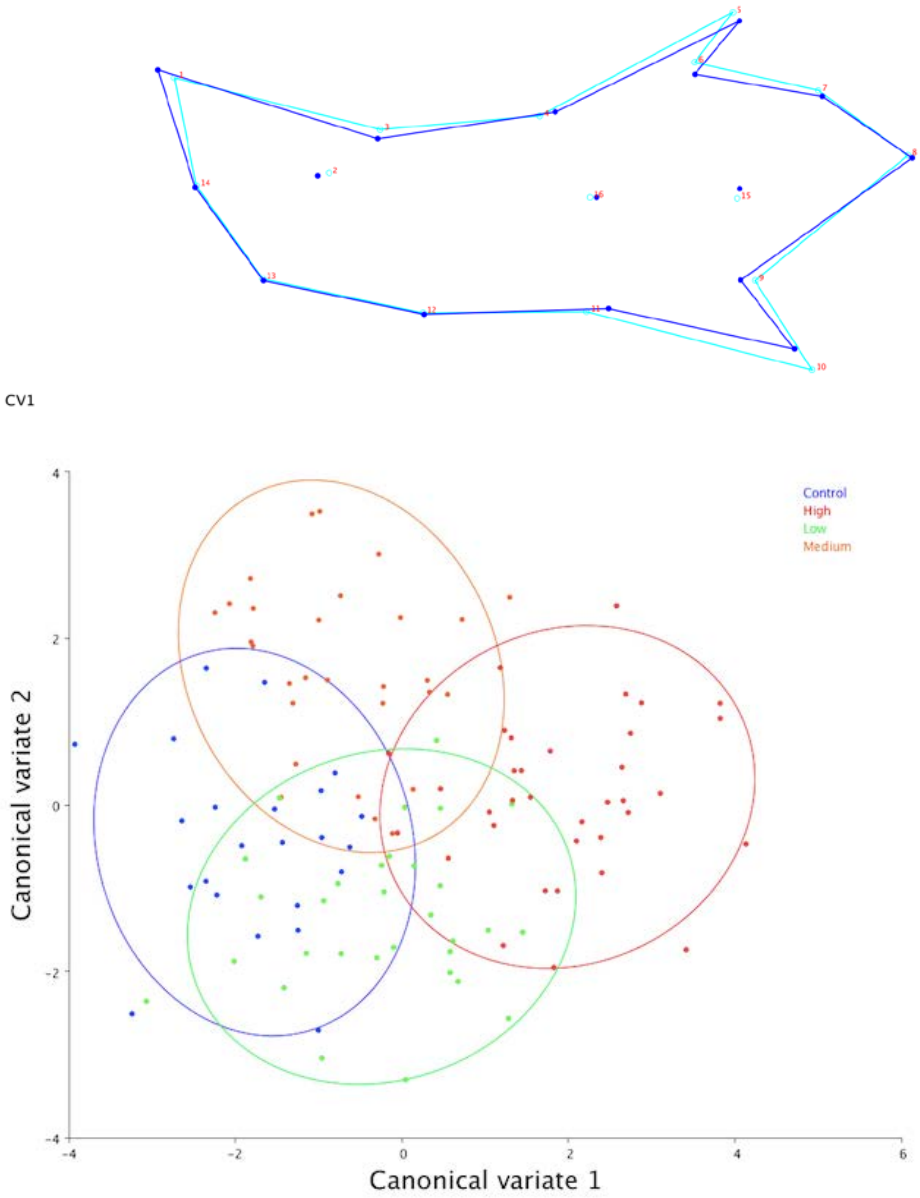

Figure 20. Sample visualizations of CVA from MorphoJ software.

2.5 DATA MANAGEMENT PROTOCOL

All data and protocol were saved on the CCDG servers for security and ease of backup. The analysis and software outputs for each test were saved, and the data master data files are also maintained on the servers. All protocols are attached as appendices, and results are presented in a manner that best display the results of the study; as such, not all analyses are presented in the results section. Further unconventional or unanticipated statistical tests and data manipulation are explained in Section 3.0 as needed. Naming protocols are detailed in protocols, and all images were exported as both .bmp and .svg outputs for visual manipulation.

3.0 RESULTS

The two methods utilized for this project, EDMA and GM, represent two separate methods of evaluating shape differences within a biological sample. While these methods are different both statistically and theoretically, they both utilize mandibular landmarks to effectively quantify the overall shape changes between age and dosage groups within the sample. It should be noted, however, that EDMA is *not* an effective method of verifying or falsifying GM results, and vice-versa. The methods are meant to complement each other and help provide a better overall picture of any shape changes occurring in the present sample.

3.1 EUCLIDEAN DISTANCE MATRIX RESULTS

3.1.1 Age-Based EDMA Results

All 16 landmarks were utilized for each of the mandibles in the study. Each sample was statistically bootstrapped (1,000 resamples) to allow for further statistical sampling utilizing a 90% confidence interval to determine statistical significance. Geometric mean of each sample was used to scale the form matrix for each sample. Additional parameters and tests not presented in the results are provided in Appendix B.

3.1.1.1 15-Day EDMA Results

A total of 28 individuals (19 low dosage and nine high dosage) were evaluated within the 15-day sample. These matrices represent the mean distance between each landmark for the two

groups. Unfortunately, due to unknown errors with the EDMA software and the dataset for this project, EDMA could not be conducted on the 15-day sample. The errors may be linked to scaling issues within the Amira software, the ability of the EDMA software to handle populations with large variance between landmark locations, or a combination of both. Contact was made with the software authors and researchers working with the rendered Amira files, but no consensus explanation could be reached. As such, the 15-day samples were not included in the EDMA analyses. As no outliers were seen in either Excel or GM analyses, it was concluded that the errors were in only the EDMA data.

3.1.1.2 20-Day EDMA Results

A total of 32 individuals were examined within the 20-day old mandibular sample (11 low dosage individuals and 21 high dosage individuals). Each linear distance for each subset was averaged across all individuals within the group to generate form matrices for the 20-day low dosage group (Table 6) and for the 20-day high dosage group (Table 7). To effectively remove size from these matrices, each value within the form matrices was again divided by the geometric mean of each sample (107.81 for the low dosage group, 108.78 for the high dosage group) to produce two new shape matrices: one for the 20-day low dosage group (Table 8) and one for the 20-day high dosage group (Table 9). The omnibus test for the 20-day old sample produced a Z-statistic of 0.3365 and associated 90% confidence interval (0.1444 to 0.5648), so the null hypothesis that the shapes of the two samples are the same was disproven. The shape matrices scaled by geometric mean were then subjected to the Monte Carlo resampling (1,000 resamples) to produce a shape-difference matrix between each landmark. This new shape-difference matrix

(SDM) was also sorted, lowest to highest, based on the arithmetic difference between each landmark (Table 10), and the 20 lowest and 20 highest of the group were plotted (Figure 21).

Within the 20-day sample, 15 linear distances rejected the null hypotheses of both groups having the same shape by having 90% confidence intervals that did not contain zero (Table 10). Fourteen of these involved Landmark 1 (anterior superior incisor alveolar rim). More specifically, the shape differences involving the position of the superior aspect of the alveolus at the incisor was significantly different in regards to every landmark with the exception of Landmark 13 (most inferior point along the mandibular symphysis; Table 10). Finally, the linear distance between Landmarks 5 and 6 (apex of the coronoid process and posterior base of the coronoid process), suggesting shape changes in this region (Figure 22). Shape changes were not significant in other posterior aspects of the mandible, specifically the condyle or mandibular angle.

Table 6. Mean form matrix for the 20-day low dose sample.

	L1	*L2*	*L3*	*L4*	*L5*	*L6*	*L7*	*L8*	*L9*	*L10*	*L11*	*L12*	*L13*	*L14*	*L15*	*L16*
L1	0															
L2	596.31	0														
L3	580.74	22.82	0													
L4	569.00	71.67	51.05	0												
L5	542.29	137.03	115.23	66.17	0											
L6	554.37	120.71	99.68	49.05	20.34	0										
L7	558.46	156.86	136.85	85.84	35.86	39.18	0									
L8	574.50	183.50	165.04	114.83	70.03	72.03	34.37	0								
L9	606.61	136.64	123.09	81.49	81.56	66.94	61.99	63.92	0							
L10	628.62	161.51	150.50	112.64	111.11	98.30	85.48	74.26	32.47	0						
L11	616.16	94.45	86.59	64.02	102.83	82.87	99.17	111.56	50.49	68.31	0					
L12	622.70	53.02	57.84	73.18	134.44	114.59	142.16	160.88	103.05	120.81	53.32	0				
L13	619.38	39.21	59.69	102.47	168.45	150.41	183.41	206.30	152.44	171.82	103.89	51.54	0			
L14	605.87	40.70	60.88	111.60	176.04	160.45	197.06	223.85	175.74	198.87	130.73	81.72	37.12	0		
L15	586.30	130.01	113.39	66.35	57.67	43.21	42.28	55.74	24.07	55.15	57.94	105.29	151.12	170.20	0	
L16	580.10	85.98	70.36	33.73	73.54	53.49	78.98	100.77	56.51	84.98	37.68	65.52	106.23	125.12	47.54	0

Table 7. Mean form matrix for 20-day high dose sample.

	L1	*L2*	*L3*	*L4*	*L5*	*L6*	*L7*	*L8*	*L9*	*L10*	*L11*	*L12*	*L13*	*L14*	*L15*	*L16*
L1	0															
L2	573.70	0														
L3	555.28	22.32	0													
L4	541.43	71.10	52.09	0												
L5	510.86	135.35	115.04	65.26	0											
L6	522.72	120.23	100.61	49.27	18.36	0										
L7	527.88	156.80	138.48	86.44	37.95	40.93	0									
L8	545.16	183.75	167.13	115.82	72.47	74.53	34.79	0								
L9	582.62	135.97	124.71	82.19	83.18	70.51	63.35	65.41	0							
L10	607.74	162.31	153.66	114.89	114.15	103.19	87.74	76.19	33.90	0						
L11	594.46	94.79	89.07	65.32	103.48	85.75	99.89	112.23	49.80	68.86	0					
L12	603.27	53.08	59.62	74.00	134.43	116.45	143.14	162.03	102.89	121.86	54.01	0				
L13	600.67	41.42	60.84	104.04	169.22	152.62	185.47	208.67	153.90	174.56	106.12	53.55	0			
L14	585.79	42.11	60.63	112.20	175.64	161.13	198.23	225.30	176.17	200.61	131.91	82.25	36.79	0		
L15	559.19	129.81	115.13	66.81	58.01	45.66	42.09	56.01	25.42	57.60	58.74	106.23	153.29	171.23	0	
L16	552.76	87.13	72.82	36.53	74.97	57.07	80.39	102.40	59.74	89.21	42.02	68.51	108.21	126.44	50.54	0

Table 8. Mean shape matrix for the 20-day low dose sample.

	L1	*L2*	*L3*	*L4*	*L5*	*L6*	*L7*	*L8*	*L9*	*L10*	*L11*	*L12*	*L13*	*L14*	*L15*	*L16*
L1	0															
L2	5.531	0														
L3	5.386	0.212	0													
L4	5.278	0.665	0.474	0												
L5	5.030	1.271	1.069	0.614	0											
L6	5.142	1.120	0.925	0.455	0.189	0										
L7	5.180	1.455	1.269	0.796	0.333	0.363	0									
L8	5.329	1.702	1.531	1.065	0.650	0.668	0.319	0								
L9	5.626	1.267	1.142	0.756	0.757	0.621	0.575	0.593	0							
L10	5.831	1.498	1.396	1.045	1.031	0.912	0.793	0.689	0.301	0						
L11	5.715	0.876	0.803	0.594	0.954	0.769	0.920	1.035	0.468	0.634	0					
L12	5.776	0.492	0.536	0.679	1.247	1.063	1.319	1.492	0.956	1.121	0.495	0				
L13	5.745	0.364	0.554	0.950	1.562	1.395	1.701	1.913	1.414	1.594	0.964	0.478	0			
L14	5.620	0.377	0.565	1.035	1.633	1.488	1.828	2.076	1.630	1.845	1.213	0.758	0.344	0		
L15	5.438	1.206	1.052	0.615	0.535	0.401	0.392	0.517	0.223	0.511	0.537	0.977	1.402	1.579	0	
L16	5.381	0.797	0.653	0.313	0.682	0.496	0.733	0.935	0.524	0.788	0.349	0.608	0.985	1.161	0.441	0

Table 9. Mean shape matrix for the 20-day high dose sample.

	L1	*L2*	*L3*	*L4*	*L5*	*L6*	*L7*	*L8*	*L9*	*L10*	*L11*	*L12*	*L13*	*L14*	*L15*	*L16*
L1	0															
L2	5.274	0														
L3	5.105	0.205	0													
L4	4.977	0.654	0.479	0												
L5	4.696	1.244	1.058	0.600	0											
L6	4.805	1.105	0.925	0.453	0.169	0										
L7	4.853	1.441	1.273	0.795	0.349	0.376	0									
L8	5.012	1.689	1.536	1.065	0.666	0.685	0.320	0								
L9	5.356	1.250	1.146	0.756	0.765	0.648	0.582	0.601	0							
L10	5.587	1.492	1.413	1.056	1.049	0.949	0.807	0.700	0.312	0						
L11	5.465	0.871	0.819	0.600	0.951	0.788	0.918	1.032	0.458	0.633	0					
L12	5.546	0.488	0.548	0.680	1.236	1.071	1.316	1.490	0.946	1.120	0.496	0				
L13	5.522	0.381	0.559	0.956	1.556	1.403	1.705	1.918	1.415	1.605	0.976	0.492	0			
L14	5.385	0.387	0.557	1.031	1.615	1.481	1.822	2.071	1.620	1.844	1.213	0.756	0.338	0		
L15	5.141	1.193	1.058	0.614	0.533	0.420	0.387	0.515	0.234	0.530	0.540	0.977	1.409	1.574	0	
L16	5.081	0.801	0.669	0.336	0.689	0.525	0.739	0.941	0.549	0.820	0.386	0.630	0.995	1.162	0.465	0

Table 10. Sorted shape difference matrix for the 20-day samples (low dose and high dose), with difference estimate, lower bound (LB), and upper bound (UB).

No.	*Landmarks*		*Estimate*	*LB*	*UB*	*No.*	*Landmarks*		*Estimate*	*LB*	*UB*
1	L6	L10	-0.037	-0.080	0.004	31	L2	L14	-0.010	-0.030	0.011
2	L11	L16	-0.037	-0.076	0.010	32	L13	L16	-0.009	-0.052	0.033
3	L10	L16	-0.032	-0.082	0.017	33	L8	L9	-0.008	-0.028	0.011
4	L6	L16	-0.028	-0.072	0.016	34	L5	L9	-0.008	-0.037	0.021
5	L6	L9	-0.027	-0.057	0.003	35	L6	L13	-0.008	-0.059	0.043
6	L9	L16	-0.025	-0.068	0.022	36	L6	L12	-0.008	-0.047	0.034
7	L15	L16	-0.024	-0.062	0.015	37	L13	L15	-0.008	-0.056	0.038
8	L4	L16	-0.023	-0.061	0.016	38	L7	L9	-0.007	-0.033	0.018
9	L12	L16	-0.022	-0.071	0.029	39	L5	L16	-0.007	-0.053	0.040
10	L6	L11	-0.020	-0.054	0.012	40	L4	L11	-0.007	-0.039	0.023
11	L6	L15	-0.019	-0.039	0.001	41	L8	L16	-0.007	-0.044	0.031
12	L5	L10	-0.019	-0.059	0.021	42	L3	L15	-0.007	-0.036	0.021
13	L10	L15	-0.018	-0.044	0.007	43	L7	L16	-0.006	-0.042	0.029
14	L2	L13	-0.017	-0.057	0.020	44	L4	L13	-0.006	-0.053	0.037
15	L6	L8	-0.017	-0.042	0.008	45	L3	L13	-0.006	-0.049	0.034
16	L3	L16	-0.017	-0.056	0.023	46	L3	L8	-0.006	-0.041	0.028
17	L5	L8	-0.017	-0.043	0.010	47	L3	L4	-0.005	-0.021	0.010
18	L3	L10	-0.017	-0.065	0.027	48	L8	L13	-0.005	-0.057	0.046
19	L5	L7	-0.016	-0.037	0.005	49	L3	L9	-0.005	-0.043	0.031
20	L3	L11	-0.016	-0.052	0.020	50	L7	L13	-0.004	-0.054	0.044
21	L12	L13	-0.014	-0.038	0.010	51	L3	L7	-0.004	-0.032	0.023
22	L7	L10	-0.014	-0.047	0.021	52	L2	L16	-0.004	-0.053	0.046
23	L6	L7	-0.013	-0.032	0.006	53	L11	L15	-0.003	-0.026	0.021
24	L11	L13	-0.012	-0.046	0.023	54	L11	L12	-0.002	-0.025	0.018
25	L8	L10	-0.012	-0.039	0.014	55	L14	L16	-0.002	-0.055	0.048
26	L3	L12	-0.012	-0.047	0.025	56	L4	L12	-0.002	-0.040	0.037
27	L4	L10	-0.011	-0.052	0.030	57	L7	L8	-0.001	-0.017	0.014
28	L10	L13	-0.011	-0.067	0.036	58	L9	L13	-0.001	-0.048	0.042
29	L9	L10	-0.011	-0.025	0.003	59	L3	L6	0.000	-0.021	0.019
30	L9	L15	-0.010	-0.026	0.006	60	L11	L14	0.000	-0.038	0.037

Table 10 (*continued*). Sorted shape difference matrix for the 20-day samples (low dose and high dose), with difference estimate, lower bound (LB), and upper bound (UB).

No.	*Landmarks*		*Estimate*	*LB*	*UB*	*No.*	*Landmarks*		*Estimate*	*LB*	*UB*
61	L12	L15	0.000	-0.034	0.034	91	L9	L12	0.010	-0.019	0.038
62	L4	L9	0.000	-0.031	0.030	92	L9	L11	0.010	-0.011	0.030
63	L4	L8	0.000	-0.027	0.027	93	L9	L14	0.010	-0.036	0.054
64	L10	L12	0.000	-0.031	0.030	94	L5	L12	0.011	-0.031	0.053
65	L10	L14	0.000	-0.053	0.051	95	L2	L4	0.011	-0.013	0.036
66	L10	L11	0.001	-0.024	0.025	96	L3	L5	0.011	-0.011	0.032
67	L4	L15	0.001	-0.021	0.021	97	L2	L15	0.013	-0.021	0.044
68	L7	L11	0.002	-0.029	0.032	98	L2	L8	0.013	-0.028	0.051
69	L4	L7	0.002	-0.019	0.022	99	L2	L7	0.013	-0.025	0.048
70	L5	L15	0.002	-0.019	0.023	100	L4	L5	0.014	-0.004	0.031
71	L12	L14	0.002	-0.026	0.029	101	L2	L6	0.014	-0.024	0.045
72	L4	L6	0.002	-0.013	0.017	102	L2	L9	0.017	-0.018	0.051
73	L8	L15	0.002	-0.011	0.016	103	L5	L14	0.018	-0.025	0.062
74	L5	L11	0.002	-0.034	0.035	**104**	**L5**	**L6**	**0.020**	**0.009**	**0.030**
75	L7	L12	0.003	-0.038	0.043	105	L2	L5	0.027	-0.003	0.055
76	L8	L12	0.003	-0.034	0.043	106	L1	L13	0.223	-0.003	0.467
77	L8	L11	0.003	-0.026	0.033	**107**	**L1**	**L12**	**0.230**	**0.005**	**0.477**
78	L4	L14	0.004	-0.031	0.038	**108**	**L1**	**L14**	**0.234**	**0.011**	**0.473**
79	L2	L12	0.004	-0.025	0.031	**109**	**L1**	**L10**	**0.244**	**0.008**	**0.479**
80	L14	L15	0.005	-0.040	0.047	**110**	**L1**	**L11**	**0.250**	**0.029**	**0.490**
81	L2	L11	0.005	-0.028	0.037	**111**	**L1**	**L2**	**0.257**	**0.043**	**0.493**
82	L8	L14	0.005	-0.048	0.054	**112**	**L1**	**L9**	**0.270**	**0.044**	**0.500**
83	L7	L15	0.005	-0.010	0.020	**113**	**L1**	**L3**	**0.282**	**0.071**	**0.514**
84	L7	L14	0.005	-0.040	0.050	**114**	**L1**	**L15**	**0.297**	**0.081**	**0.522**
85	L2	L10	0.006	-0.038	0.048	**115**	**L1**	**L16**	**0.299**	**0.085**	**0.532**
86	L13	L14	0.006	-0.022	0.032	**116**	**L1**	**L4**	**0.300**	**0.092**	**0.525**
87	L2	L3	0.006	-0.012	0.026	**117**	**L1**	**L8**	**0.317**	**0.097**	**0.541**
88	L5	L13	0.007	-0.047	0.058	**118**	**L1**	**L7**	**0.327**	**0.116**	**0.550**
89	L6	L14	0.007	-0.034	0.050	**119**	**L1**	**L5**	**0.333**	**0.123**	**0.556**
90	L3	L14	0.007	-0.008	0.035	**120**	**L1**	**L6**	**0.337**	**0.128**	**0.561**

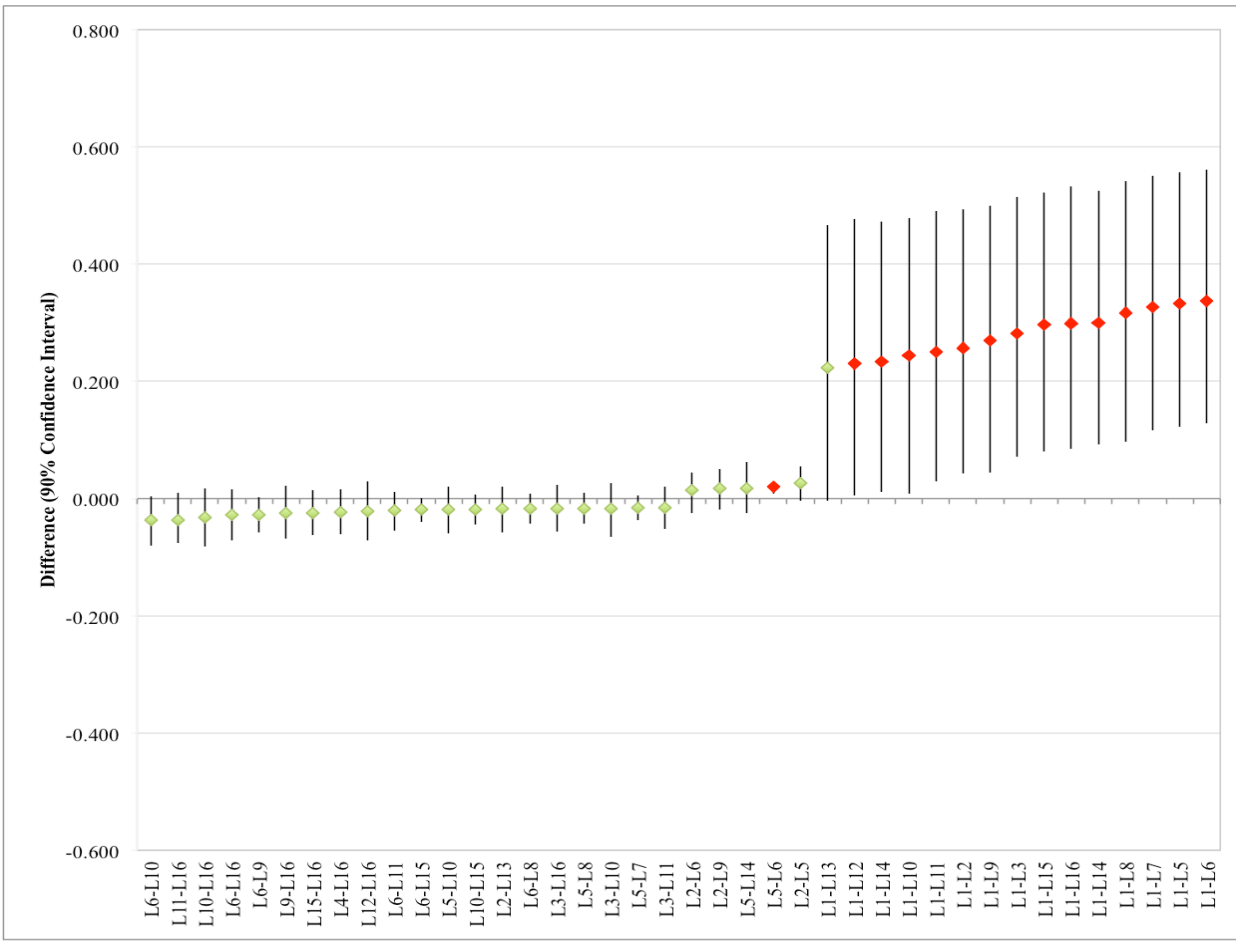

Figure 21. High and low subsets of scaled linear distances for 20-day low and high dose samples. The 20 lowest (left half of the diagram) and 20 highest (right half of the diagram) represent the 40 tails of scaled linear distances between landmarks with associated 90% confidence interval (bootstrapping with 1,000 resampled). Significantly different landmarks between the two samples (CI's do not include zero) are shown in red.

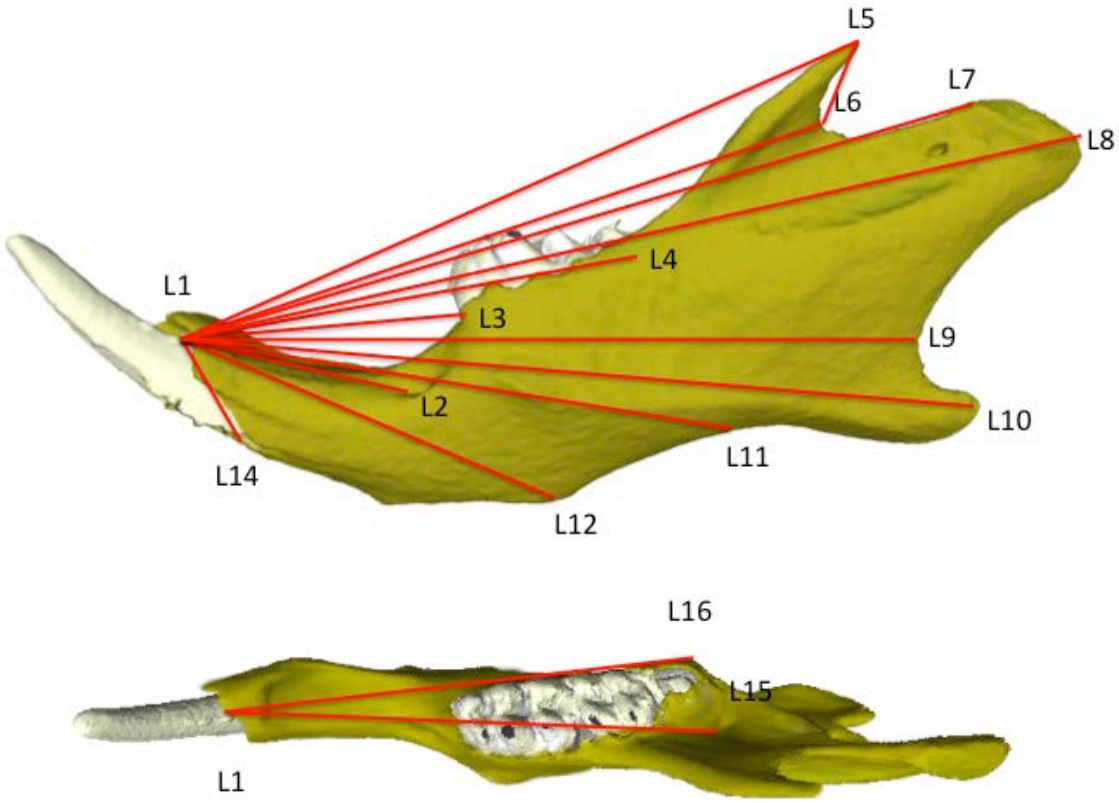

Figure 22. Significant shape changes in the EDMA results between the 20-day low dosage and 20-day high dosage samples. Red lines indicate a significant (p< 0.10) increase in size, and blue lines indicate a significant (p< 0.10) decrease in size.

3.1.1.3 25-Day EDMA Results

Due to high variance within the population likely tied to AMIRA filters and rendering outputs of the micro-CT scans, EDMA was not possible on the 25-day low dosage group. In lieu of these data, the 25day control sample was compared to the 25-day high dosage group to determine and shape differences between the untreated sample and the population with the highest dosage. A total of 58 individuals were evaluated within the 25-day old sample (23 control specimens and 35 high dosage individuals). Similar to the 20-day samples, linear distance for each subset was averaged across all individuals within the group to create form matrices for the 25-day

control group (Table 11) and for the 25-day high dosage group (Table 12). Each matrix was again divided by the geometric mean of each sample (112.88 for the control group, 112.18 for the high dosage group) to produce two new shape matrices: one for the 25-day control group (Table 13) and one for the 25-day high dosage group (Table 14). The omnibus test for the 25-day old sample produced a Z-statistic of 0.43995 and associated 90% confidence interval (0.2029 to 0.66977), so the null hypotheses that the two sample shapes are the same was rejected. The shape matrices were then subjected to Monte Carlo resampling (1,000 resamples) to produce a shape-difference matrix between each landmark. This new shape-difference matrix (SDM) was sorted, lowest to highest, based on the arithmetic difference between each landmark (Table 15), and the 20 lowest and 20 highest of the group were plotted (Figure 23).

Within the 25-day sample, nearly one third of the entire set of linear distances (n=120) was significantly different between the control group and the high dosage group, with 35 linear measurements having confidence intervals not containing zero (Table 15). Landmarks 2, 10, and 11 (anterior edge of mental foramen, posterior tip of mandibular angle, and most superior point of the inferior border of the mandibular angle) were represented the most in the sorted linear distance estimate table, suggesting shape changes in these regions. Landmark 10 has 10 significantly different linear metrics between the two samples, while Landmarks 2 and 11 both have seven (Figure 23). Other shape changes are seen in nearly every other aspect of the mandible, including the coronoid process, condyle, inferior margin, and alveolus (Figure 24). Interestingly, Landmark 1 *did not* have any significant shape differences between the control and high dose samples; this can be explained either by issues arising from the EDMA complications and data compilation, or from shape changes appearing at different ages within the sample. These arguments are explored further in the discussion section of this dissertation.

Table 11. Mean form matrix for the 25-day control sample.

	L1	*L2*	*L3*	*L4*	*L5*	*L6*	*L7*	*L8*	*L9*	*L10*	*L11*	*L12*	*L13*	*L14*	*L15*	*L16*
L1	0															
L2	578.04	0														
L3	559.46	22.10	0													
L4	547.44	69.44	51.12	0												
L5	511.50	139.89	119.91	71.51	0											
L6	526.18	123.42	104.27	54.06	20.48	0										
L7	532.00	161.35	143.43	92.43	38.86	41.75	0									
L8	553.03	188.29	172.22	121.71	74.56	75.95	36.00	0								
L9	592.22	143.61	132.87	89.87	88.35	74.23	66.10	64.57	0							
L10	620.92	170.97	162.89	123.48	121.07	108.68	93.01	78.06	35.36	0						
L11	603.86	93.82	89.10	65.63	109.41	89.31	106.39	118.49	58.50	78.93	0					
L12	612.25	54.82	61.95	74.26	140.45	120.51	148.76	166.99	110.14	129.94	52.19	0				
L13	609.43	44.04	63.07	104.42	175.70	157.44	191.64	214.47	162.10	183.63	105.17	54.58	0			
L14	592.44	44.54	62.87	113.21	182.78	166.94	205.26	232.21	185.68	210.90	132.18	84.36	38.15	0		
L15	566.79	132.60	118.54	70.63	61.39	46.79	45.12	57.94	27.52	62.14	62.63	109.22	157.14	176.21	0	
L16	562.01	88.60	75.04	39.06	79.82	59.84	84.71	106.30	65.41	96.27	42.35	69.94	110.22	129.85	52.50	0

Table 12. Mean form matrix for the 25-day high dose sample.

	L1	*L2*	*L3*	*L4*	*L5*	*L6*	*L7*	*L8*	*L9*	*L10*	*L11*	*L12*	*L13*	*L14*	*L15*	*L16*
L1	0															
L2	575.07	0														
L3	556.56	22.22	0													
L4	540.70	71.94	52.77	0												
L5	505.25	140.63	120.15	69.64	0											
L6	519.38	123.32	103.56	51.44	20.98	0										
L7	522.10	160.73	142.06	89.41	37.51	41.11	0									
L8	539.56	187.63	170.64	118.75	72.69	74.95	35.48	0								
L9	578.99	141.20	129.29	85.99	86.11	71.78	64.87	65.01	0							
L10	602.59	167.07	157.52	117.72	115.80	103.46	88.54	75.37	32.89	0						
L11	592.03	96.02	89.43	65.19	106.42	86.05	102.19	114.29	53.02	72.43	0					
L12	603.79	54.76	60.36	74.69	139.11	118.53	146.39	164.82	106.67	125.53	54.18	0				
L13	603.81	42.30	61.35	104.99	174.44	155.39	189.11	211.95	158.02	178.45	106.50	53.76	0			
L14	589.99	42.70	61.64	113.87	181.77	165.05	202.81	229.71	181.58	205.56	133.27	83.63	37.71	0		
L15	554.43	132.45	117.15	67.97	58.67	44.27	42.81	56.89	27.75	59.29	60.23	108.29	155.53	174.33	0	
L16	551.82	88.63	73.89	37.03	78.02	57.47	82.44	104.23	61.71	90.72	40.65	68.77	109.35	128.54	50.74	0

Table 13. Mean shape matrix for the 25-day control sample.

	L1	*L2*	*L3*	*L4*	*L5*	*L6*	*L7*	*L8*	*L9*	*L10*	*L11*	*L12*	*L13*	*L14*	*L15*	*L16*
L1	0															
L2	5.121	0														
L3	4.956	0.196	0													
L4	4.850	0.615	0.453	0												
L5	4.531	1.239	1.062	0.634	0											
L6	4.661	1.093	0.924	0.479	0.181	0										
L7	4.713	1.429	1.271	0.819	0.344	0.370	0									
L8	4.899	1.668	1.526	1.078	0.661	0.673	0.319	0								
L9	5.246	1.272	1.177	0.796	0.783	0.658	0.586	0.572	0							
L10	5.501	1.515	1.443	1.094	1.073	0.963	0.824	0.691	0.313	0						
L11	5.349	0.831	0.789	0.581	0.969	0.791	0.943	1.050	0.518	0.699	0					
L12	5.424	0.486	0.549	0.658	1.244	1.068	1.318	1.479	0.976	1.151	0.462	0				
L13	5.399	0.390	0.559	0.925	1.556	1.395	1.698	1.900	1.436	1.627	0.932	0.484	0			
L14	5.248	0.395	0.557	1.003	1.619	1.479	1.818	2.057	1.645	1.868	1.171	0.747	0.338	0.000		
L15	5.021	1.175	1.050	0.626	0.544	0.415	0.400	0.513	0.244	0.550	0.555	0.968	1.392	1.561	0	
L16	4.979	0.785	0.665	0.346	0.707	0.530	0.750	0.942	0.579	0.853	0.375	0.620	0.976	1.150	0.465	0

Table 14. Mean shape matrix for the 25-day high dose sample.

	L1	*L2*	*L3*	*L4*	*L5*	*L6*	*L7*	*L8*	*L9*	*L10*	*L11*	*L12*	*L13*	*L14*	*L15*	*L16*
L1	0															
L2	5.197	0														
L3	5.029	0.201	0													
L4	4.886	0.650	0.477	0												
L5	4.566	1.271	1.086	0.629	0											
L6	4.693	1.114	0.936	0.465	0.190	0										
L7	4.718	1.452	1.284	0.808	0.339	0.371	0									
L8	4.876	1.695	1.542	1.073	0.657	0.677	0.321	0								
L9	5.232	1.276	1.168	0.777	0.778	0.649	0.586	0.587	0							
L10	5.445	1.510	1.423	1.064	1.046	0.935	0.800	0.681	0.297	0						
L11	5.350	0.868	0.808	0.589	0.962	0.778	0.923	1.033	0.479	0.655	0					
L12	5.456	0.495	0.545	0.675	1.257	1.071	1.323	1.489	0.964	1.134	0.490	0				
L13	5.456	0.382	0.554	0.949	1.576	1.404	1.709	1.915	1.428	1.613	0.962	0.486	0			
L14	5.331	0.386	0.557	1.029	1.643	1.491	1.833	2.076	1.641	1.858	1.204	0.756	0.341	0		
L15	5.010	1.197	1.059	0.614	0.530	0.400	0.387	0.514	0.251	0.536	0.544	0.979	1.405	1.575	0	
L16	4.986	0.801	0.668	0.335	0.705	0.519	0.745	0.942	0.558	0.820	0.367	0.621	0.988	1.162	0.458	0

Table 15. Sorted shape difference matrix for the 25-day samples (control and high dose), with difference estimate, lower bound (LB), and upper bound (UB).

No.	*Landmarks*		*Estimate*	*LB*	*UB*	*No.*	*Landmarks*		*Estimate*	*LB*	*UB*
1	L1	L14	-0.083	-0.265	0.101	31	L8	L13	-0.015	-0.032	0.002
2	L1	L2	-0.076	-0.254	0.104	32	L7	L14	-0.014	-0.036	0.009
3	L1	L3	-0.073	-0.251	0.109	33	L14	L15	-0.014	-0.030	0.002
4	L1	L13	-0.057	-0.235	0.115	34	L13	L15	-0.013	-0.028	0.001
5	**L2**	**L11**	**-0.037**	**-0.051**	**-0.022**	35	L3	L7	-0.013	-0.031	0.005
6	L1	L4	-0.036	-0.215	0.145	36	L5	L12	-0.013	-0.032	0.007
7	**L2**	**L4**	**-0.035**	**-0.046**	**-0.024**	37	L6	L14	-0.013	-0.029	0.006
8	L1	L5	-0.034	-0.219	0.152	38	L3	L6	-0.012	-0.024	0.002
9	**L11**	**L14**	**-0.033**	**-0.053**	**-0.014**	39	L13	L16	-0.012	-0.029	0.004
10	L1	L12	-0.032	-0.210	0.147	40	L14	L16	-0.011	-0.037	0.014
11	L1	L6	-0.032	-0.217	0.149	41	L7	L13	-0.011	-0.031	0.009
12	**L2**	**L5**	**-0.032**	**-0.048**	**-0.015**	42	L12	L15	-0.011	-0.023	0.001
13	**L11**	**L13**	**-0.031**	**-0.047**	**-0.014**	43	L8	L12	-0.010	-0.027	0.008
14	**L2**	**L8**	**-0.027**	**-0.045**	**-0.010**	44	L6	L13	-0.009	-0.027	0.010
15	**L11**	**L12**	**-0.027**	**-0.039**	**-0.016**	45	L2	L12	-0.009	-0.022	0.004
16	**L4**	**L14**	**-0.026**	**-0.038**	**-0.014**	46	L3	L15	-0.008	-0.020	0.002
17	**L3**	**L4**	**-0.024**	**-0.033**	**-0.015**	47	L12	L14	-0.008	-0.026	0.009
18	**L4**	**L13**	**-0.024**	**-0.038**	**-0.010**	48	L5	L6	-0.008	-0.017	0.000
19	**L3**	**L5**	**-0.023**	**-0.037**	**-0.008**	49	L1	L16	-0.008	-0.182	0.172
20	**L5**	**L14**	**-0.023**	**-0.042**	**-0.004**	50	L4	L11	-0.008	-0.021	0.006
21	**L2**	**L7**	**-0.023**	**-0.042**	**-0.004**	51	L9	L15	-0.007	-0.017	0.003
22	**L2**	**L15**	**-0.022**	**-0.035**	**-0.009**	52	L7	L12	-0.005	-0.024	0.013
23	**L2**	**L6**	**-0.021**	**-0.035**	**-0.006**	53	L1	L7	-0.005	-0.187	0.173
24	L5	L13	-0.020	-0.040	0.001	54	L2	L3	-0.005	-0.013	0.003
25	**L3**	**L11**	**-0.019**	**-0.032**	**-0.005**	55	L6	L8	-0.004	-0.019	0.009
26	L8	L14	-0.019	-0.038	0.001	56	L2	L9	-0.004	-0.018	0.010
27	**L4**	**L12**	**-0.017**	**-0.032**	**-0.001**	57	L6	L12	-0.003	-0.020	0.014
28	L3	L8	-0.016	-0.033	0.000	58	L3	L16	-0.003	-0.022	0.016
29	L2	L16	-0.016	-0.039	0.007	59	L13	L14	-0.003	-0.019	0.012
30	**L8**	**L9**	**-0.015**	**-0.030**	**-0.001**	60	L12	L13	-0.002	-0.014	0.009

Table 15 (*continued*). Sorted shape difference matrix for the 25-day samples (control and high dose), with difference estimate, lower bound (LB), and upper bound (UB).

No.	*Landmarks*		*Estimate*	*LB*	*UB*	*No.*	*Landmarks*		*Estimate*	*LB*	*UB*
61	L12	L16	-0.002	-0.023	0.018	91	L10	L14	0.011	-0.011	0.031
62	L7	L8	-0.002	-0.013	0.011	92	L4	L7	0.011	-0.008	0.029
63	L6	L7	-0.002	-0.015	0.012	93	L1	L15	0.011	-0.168	0.188
64	L8	L15	-0.001	-0.012	0.010	94	L4	L16	0.011	-0.009	0.032
65	L7	L9	-0.001	-0.017	0.017	95	L4	L15	0.011	-0.001	0.023
66	L1	L11	0.000	-0.179	0.176	**96**	**L9**	**L12**	**0.012**	**0.002**	**0.023**
67	L8	L16	0.000	-0.021	0.021	**97**	**L7**	**L15**	**0.013**	**0.001**	**0.026**
68	L3	L14	0.000	-0.010	0.011	98	L6	L11	0.014	-0.003	0.031
69	L5	L16	0.002	-0.020	0.027	99	L5	L15	0.014	-0.001	0.028
70	L3	L12	0.003	-0.010	0.016	**100**	**L4**	**L6**	**0.014**	**0.001**	**0.028**
71	L5	L8	0.004	-0.013	0.019	101	L10	L13	0.014	-0.005	0.033
72	L9	L14	0.004	-0.015	0.022	102	L1	L9	0.014	-0.163	0.189
73	L4	L5	0.004	-0.012	0.021	**103**	**L6**	**L15**	**0.015**	**0.002**	**0.026**
74	L3	L13	0.004	-0.006	0.015	**104**	**L10**	**L15**	**0.015**	**0.000**	**0.029**
75	L5	L9	0.005	-0.016	0.024	**105**	**L9**	**L10**	**0.016**	**0.004**	**0.027**
76	L2	L10	0.005	-0.014	0.023	**106**	**L10**	**L12**	**0.017**	**0.001**	**0.032**
77	L4	L8	0.005	-0.012	0.021	107	L8	L11	0.017	-0.002	0.035
78	L5	L7	0.005	-0.009	0.018	**108**	**L4**	**L9**	**0.019**	**0.002**	**0.035**
79	L7	L16	0.005	-0.014	0.026	109	L7	L11	0.019	-0.001	0.037
80	L15	L16	0.007	-0.014	0.026	**110**	**L3**	**L10**	**0.020**	**0.001**	**0.038**
81	L5	L11	0.007	-0.012	0.027	**111**	**L9**	**L16**	**0.022**	**0.000**	**0.040**
82	L2	L13	0.008	-0.004	0.020	112	L1	L8	0.023	-0.162	0.202
83	L11	L16	0.008	-0.015	0.029	**113**	**L7**	**L10**	**0.024**	**0.002**	**0.044**
84	L9	L13	0.008	-0.006	0.022	**114**	**L5**	**L10**	**0.026**	**0.001**	**0.049**
85	L2	L14	0.009	-0.002	0.020	**115**	**L6**	**L10**	**0.028**	**0.005**	**0.049**
86	L3	L9	0.009	-0.005	0.023	**116**	**L4**	**L10**	**0.030**	**0.009**	**0.050**
87	L6	L9	0.009	-0.009	0.026	**117**	**L10**	**L16**	**0.033**	**0.006**	**0.057**
88	L8	L10	0.010	-0.006	0.027	**118**	**L9**	**L11**	**0.039**	**0.026**	**0.053**
89	L11	L15	0.011	-0.002	0.024	**119**	**L10**	**L11**	**0.045**	**0.026**	**0.062**
90	L6	L16	0.011	-0.009	0.032	120	L1	L10	0.055	-0.118	0.227

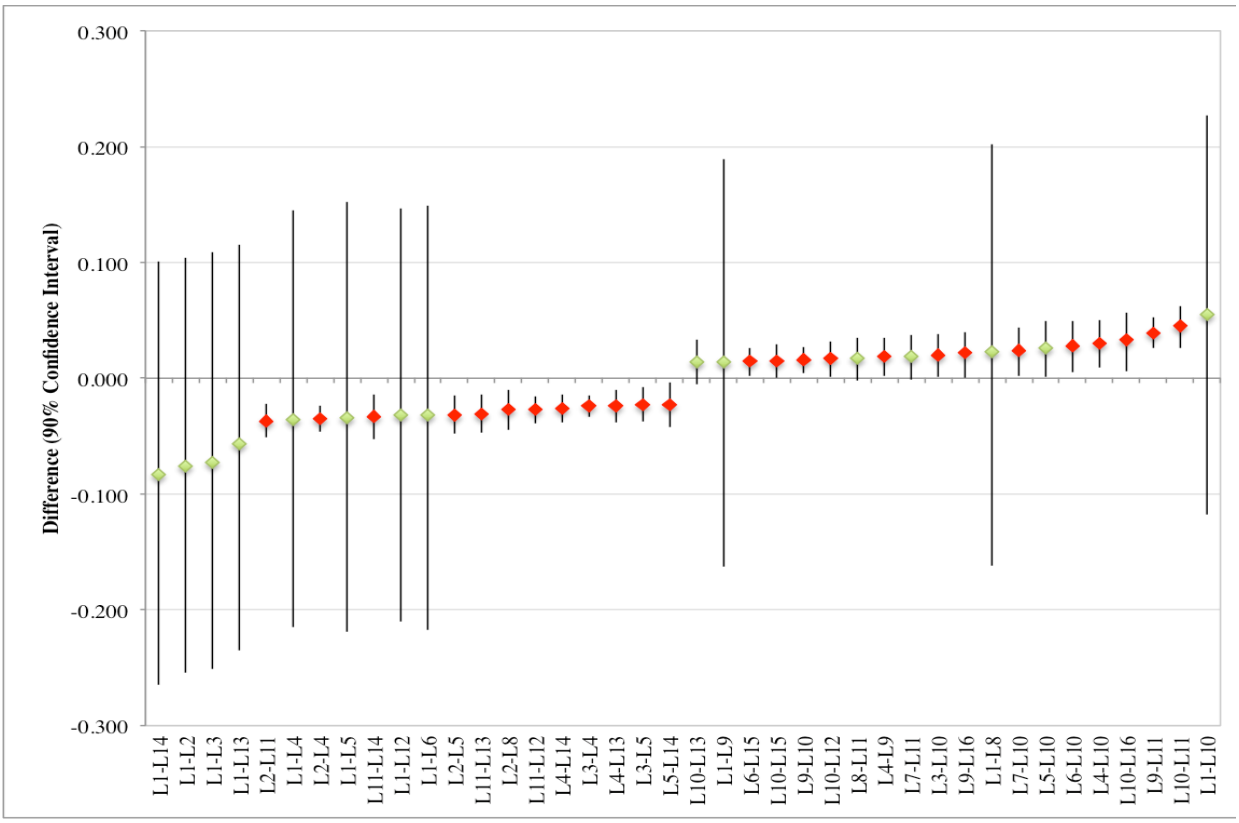

Figure 23. High and low subsets of scaled linear distances for 25-day control and high dose samples. The 20 lowest (left half of the diagram) and 20 highest (right half of the diagram) represent the 40 tails of scaled linear distances between landmarks with associated 90% confidence interval (bootstrapping with 1,000 resampled). Significantly different landmarks between the two samples (CI's do not include zero) are shown in red.

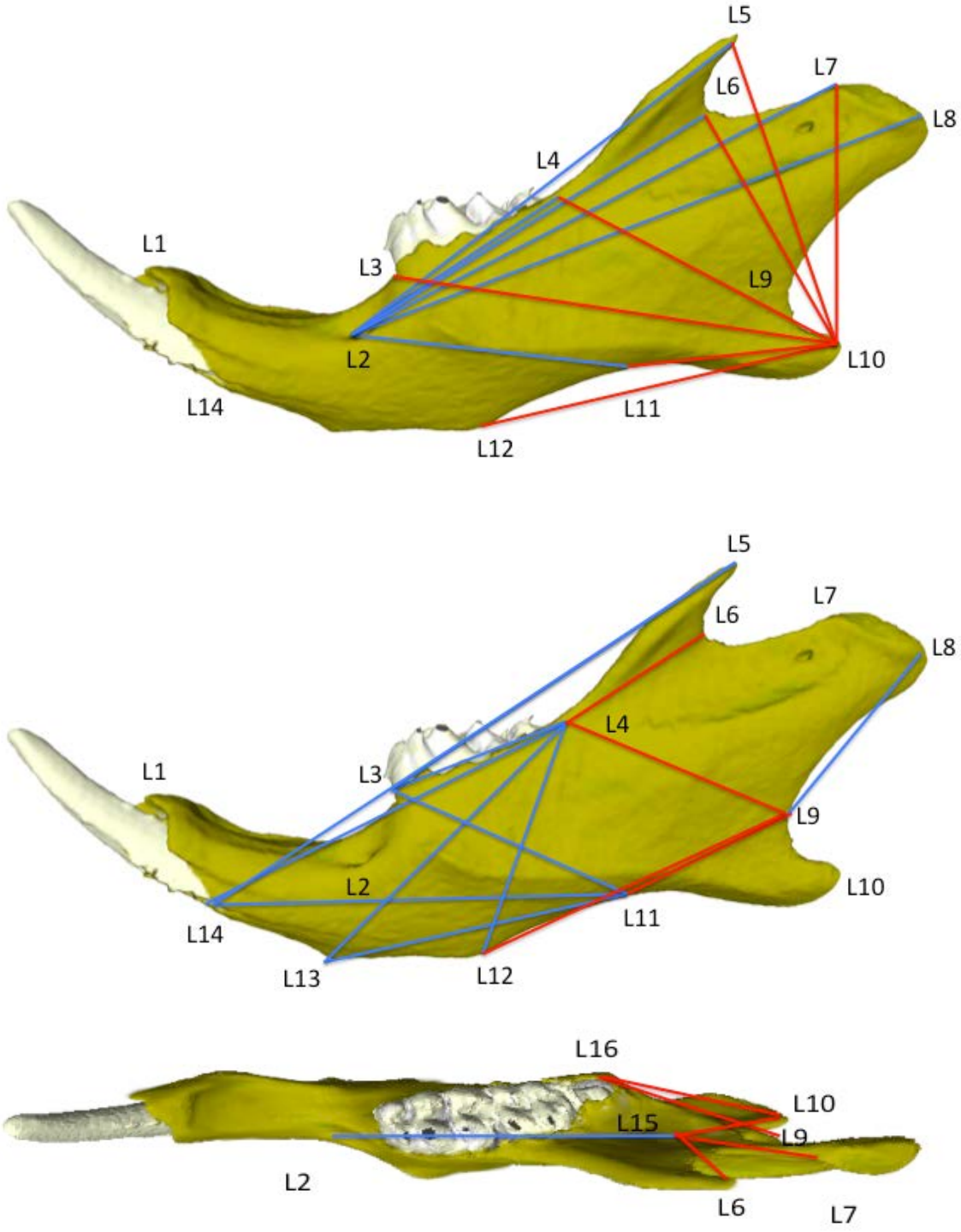

Figure 24. Significant shape changes in the EDMA results between the 25-day control and 25-day high dosage samples. Red lines indicate a significant (p< 0.10) increase in size, and blue lines indicate a significant (p< 0.10) decrease in size.

3.1.2 EDMA Results Summary

Overall, the EDMA results show marked shape changes between dosage groups for both age groups within the sample. These results suggest shape changes in the 20-day sample occur primarily in the anterior aspect of the mandible, primarily the position of the incisor. The 25-day results, albeit using control rather than low dose samples due to complications and errors that could not be reconciled with WINEDMA, demonstrate marked shape changes in the posterior aspect of the mandible, namely the coronoid process, mandibular condyle, and the angle of the mandible. The cause of these differences across age groups is not readily apparent, and is explored further in the Discussion chapter of this dissertation. The high variance seen in many of the landmarks could be indicative or EDMA errors, though it was evident in test runs utilizing even high numbers of resamples (2,000 to 10,000 runs).

3.2 GEOMETRIC MORPHOMETRIC RESULTS

Geometric morphometric analysis revealed many interesting aspects of offspring mandibular shape change as both age and treatment level increased. The analyses were conducted on the entire group, allowing for estimation of shape changes between the three age groups. The offspring sample was also evaluated within each age group to determine any mandibular shape changes within the varying dosage groups. Principle component analysis (PCA) was conducted across all three age groups and on the overall sample combined. Due to the loss of medium dose data and overall smaller sample sizes within each group, canonical variate analysis (CVA) was

only conducted using the entire sample, corrected for the effects of sex, to better describe shape changes between treatment groups.

3.2.1 ANOVA

All specimens were evaluated using PCA to determine any shape changes that occurred as a result of thyroxine dosage. All mandible landmark data were subjected to a Procrustes ANOVA, comparing both treatment groups and ages, to determine if significant differences exist between the samples. Within MorphoJ, ANOVA tests were conducted comparing both centroid size and Procrustes coordinates; significant differences ($p < 0.05$) between centroid sizes suggest size differences between populations, whereas significant differences ($p < 0.05$) between Procrustes coordinates suggest shape differences between the groups.

ANOVA tests found significant size ($p = 0.0051$) and shape ($p < 0.001$) differences between treatment groups within the combined mandibular landmark data (Table 16). This result suggests that dosage does, in fact, have a significant effect on mandibular shape. Further ANOVA tests found significant centroid size ($p < 0.001$) and Procrustes coordinate ($p < 0.001$) differences between age groups within the combined mandibular sample (Table 16). These results do not necessarily suggest that dosage is the prime cause of size and shape differences between the age groups, as confounding factors (e.g., sex) may also play primary roles in the ontogeny of offspring mandible.

Table 16. ANOVA results for treatment for both size (centroid) and shape (Procrustes coordinates) for the combined landmark data.

		SS	MS	df	F	p
Treatment	**Centroid Size**					
	Individual	3463.3	1154.4	3	4.37	0.005**
	Residuals	62641.7	264.3	237		
	Procrustes Coordinates					
	Individual	0.012	<0.0001	123	2.64	<0.001**
	Residuals	0.351	<0.0001	9717		
Age	**Centroid Size**					
	Individual	34448.8	17224.4	2	129.5	<0.001**
	Residuals	31656.2	133.0	238		
	Procrustes Coordinates					
	Individual	0.065	0.0008	82	26.23	<0.001**
	Residuals	0.297	<0.0001	9758		

**indicates significant ($p<0.05$) differences within the group

Overall, PC analysis of the sample demonstrated shape differences across all three age groups. These changes can be explained as differences arising from thyroxine dosage as age of the sample increased, but could also be explained as sex differences within the sample. To ensure that the shape changes seen in the GM analyses of the samples were not a direct result of either sampling bias in sex or size differences between the sexes, ANOVA tests were again run using the Procrustes distances of the control groups for each age. Significant results ($p< 0.05$) between sexes in the Procrustes distances within the untreated control groups suggest that sex may explain the shape differences more than thyroxine dosage. Due to the loss of sex data in the 15-day control group, the tests could only be run on the 20- and 25-day samples. Within each of these two age groups, the control samples were imported in to MorphoJ and given a Procrustes fit. ANOVA tests between males and females were then run on both the centroid sizes and Procrustes coordinates; significant differences ($p< 0.05$) in the centroid size in a group suggests that there are size

differences between the sexes, while significant differences ($p < 0.05$) between the Procrustes coordinates suggests that there are shape differences between females.

Using sex as the individual classifier with both samples, the ANOVA tests did not show any significant differences in centroid size or Procrustes coordinate differences between males and females in either the 20-day or 25-day samples (Table 17). These results within the control groups demonstrate that sexual dimorphism *does not* result in either size or shape differences within the sample mandibular sample. Therefore, any resulting size or shape differences seen in the sample are best explained by differences in thyroxine dosage.

Table 17. ANOVA results comparing sex for both size (centroid) and shape (Procrustes coordinates) within the 20-day and 25-day samples.

		SS	MS	df	F	p
20-day Sample	**Centroid Size**					
	Individual	74.32	74.32	1	0.42	0.5235
	Residuals	977.81	175.17	17		
	Procrustes Coordinates					
	Individual	0.001	<0.001	95	0.95	0.6133
	Residuals	0.021	<0.001	1615		
25-day Sample	**Centroid Size**					
	Individual	54.81	54.81	1	0.29	0.5932
	Residuals	3912.14	186.29	21		
	Procrustes Coordinates					
	Individual	0.001	<0.001	95	1.02	0.4234
	Residuals	0.022	<0.001	1995		

**indicates significant ($p<0.05$) differences within the group

3.2.2 Principle Component Analysis Results

Within each age group, principal component scores were exported from MorphoJ and imported in to SPSS for ANOVA tests to identify significant differences between principle components (PC's) within each age group. Significant ($p < 0.05$) results for a PC indicate that that particular PC explains shape differences between samples and should be further evaluated. Further Bonferroni corrections were applied within SPSS to evaluate p-values for each PC to determine the interaction of each PC with each treatment group. The relevant PC's are described within each age group below, and results of the ANOVA are presented in Appendix C.

3.2.1.1 15-Day Sample

Due to loss of medium dose data, only control, low, and high dosage offspring were evaluated for the 15-day old sample (n= 49 individuals). A total of 41 PC's were extracted to explain 100% of the overall shape variation seen within the 15-day sample (Figure 25), with more than 90% of all shape variation was explained by the first 15 PC's (Table 18). Only one principle component within the 15-day old sample, PC 9 (3.5% of all variation within the sample), demonstrated significant differences ($p=0.013$) between the low- and high dosage groups in preliminary ANOVA tests. This PC also demonstrated a distinct separation of treatment groups (Figure 26). PC9 is associated with pronounced shape changes in the high dose group in nearly all aspects of the mandible most notably an anterior movement in the coronoid process and superior movement of the mandibular angle; both of these shape changes appear as reduction in both regions (Figure 27). There is also an anterior movement of Landmark 2 (mental foramen) and a posterior and lingual displacement of Landmark 16 (mandibular foramen). Shape changes

described by PC9 also demonstrate a marked rotation of the mandibular condyle as dosage increases (Figure 27).

Table 18. PCA results accounting for over 90% of all shape variation within the 15-day old sample.

PC	Eigenvalues	% Variance	Cumulative Variance
1.	0.00025826	18.288	18.288
2.	0.00022402	15.863	34.151
3.	0.00015834	11.212	45.363
4.	0.00011954	8.465	53.828
5.	0.00009445	6.688	60.516
6.	0.00008003	5.667	66.183
7.	0.00006953	4.923	71.106
8.	0.00006227	4.409	75.515
9.	0.00004930	3.491	79.007
10.	0.00004214	2.984	81.990
11.	0.00003031	2.146	84.137
12.	0.00002594	1.837	85.973
13.	0.00002201	1.558	87.532
14.	0.00002050	1.451	88.983
15.	0.00001897	1.343	90.326

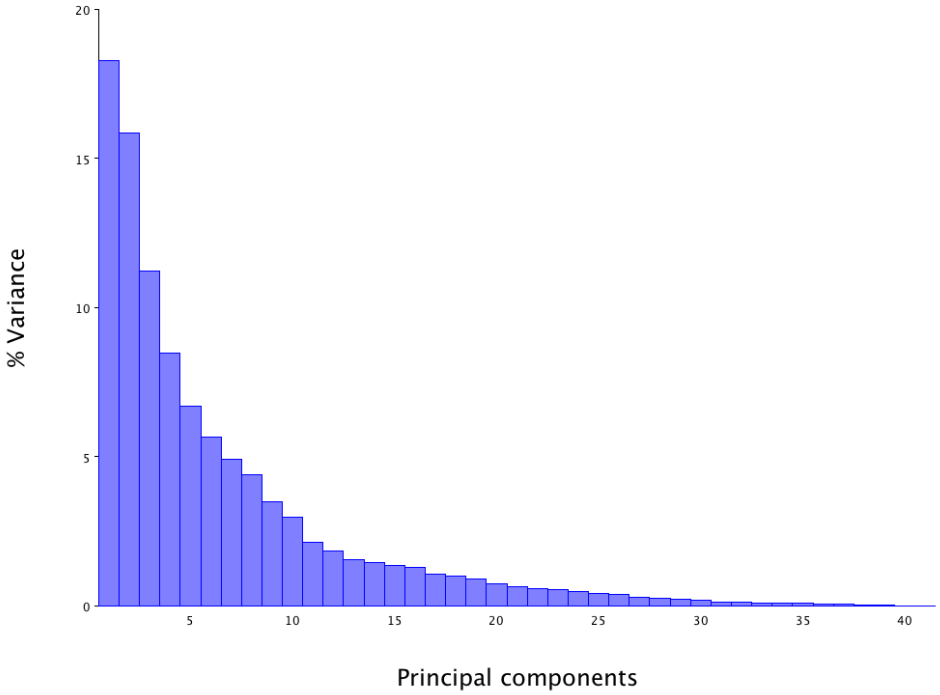

Figure 25. Eigenvalues for the 15-day old sample displaying the % of shape variation explained by each principle component.

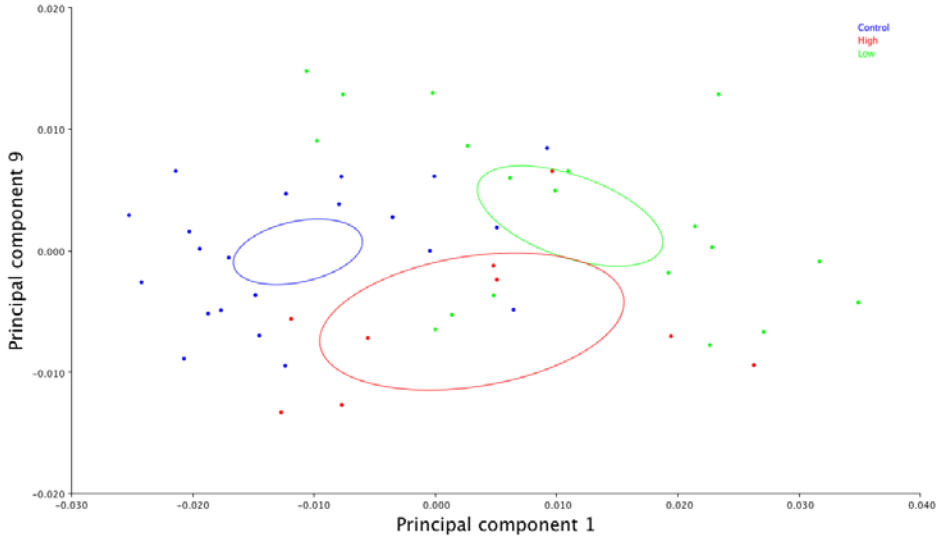

Figure 26. Scatterplot demonstrating separation of treatment groups along PC9 axis. Ellipses represent 90% confidence for sample means.

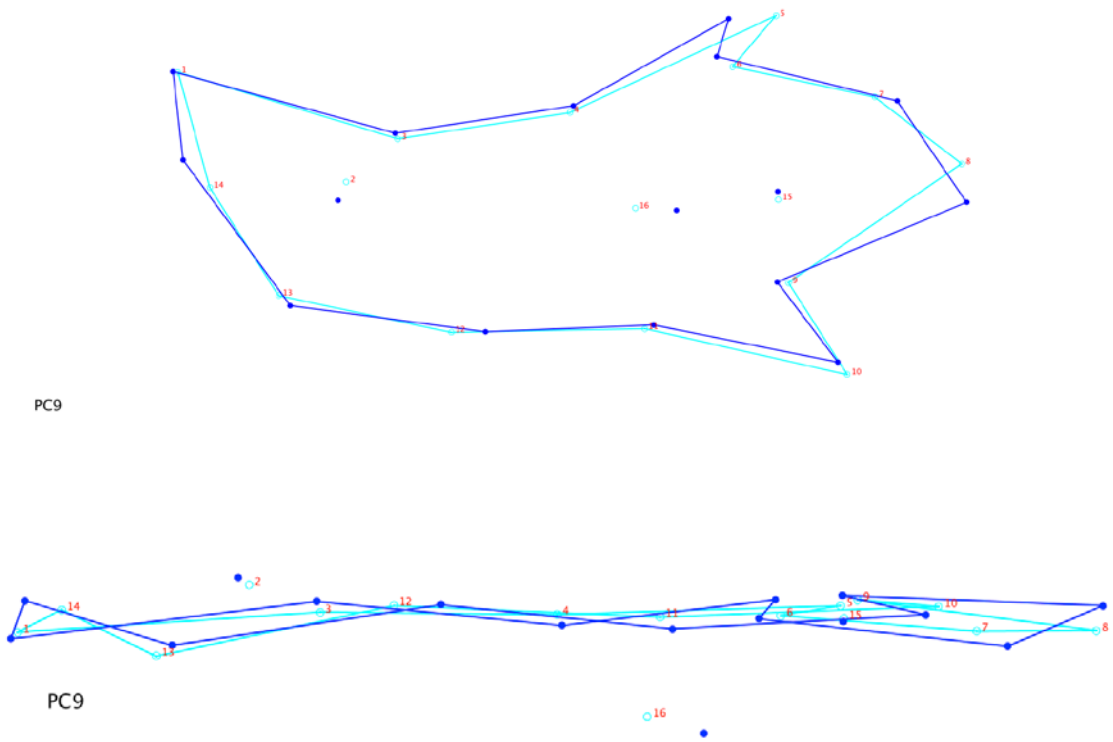

Figure 27. Wireframe deformations for PC9 within the 15-day old sample (scaling factor = 0.1). The light blue wireframe represents the mean shape of the 15-day old sample, and the dark blue represents the shape changes towards the high dosage group described by the PC.

Overall, GM analysis of the 15-day old sample showed shape changes throughout the mandible. PCA demonstrates that these shape changes occur primarily in the anterior-posterior dimensions, with minor changes appearing in the mediolateral plane. The most apparent of the shape changes occurred in the coronoid process and angle of the mandible, with mediolateral rotation of the mandibular condyle.

3.2.1.2 20-Day Sample

A total of 41 PC's were calculated for the 20-day old sample (n= 74 individuals), and included all dosage groups. The first 15 PC's accounted for 90% of all variation within the sample (Table 19), with the first four PC's explaining roughly 50% of all variation (Figure 28). Within the 20-day sample, preliminary ANOVA results suggest PC3 demonstrated significant difference (p= 0.035) between treatment groups. These results are corroborated by a clear distinction between treatment groups in a scatterplot of PC scores, particularly between the control group and treatment groups (Figure 29). The shape changes associated with PC3 (11.5% of all variation within the sample) are seen a reduction of the coronoid process and mandibular angle in the high dosage group, a posterior movement of the mandibular condyles, and slight anterior movement of the mental foramen (Figure 30). A distinct narrowing of the mandible can be seen in the mandibular condyle, with all landmarks in this region demonstrating a marking change in location towards the midline of the mandible as thyroxine dose increases (Figure 30).

Table 19. PCA results accounting for over 90% of all shape variation within the 20-day old sample.

PC	Eigenvalues	% Variance	Cumulative Variance
1.	0.00020160	15.706	15.706
2.	0.00016911	13.176	28.882
3.	0.00014799	11.530	40.412
4.	0.00011177	8.708	49.120
5.	0.00009384	7.311	56.431
6.	0.00008296	6.464	62.894
7.	0.00006438	5.016	67.910
8.	0.00005346	4.165	72.075
9.	0.00004964	3.867	75.943
10.	0.00003753	2.924	78.867
11.	0.00003412	2.658	81.525
12.	0.00002999	2.337	83.862
13.	0.00002567	2.000	85.862
14.	0.00002454	1.912	87.774
15.	0.00001957	1.525	89.299

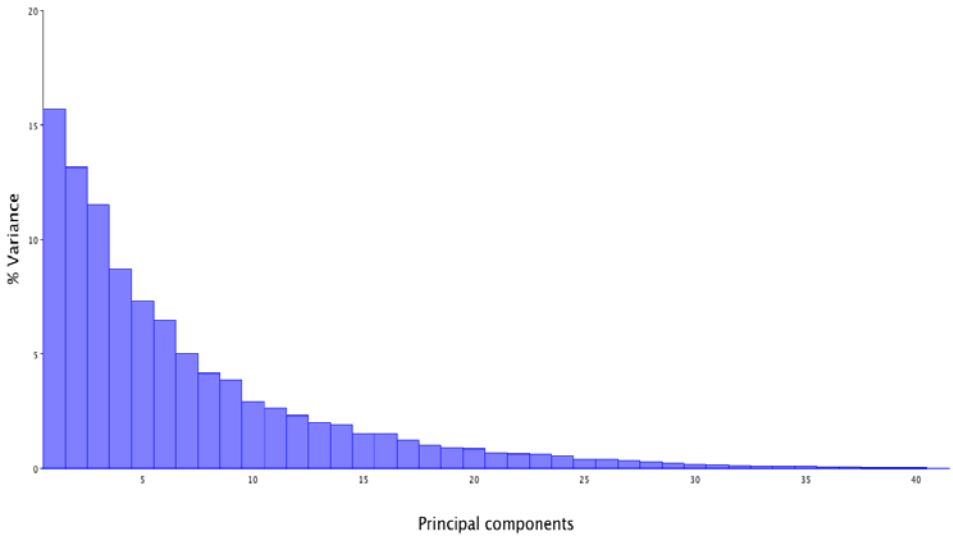

Figure 28. Eigenvalues for the 20-day old sample displaying the % of shape variation explained by each principle component.

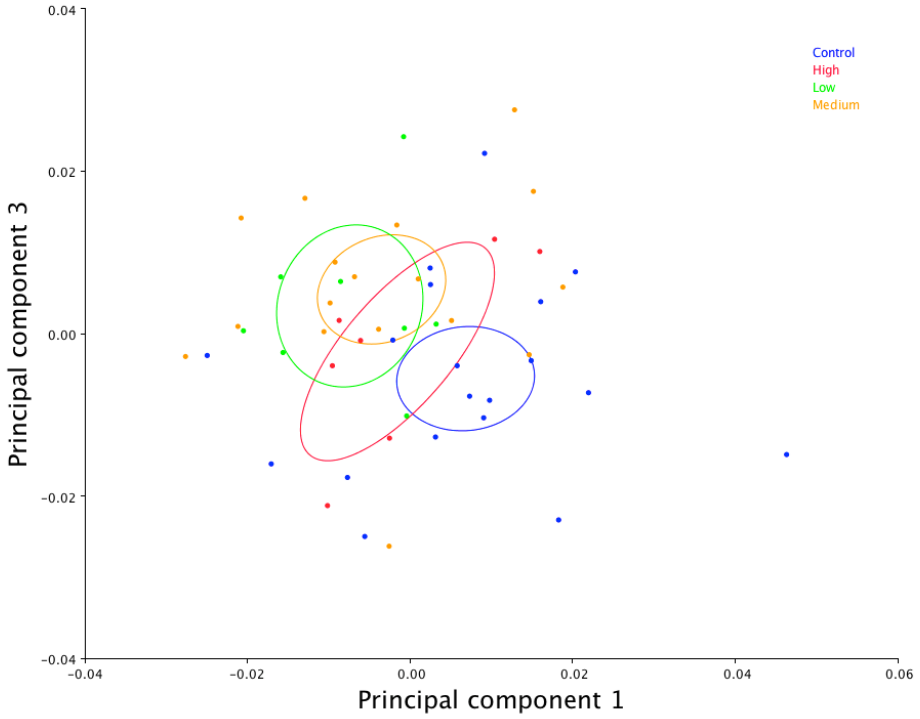

Figure 29. Scatterplot demonstrating separation of treatment groups along PC3 axis. Ellipses represent 90% confidence for sample means.

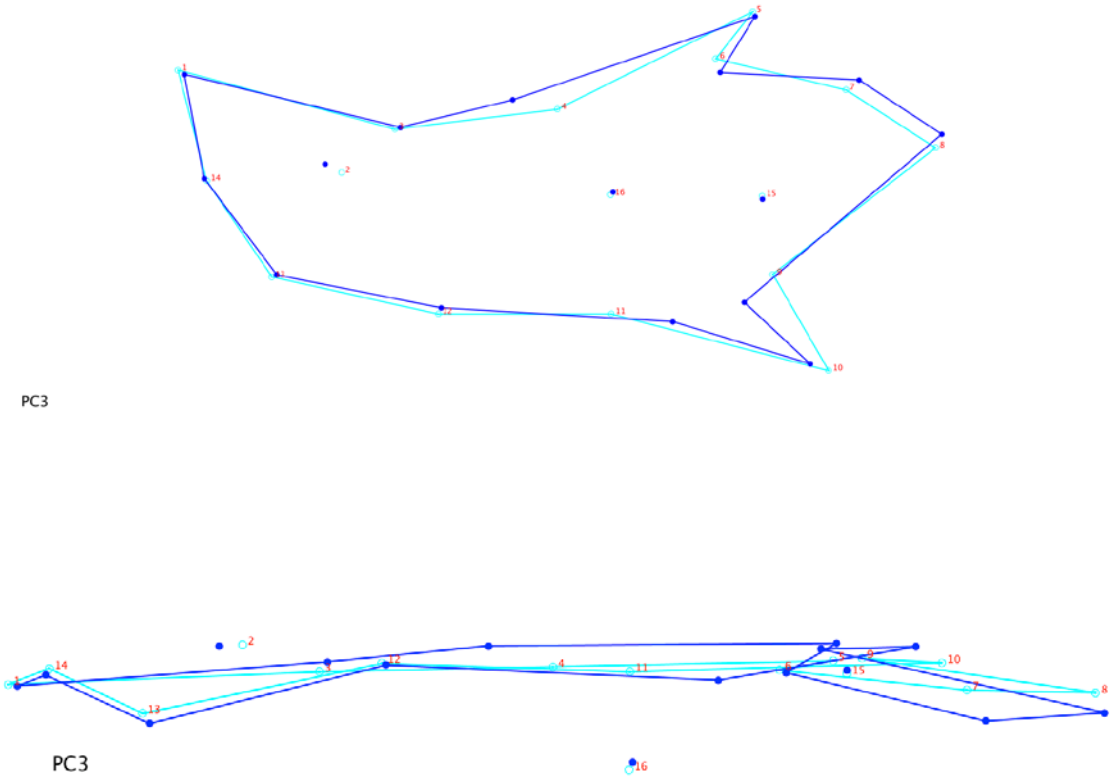

Figure 30. Wireframe deformations for PC3 (scaling factor = 0.1). The light blue wireframe represents the mean shape of the 20-day old sample, and the dark blue represents the shape changes described by the PC.

Overall shape changes seen in the 20-day sample are more apparent than those seen in the 15-day sample, though the regions are the same: coronoid process, mandibular angle, and mandibular condyles. Shape changes are also seen in the inferior aspect of the mandible in the mediolateral dimension as dose increases.

3.2.1.3 25-Day Sample

Forty-one PC's were calculated for the 25-day offspring (n= 118 individuals) across all dosage groups, with the first 18 accounting over 90% of all variation within the sample (Table 20 and Figure 31). Preliminary ANOVA results show eight PC's with significant differences ($p < 0.05$) in shape (Appendix C). These eight PC's also demonstrate substantial separation between the control group and treatment groups (Figure 32). Of the eight significant PC's, only five account for more than 3% of total variation: PC1, PC3, PC5, PC6, and PC7 (Table 20).

Table 20. PCA results accounting for over 90% of all shape variation within the 25-day old sample.

PC	Eigenvalues	% Variance	Cumulative Variance
1.	0.00020352	16.724	16.724
2.	0.00016926	13.908	30.631
3.	0.00011288	9.275	39.907
4.	0.00009083	7.464	47.370
5.	0.00007700	6.327	53.698
6.	0.00006842	5.622	59.320
7.	0.00006427	5.281	64.601
8.	0.00005320	4.371	68.972
9.	0.00004156	3.415	72.387
10.	0.00003596	2.954	75.341
11.	0.00003181	2.614	77.955
12.	0.00002813	2.311	80.266
13.	0.00002458	2.020	82.286
14.	0.00002357	1.936	84.222
15.	0.00002207	1.814	86.036
16.	0.00001630	1.340	87.376
17.	0.00001571	1.291	88.667
18.	0.00001465	1.204	89.871

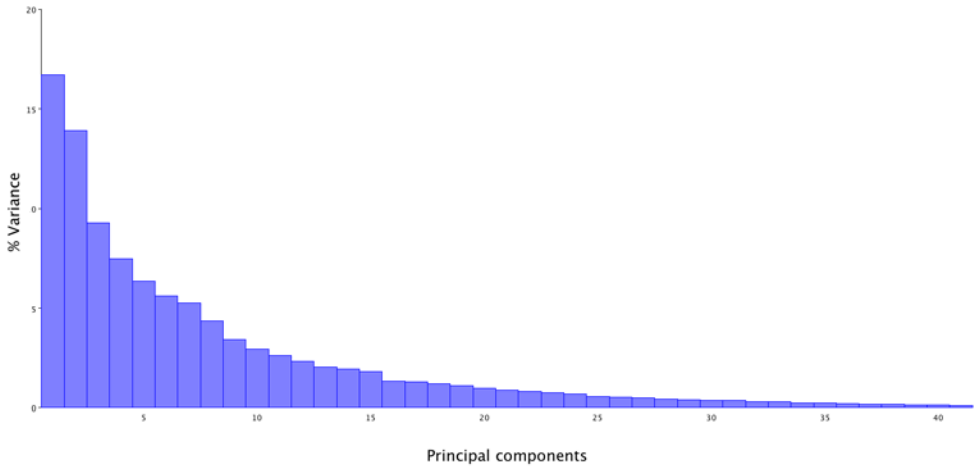

Figure 31. Eigenvalues for the 25-day old sample displaying the % of shape variation explained by each principle component.

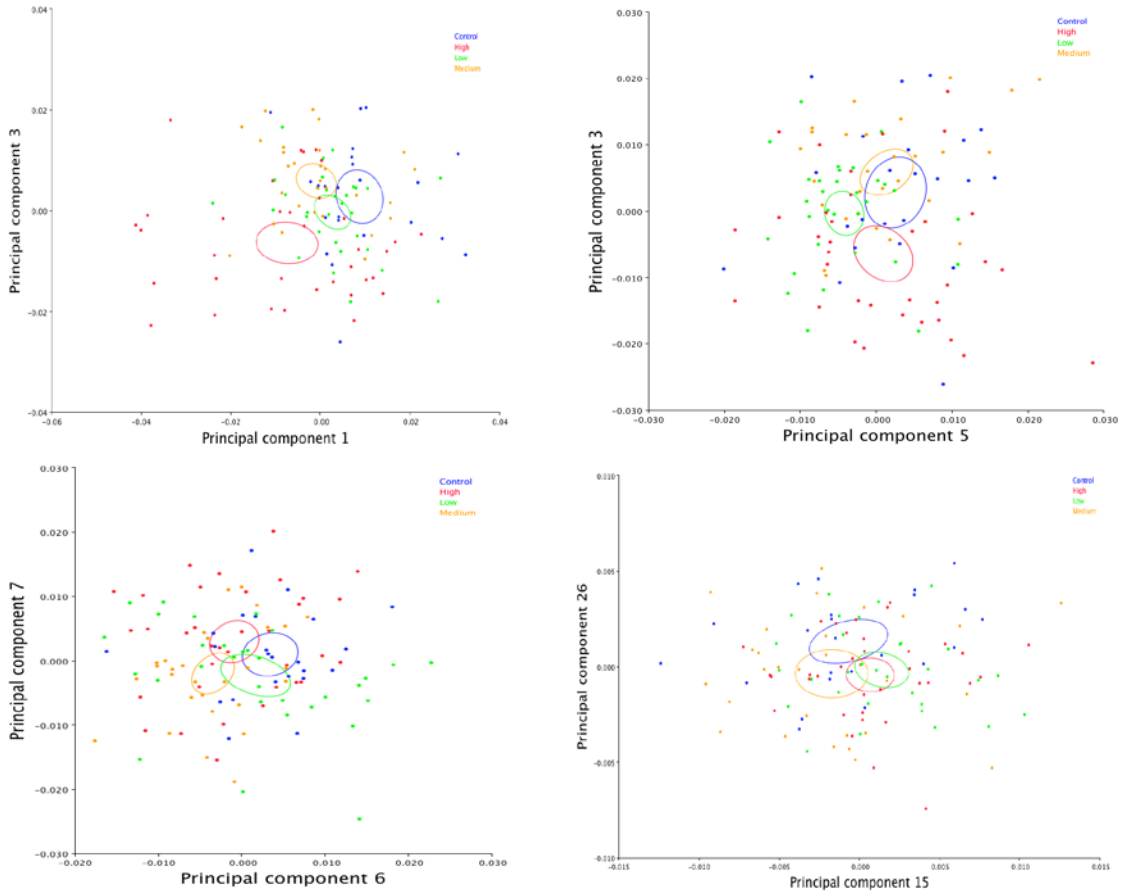

Figure 32. Scatterplot demonstrating separation of treatment groups by PC's along both axes. Ellipses represent 90% confidence for sample means.

Shape changes associated with PC1 (16.7% of overall variation) are primarily associated with the angle of the mandible in the high dosage group, with minor changes with the alveolus near the incisor and near the mandibular condyles; these changes are also associated with a medial movement of the condyles (Figure 33). The shape changes explained by PC3 (9.3% of overall variation) also involve the angle of the mandible and alveolus near the incisor, but are much more marked in the coronoid process and mandibular condyles, as well as minor shape changes along the alveolus of the molar as dose increases (Figure 33). PC5 and PC6, accounting for a combined 12% of overall variation, are associated with shape changes throughout the mandible, most notably in the mandibular condyles and coronoid process, though there is very little medial-lateral shape change in either PC (Figure 34). The shape changes explained by PC7 (5.3% of overall variation) are also located in the posterior aspect of the mandible, though the changes in the anterior mandible are drastically reduced (Figure 35).

Overall, the shape changes seen in the 25-day sample involve nearly all aspects of the mandible as thyroxine dose increases, with the most marked changes seen in the posterior portion: mandibular condyle, mandibular angle, and coronoid process. These changes are also more marked than those seen in either the 15- or 20-day samples, especially in regards to the condyle and coronoid process.

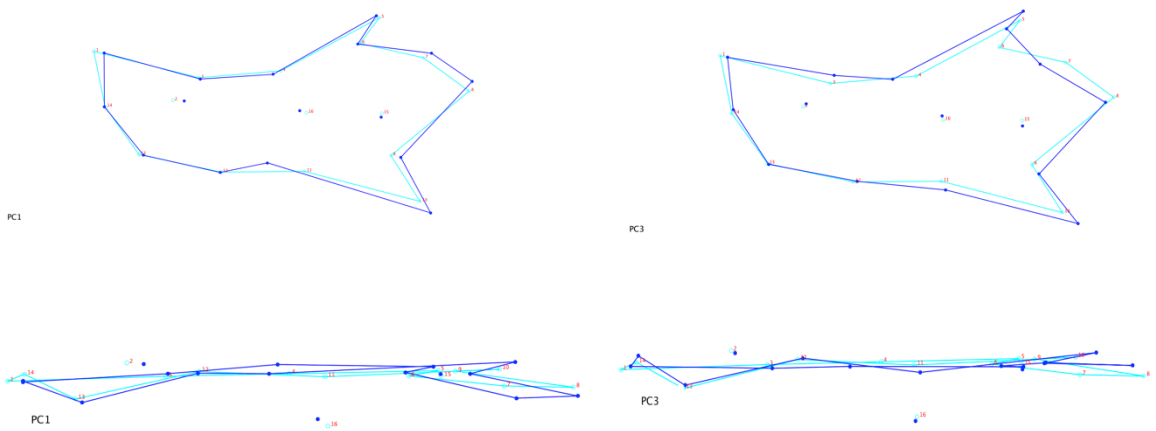

Figure 33. Wireframe deformations for PC1 and PC3 (scaling factor = 0.1). The light blue wireframe represents the mean shape of the 25-day old sample, and the dark blue represents the shape changes described by the PC.

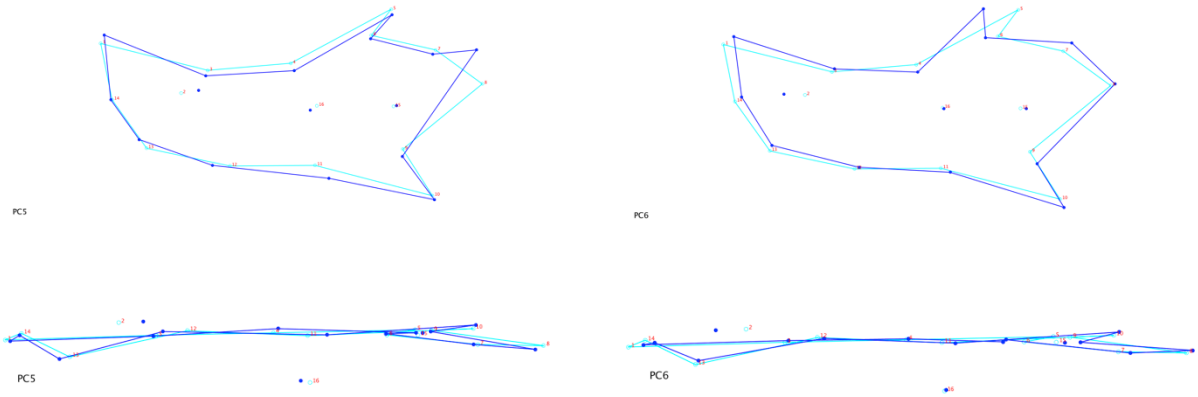

Figure 34. Wireframe deformations for PC5 and PC6 (scaling factor = 0.1). The light blue wireframe represents the mean shape of the 25-day old sample, and the dark blue represents the shape changes described by the PC.

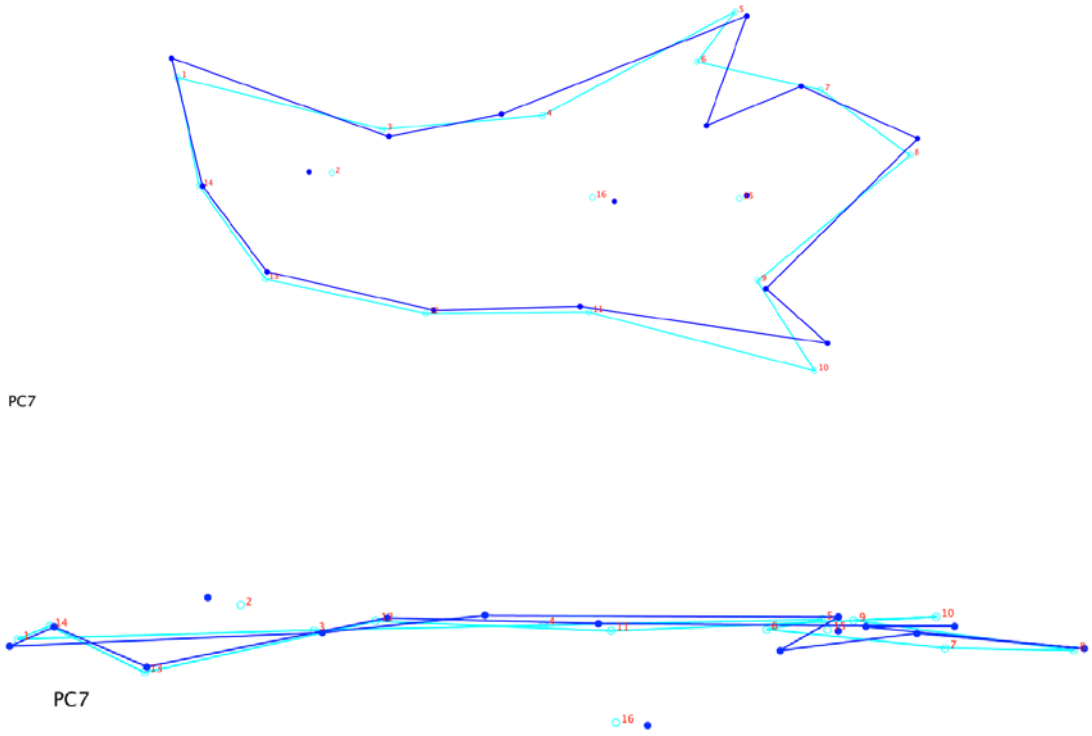

Figure 35. Wireframe deformations for PC7 (scaling factor = 0.1). The light blue wireframe represents the mean shape of the 25-day old sample, and the dark blue represents the shape changes described by the PC.

3.2.3 Canonical Variate Analysis Results

Due to the smaller samples size and missing data for some subgroups, canonical variance analysis was conducted on the Procrustes transformation of the combined data using the MorphoJ software. Canonical variate analysis allows comparison between dosage groups after potential confounding factors have been regressed out of the sample. Furthermore, this method allows comparison between dosage groups in some of smaller sample sizes present in groups within the

present sample. Age and centroid size were set as covariates and regressed out within the program, and a new covariation matrix was created on the residuals of the regression for CVA analysis. This was done regressing age out of the sample and performing CVA on the residuals.

3.3.2.1 Combined Mandibular Sample

For the 241 specimens within the combined sample, CVA using 5,000 permutations produces significant differences ($p < 0.001$) between the four treatment groups in both Procrustes distance and Mahalanobis distances (Table 21), which are more clearly demonstrated in the group clustering of differences between treatment groups (Figure 36). Canonical variate 1 (CV1) accounts for 54.7% of the overall variance related to the high dose group, with CV2 accounting for 27.7% and CV3 the remaining 17.7% of variation. The mandibular shape changes associated with each CV are depicted as wireframe deformations demonstrating the variation related to increased dosage explained by the permutations (Figure 37-Figure 39).

Table 21. Between group distance statistics (p-values) from CVA for all mandibles, with Procrustes distance above the diagonal and Mahalanobis distance below the diagonal.

	Control	Low	Medium	High
Control	-	0.0008*	0.0026	0.0002*
Low	<0.0001*	-	0.0008*	0.1616
Medium	<0.0001*	<0.0001*	-	0.0078
High	<0.0001*	0.0010*	<0.0001*	-

**P*<0.001 based on 5,000 permutations

Canonical variate analysis demonstrates marked shape changes between treatment groups once corrected for age. CV1, which accounts for more than half of all variation seen in the

combined sample, is associated with shape changes throughout the mandible, and more pronounced changes in the coronoid process, mandibular angle, and alveolus near the incisor (Figure 37). This CV is also linked to mediolateral shape changes of the inferior margin of the mandible (Landmark 13) and the anterior positioning of the mental foramen (Landmark 2; Figure 37).

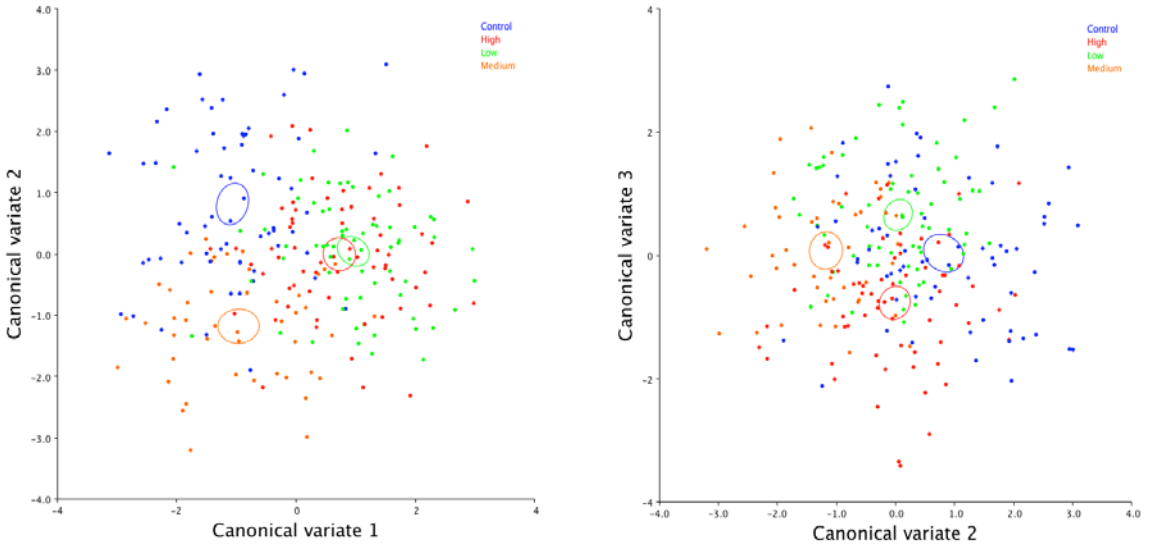

Figure 36. Canonical variance analysis of the combined sample based on Procrustes coordinates demonstrating grouping produced by the three CV's (90% confidence for sample means).

Accounting for almost one-third of all shape variation within the combined sample, CV2 also displays prominent shape changes in the coronoid process, mandibular angle, and alveolus of the incisor, with added variation in the position and orientation of the mandibular condyle (Figure 38). Mediolateral shape changes associated with CV2 are minor in comparison to CV1, with minimal shape changes near the alveolus of the incisor (Landmarks 1 and 14). As with the first two CV's, CV3 encapsulates shape changes primarily in the posterior mandible (coronoid process,

mandibular condyle, and mandibular angle), with only minor shape changes in the anterior mandible (Figure 39).

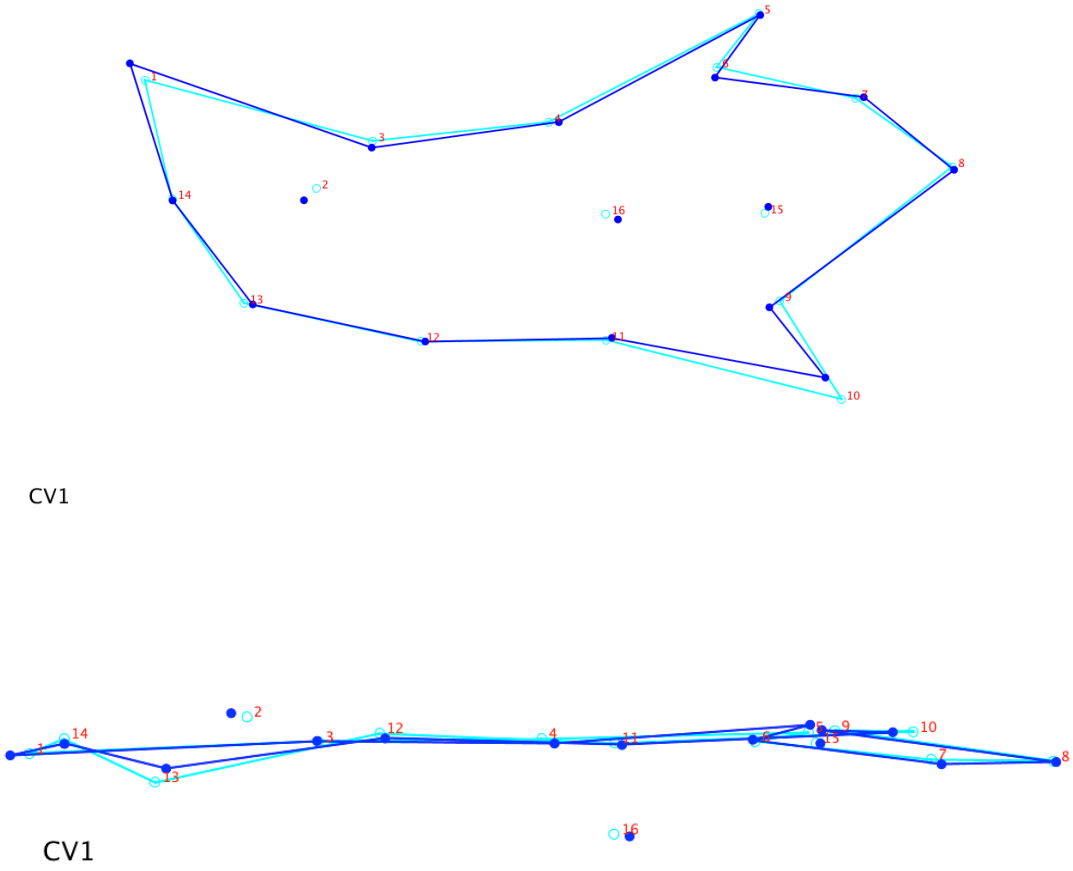

Figure 37. Canonical variance analysis of the combined sample demonstrating wireframe deformations of shape variation explained by CV1 (54.7% of all variation within the sample. The light blue represents the non-deformed shape, and the dark blue the deformed shape of CV1 related to the high dose group (scaling factor = 10.0).

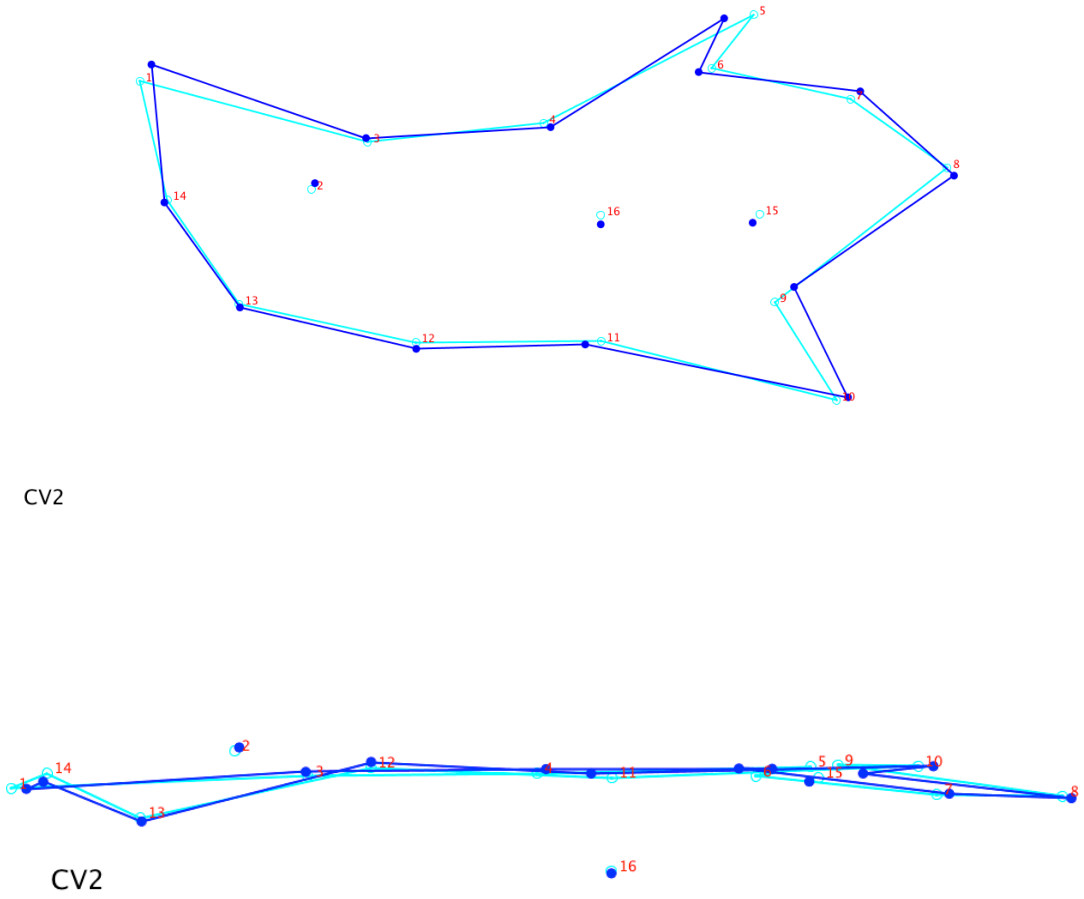

Figure 38. Canonical variance analysis of the combined sample demonstrating wireframe deformations of shape variation explained by CV2 (27.7% of all variation within the sample. The light blue represents the non-deformed shape, and the dark blue the deformed shape of CV2 (scaling factor = 10.0).

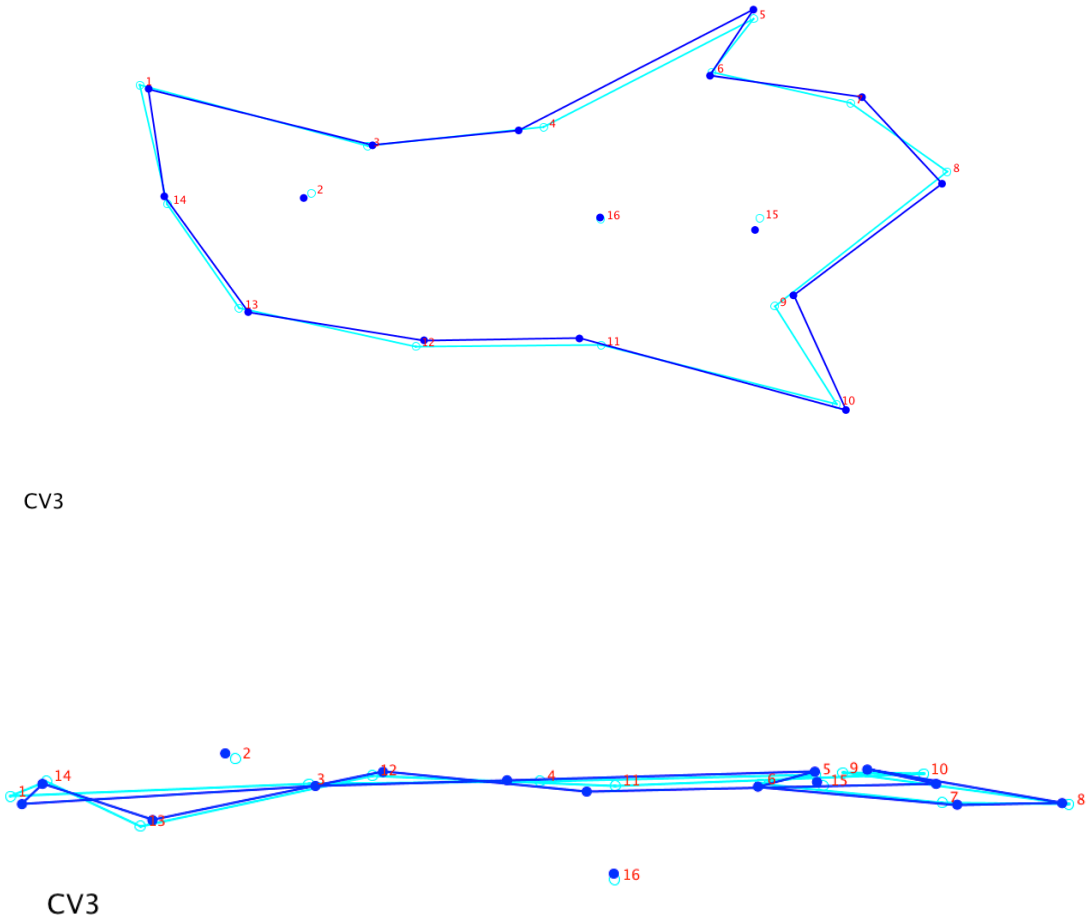

Figure 39. Canonical variance analysis of the combined sample demonstrating wireframe deformations of shape variation explained by CV3 (17.7% of all variation within the sample. The light blue represents the non-deformed shape, and the dark blue the deformed shape of CV3 (scaling factor = 10.0).

Overall, CVA on the combined data once corrected for age demonstrated noticeable shape changes in the mandible in regards to dosage. The grouping of the different treatment groups (Figure 36) corroborates the notable variation explained seen in the wireframe reconstructions (Figure 37-Figure 39). As previously stated, ANOVA tests on the Procrustes distances and centroid

sizes demonstrates no statistical difference between male and females in control groups, precluding sex as an explanatory factor in these shape changes. The shape changes seen in CVA also mirror those seen in PCA, suggesting an overall shape change within the sample associated with thyroxine dosage.

3.2.4 GM RESULTS SUMMARY

Shape changes seen in the GM results demonstrate marked shape changes in the mandible across both age and dosage groups. These shape changes could be linked to thyroxine dosage, or could be explained by other biomechanical factors as a result of maternal thyrotoxicosis. Across all three age groups, shape changes were particular apparent in the coronoid process, mandibular condyle, angle of the mandible, and the alveolus of the incisor. These changes are similar to those seen in the EDMA analyses, but it should be restated that EDMA and GM results are not effective under direct comparison, and should be treated as compliments to one another (Lele and Richtsmeier 1991). The shape changes seen in the GM results and relevant discussion regarding similarities and differences to the EDMA results are discussed in the Discussion chapter of this dissertation.

4.0 DISCUSSION

This study compared the micro-CT images of the offspring of pregnant dams given control, low, medium, and high doses of thyroxine during pregnancy in an attempt to quantify and explain shape changes in the offspring mandible. As discussed in Chapter 1 of this dissertation, thyroxine has an effect on bone growth and development, specifically in the cranial base and other areas of endochondral ossification. What is not entirely clear is the role of maternal thyroxine in the growth and development of the offspring mandible, and bone with complex formation process involving aspects of intramembranous and endochondral ossification, and formation and development of secondary cartilage in the condyles. This research utilized two separate methods of evaluating and conceptualizing shape changes in biological samples: Euclidean Distance Matrix Analysis (EDMA) and geometric morphometric (GM) analysis. These two methodologies were not included to test, prove, or disprove one another, but rather to complement each other and better describe the shape changes, if any, that occur in both age and dosage ranges. These variations could result from embryological changes in the mandible itself, biomechanical changes either pre- or postnatal associated with shape changes in the cranial base, muscles of mastication, or behavioral changes related to chewing, or as a result of unanticipated changes as a result of the administration of levothyroxine.

One overarching hypothesis was proposed at the outset of this study:

> Mice exposed to exogenous thyroxine during fetal development will demonstrate altered mandibular shape compared to unexposed mice.

Three secondary hypotheses were also proposed:

(1) The regions of shape change in the mandible will be in areas associated with muscle attachment (e.g., gonial angle, coronoid process).

(2) The shape changes in exposed mice will be more pronounced as age increases.

(3) The shape changes in exposed mice will be more pronounced as dosage increases.

The results of both the EDMA and GM analyses paint a complicated picture of shape changes across both age and dosage groups within the present sample. Both methods demonstrate marked shape changes between treated and untreated group, suggesting that the overarching hypothesis set forth is supported: offspring exposed to exogenous thyroxine during embryological development demonstrate shape changes in the mandible. The results related to the secondary hypotheses, however, provide a more complex picture, with each method displaying varying shape changes in different regions of the mandible. These differences can be explained by multiple causes, ranging from cellular, biomechanical, behavioral, or even issues related to data collection and differences between the evaluation methods. To better conceptualize what is happening with the present data, the separate results from each method will be further discussed below.

4.1.1 EDMA Shape Changes

At first glance, EDMA results demonstrate marked shape changes in mandible shape. The data were separated in to age groups (15-, 20-, and 25-day samples) to test both the overall hypotheses and the three secondary hypotheses. Unfortunately, due to unresolvable errors with both the data and software, the 15-day sample had to be removed from analysis. In looking for significant differences between the treated and untreated samples, only the 20-day sample could support or disprove the overall hypotheses. However, the three secondary hypotheses could all be

questioned using high dosage samples. The secondary hypotheses assume that the high dosage samples in both age groups *should* show increased shape changes when compared to the low dosage groups. Furthermore, the high dosage groups in the 25-day sample should exhibit more marked shape changes than those seen in the 20-day sample. Finally, the shape changes seen, particularly those in the high dosage group, should be seen in areas of muscle attachment, such as the coronoid process or mandibular angle.

To better visualize the shape changes presented in the EDMA results, the significant shape changes between landmarks (those with 90% confidence intervals not containing zero after 1,000 resamples) can be mapped on to mandible images to better conceptualize shape changes. Within the 20-day sample, 15 linear distances were significantly different between the low and high dosage groups (*see* Table 10). All of the significant shape changes in the 20-day sample involve an increase in size, primarily in the overall length of the anterior mandible (Figure 22). In fact, the location of the incisor (Landmark 1) is significantly more anterior in every linear distance in the mandible with the exception of Landmark 13, strongly indicating an overall increase in mandibular size in the anterior direction. There is no reduction in size seen anywhere in the 20-day mandibular sample.

The overall lengthening of the mandible in the 20-day sample supports the overarching hypotheses of this dissertation, as well as the secondary hypotheses regarding dose dependence. The first secondary hypotheses regarding areas of change at sites of muscle attachment is also supported by this sample, at least to a small degree, as there are shape changes associated with the attachment site of the temporalis muscle at the coronoid process. The overall increase in size, as well as increase in linear measurements increasing in size, supports the other secondary hypothesis that shape changes will increase with age. These shape changes can be explained as compensatory

growth in regards to changing cranial base shape. The 20-day sample does show a lack of width change anywhere in the mandible, suggesting that there is little to no mediolateral shape change within the sample.

The 25-day low dosage sample was removed from EDMA analysis due to a large number of software errors when attempting shape analyses. These errors, suggesting either large variance within one particular landmark, could be related to scaling and rendering issues with the original micro-CT scans. As such, the 25-control sample was used in comparison to the 25-day high dosage sample. Based on the 20-day sample results, one would expect the shape differences to be much more pronounced; this is demonstrated clearly by the 35 linear distances that were statistically significant ($p < 0.10$) between the control and high dosage group (*see* Table 15). Many linear distances within the 25-day sample displayed very large confidence intervals, further suggesting that EDMA may have difficulty dealing with the scaling of the present dataset. According to the EDMA results, increases in size of the mandibular angle were seen with nearly all other aspects of the mandibular body (Figure 24). The shape changes in this region of the mandible were also apparent in the mediolateral dimension, with significant ($p < 0.10$) widening of the posterior mandible. Concurrent with these size increases were decreases associated with the anterior mandible, namely the mental foramen and aspects of the mandibular body not associated with the alveolus (Figure 24). These changes between the superior and inferior margins of the mandibular body are also mirror in a reduction in height of the coronoid process and reduction in size between the posterior aspect of the condyle and the body of the mandible.

The size changes seen in the 25-day sample once again support the overall hypotheses that exogenous thyroxine will alter the overall shape of the offspring mandible. The 25-day EDMA comparison also supports the first and third secondary hypotheses, suggesting that increased

dosage is associated with an increase in shape changes. Finally, the 25-day sample demonstrates marked changes in the areas associated with muscle attachments, specifically the attachment of the masseter and medial pterygoid at the mandibular angle (Figure 24). The observed shape changes are suggestive of a number of possible explanatory factors. The mandible could be compensating for overall cranial base growth, where the high dosage individuals exhibit significant growth changes affecting both condyle location and occlusion. According to Enlow and Moss, this manner of shape change could explain the mandible lengthening to meet both occlusal demands and accommodate condylar change (Moss and Rankow 1968; Enlow 1982; Enlow 1990; Enlow and Hans 1996).

The increase in size of the mandibular angle is particularly interesting, as no shape increases were seen in this region in either of the earlier age groups. Existing literature suggests that this is a result of increased biomechanical demands by the muscles of the region (masseter, medial pterygoid), though no soft tissue was preserved for this study to determine if this is the case. The reduction in size related to the location of the mental foramen could be cause by two potential shape changes: a posterior movement of the foramen itself, or an overall flexion of the entire mandible (seen as a clockwise increase in growth in the images in this project). The later theory is supported by the 20-day sample, as it exhibits an increase in size in the anterior aspect of the mandible (Figure 22). However, caution must be place in such a straight-forward explanation of the size changes in the 25-day sample, as it assumes that the thyroxine is affecting only the bone and cartilage of the mandible and not the musculature, teeth, mastication process, or occlusion.

Overall, the shape changes seen between the 25-day control and high dosage groups suggest that all proposed hypotheses be supported. With nearly one third of all linear distances exhibiting shape changes in the 25-day sample, far more than that seen in the 20-day sample, it is

possible that increased age is directly linked to increase shape changes; however, the comparisons allowed by EDMA between the 20- and 25-day sample are limited to dosage, and age changes between the two samples cannot be ruled out as contributing factor to the observed shape changes. It is also apparent that the increased dosage is causing increased shape changes, as demonstrated by the low and high dose comparisons in the youngest sample. The areas of change are seen throughout the mandible, and not all are associated with muscle attachments, suggesting this topic be addressed with increased scrutiny in the future.

Overall, the EDMA analyses demonstrate marked shape changes in both tested age groups and dosages, and all of the proposed hypotheses are supported. Both of the age groups demonstrate shape changes between either the control or low dosage groups and the high dosage groups. The shape changes seen in the EDMA results also increase with age and with dosage. The one questionable result involved the secondary hypotheses concerning shape changes occurring at areas of muscle attachment. While this was certainly true of the 25-day sample, it is only associated with changes of the coronoid process in the 20-day sample. This could be the result of the thyroxine causing shape changes in different regions of the mandible at different times, or these changes not becoming apparent until a later age. To better answer these questions, daily samples would be necessary. Furthermore, the loss of EDMA data of the 15-day controls and 25-day low dosage further hindered this question, and finer smoothing and more control within the data may be necessary to definitively tease out the answer to the question of timing of these shape changes.

This study demonstrated marked shape changes between the dosage groups, particularly within the high dose sample. The causes of these changes, however, require further evaluation. The shape changes as a result of exogenous thyroxine *could* be linked to compensatory growth of the anterior mandible in response to cranial base changes. However, thyroxine can affect muscle

tissues, so shape changes of the mandibular angle could be a result of thyroxine acting on those tissues rather than the bone itself (Kemp and Hoyt 1969b; Hall 1973). If the cranial base narrows, or if the glenoid fossa shift in position, the mandible follows suit (Moss and Rankow 1968; Enlow 1968). The anterior aspect of the mandible in this sample appears to follow this principle of craniofacial growth and development (Figure 40). The shape changes in the posterior aspect of the mandible, namely the coronoid process, the condyles, and the mandibular angle, also appear to move in relation to cranial base changes seen in other studies (*discussed in detail below*; Parsons et al. 2015; Cray, *unpublished*). To further understand the shape changes occurring across the different age groups, GM analyses must also be evaluated.

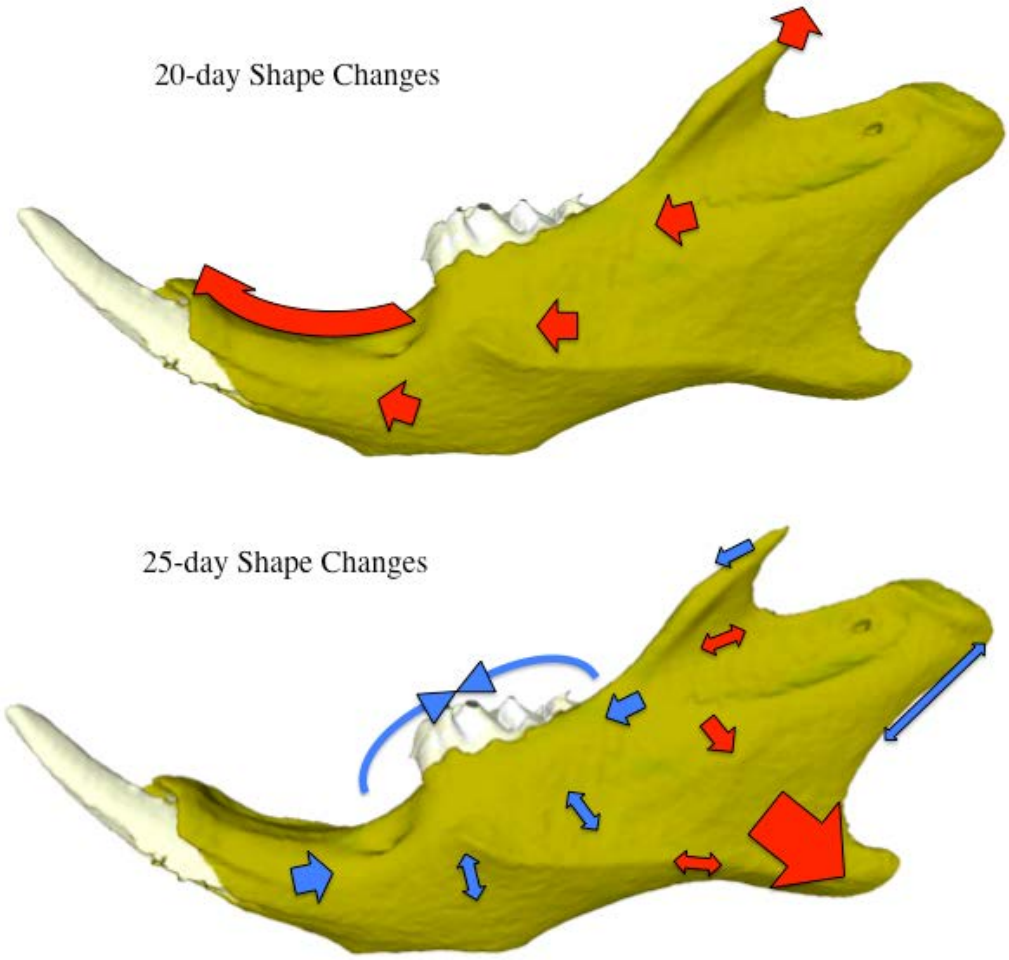

Figure 40. Schematic interpretation of overall mandibular shape changes seen in EDMA results as both age and thyroxine dosage increase. Red arrows indicate areas of growth and blue lines indicate areas of reduction.

4.1.2 GM Shape Changes

4.1.2.1 Principle Component Analysis

All available samples within the three age and four dosage groups were evaluated using GM techniques. Once fitted to Procrustes coordinates, the sample was evaluated using ANOVA to determine if significant differences ($p < 0.05$) existed between age groups treatment groups

within the population (Table 16). When comparing treatment groups (control, low, medium, and high dosage), ANOVA tests indicate significant differences in both size ($p = 0.0051$) and shape ($p < 0.001$), demonstrating that dosage does, in fact, alter the overall shape of the offspring mandible. Age groups were also compared, and both size ($p < 0.001$) and shape ($p < 0.001$) exhibit significant differences; this later result is not surprising, as one would expect older individuals to have larger mandibles, and that shape changes would exist between age groups as biomechanical loads and mastication demands changes as an individual ages. Unfortunately, sex was not recorded for the 15-day sample, so ANOVA tests were run using the 20- and 25-day samples to determine if sex played a role in the observed shape changes (Table 17). No significant size ($p = 0.534$) or shape ($p = 0.613$) differences existed between males or females in the 20-day control sample. Furthermore, no significant size ($p=0.593$) or shape ($p = 0.423$) differences existed between the sexes in the 25-day control sample. By demonstrating that sex does not play a significant role in shape differences of the mandibles across age groups, the argument can then be made that any observed shape differences are more likely a result of thyroxine dosage.

Once sex was eliminated as a possible explanation for the demonstrable shape differences, the sample was evaluated using PCA to determine where any dose-dependent shape changes are occurring in the mandible in each of the three age groups. With over 40 PC's created to explain all shape variation for each sample, ANOVA and Bonferroni tests were used to determine which PC's should be reviewed first to best explain variation. Only one PC in the 15-day sample (PC9, 3.5% of all variation) demonstrated a significant difference between dosage groups. Since the medium dosage data for the 15-day animals were lost, only control, low, and high could be compared. The shape changes seen in the 15-day sample are localized in the posterior and anterior mandible (Figure 27). The shape changes seen between dosage groups along PC9 are seen in the anterior

aspect of the mandible, namely the position of the incisor, and more markedly in the posterior mandible at the coronoid process and mandibular angle. Since the functional matrix of the anterior mandible results from occlusion, these shape changes suggest a slight alteration in form of the mandible towards the incisors, which may be indicative of compensatory changes to maintain occlusion (Moss and Rankow 1968; Enlow 1990).

The changes seen in the coronoid process and mandibular angle suggest a reduction in biomechanical loading caused by the temporalis and masseter/pterygoid muscles, respectively. Whether these changes are caused by an overall reduction in function of these muscles, or if these changes are due to different functional demands due to fluctuations in shape of the cranial base cannot be determined by the present study. Mediolaterally, shape changes explained by PC9 are observable in the movement towards the midline of the mandibular angle and the lateral flaring of the condyle, and to a lesser extent the medial movement of both the anterior aspect of the mandible around the incisor. Overall, the 15-day sample GM results support the overarching hypothesis that thyroxine will alter mandibular shape, as well as the secondary hypotheses regarding the shape changes occurring at sites of muscle attachment.

As with the 20-day sample, only one PC was determined to be significantly different by the ANOVA and Bonferroni tests: PC3. This PC, which explains 11.5% of all variation within the sample, is particularly useful in separating the control group and high dosage group from the rest of the sample (Figure 27). These shape changes are localized in the posterior aspect of the mandible, primarily a reduction of the mandibular angle and slight reduction in the coronoid process. There is also a posterior movement of the condyle and alveolus, both of which could be a result of compensatory growth to maintain occlusion. The mediolateral shape changes are more pronounced than those seen in the younger sample, with a distinct narrowing of the alveolus near

the incisor, and again a lateral flaring of the condyle and medial movement of the mandibular angle. These medial and lateral movements represent magnifications of the shape changes seen in the 15-day sample, suggesting an increase in shape changes as age increases.

Shape changes seen in the GM results of the 25-day sample are more difficult to conceptualize, as five PC's successfully discriminated between treatment groups and accounted for more than 3% of overall variation individually (Figure 31). The shape changes explained by PC1 (16.7% of overall variation) are localized in the condyle, mandibular angle, and the alveolus of the incisor, as well as lateral flaring of the condyle. Contrary to this, PC3 (9.4% of all shape variation) is associated with a *medial* movement of the condyle and anterior *reduction* in the condyle; PC3 is also associated with a more marked superior movement of the coronoid process. As with PC1, shape changes along PC3 decrease as dosage increases. PC5 and PC6 accounted for 12% of all variation within the 25-day sample, and are associated with significant rotation of the anterior aspect of the mandible, posterior displacement of the mandibular condyle resulting in a shorter span between incisor and coronoid process, increased dimensions of the mandibular angle, and little to no shape changes in the mediolateral direction. PC7 accounted for just 5.3% of overall shape variation, but is associated with shape changes throughout the mandible: superior rotation of the anterior aspect of the mandible, drastic changes in both coronoid process and condyle location, and posterior flaring of the mandibular angle. In sum, the shape changes of the 25-sample demonstrated an increased effect of thyroxine of with both age and dosage, and these changes are primarily associated with areas of muscle attachment.

4.1.2.2 Canonical Variate Analysis

To further corroborate the shape changes seen from PCA, canonical variate analysis (5,000 permutations) was conducted across the entire sample to test for significant ($p < 0.001$) differences between the four dosage groups. Prior to conducting CVA, regression was used to correct for age, allowing for effective comparison of dosage alone. Significant differences in Mahalanobis distance exist between each of the four dosage groups (all $p < 0.0001$), which demonstrate a distinct difference in shape as a result of thyroxine dosage. Furthermore, Procrustes distances were significantly different between control → low, control → high, and low → medium comparisons (*see* Table 21). Accounting for more than half of all variation in the population, CV1 is linked with a superior rotation of the anterior mandible, reduction of the mandibular angle, and a less pronounced reduction in coronoid process (Figure 41). CV2, which accounts for roughly 28% of all variance, is also associated with a superior rotation of the anterior mandible, as well as a reduction in coronoid process resulting in a more flexed mandible, and a marked increase in mandibular angle (Figure 41). CV3 (18% of all variance) is linked primarily to shape changes in the coronoid process and mandibular angle, with slight reduction in anterior mandible length (Figure 41). These CVA results corroborate those seen in PCA, linking increased dosage with a superior displacement of the incisor and an increase in mandibular angle and movement of the condyles. These changes are best explained by compensatory growth of the mandible to maintain occlusion and deal with changes of the cranial base, though the effect of the thyroxine on the muscles themselves leading to altered biomechanical loads may be a contributing factor.

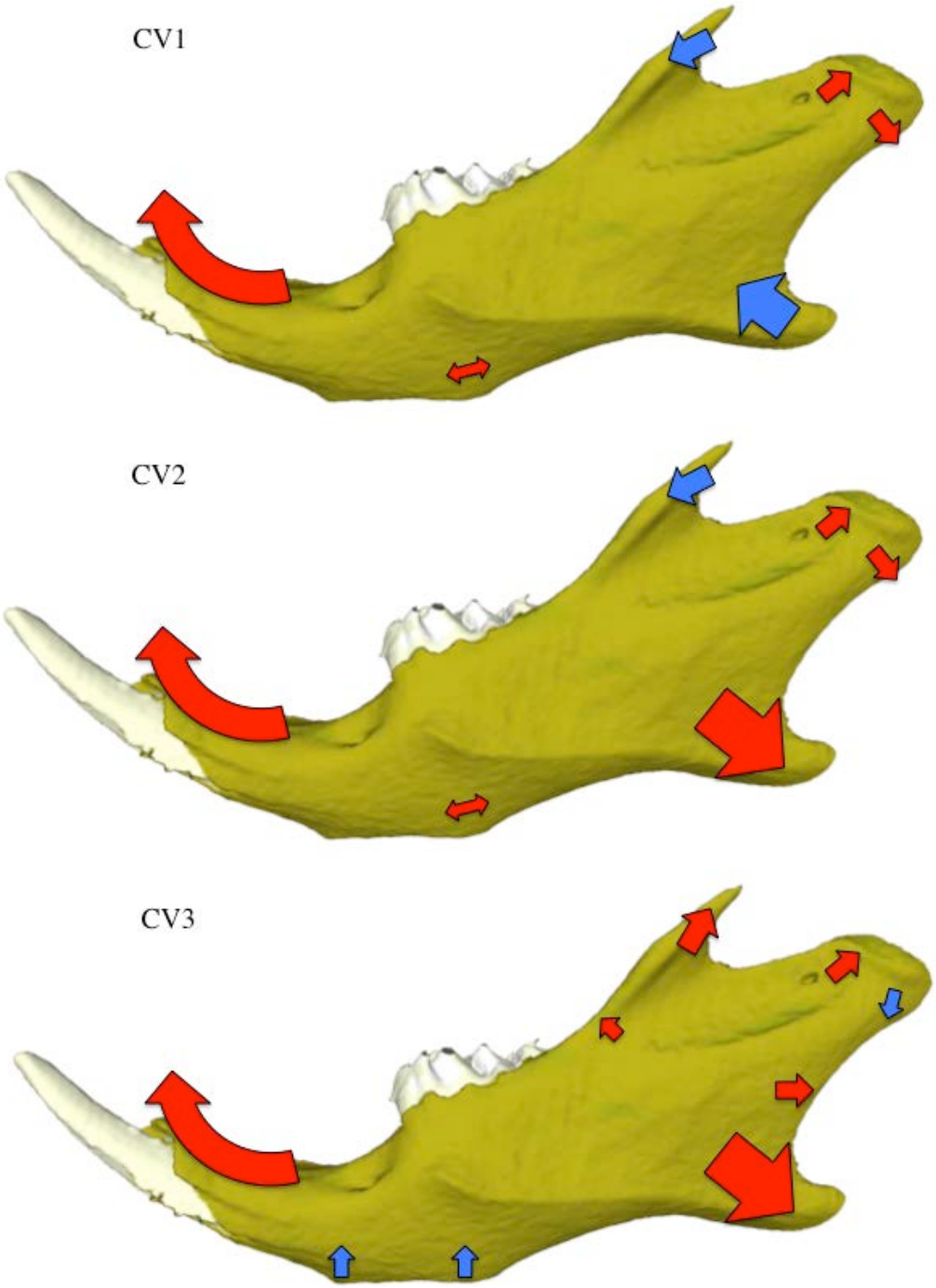

Figure 41. CVA results across all dosage groups, corrected for age. Red arrows indicate areas of growth and blue lines indicate areas of reduction.

4.1.3 Comparison of EDMA and GM Results

4.1.3.1 15-day Sample Comparison

Due to the errors associated with the collection and analysis of the 15-day EDMA, evaluation of the two methods for the 15-day sample is not possible. It should be noted that EDMA and GM are not directly comparable methods, and should instead be seen as separate paths towards answering the same questions (Lele and Richtsmeier 2001). The 15-day GM sample displays a slight rotation of the anterior mandible, a slight reduction of the mandibular angle and both a marked reduction of the coronoid process and rotation of the mandibular condyle.

4.1.3.2 20-day Sample Comparison

The EDMA results comparing the 20-day low dosage group and high dosage groups resulted in significant shape changes in the anterior mandible, specifically an increase in size and superior rotation of the alveolus towards the cranial base. There was also a slight increase of the coronoid process in the vertical dimension. The GM results also display a similar change in shape of the anterior mandible, and shape changes in the 20-day sample using this method were much more marked in a reduction of the mandibular angle and a rotation of the mandibular condyle. The shape changes seen in the mandibular angle between the two methods are also very similar as GM results suggest an anterior movement of Landmark 9 (most anterior point of subcondylar incisive) with little vertical change in the position of Landmark 10 (posterior tip of mandibular angle. The GM analysis also demonstrates that the superior margin of the mandible moves towards the cranial base, potentially in relation to mandibular rotation, which is also seen in the EDMA results. The only shape changes not corroborated by the two methods are in the position of the mandibular

condyle. The EDMA results show only an increase in distance between the posterior margin of the mandibular condyle and the incisor, whereas the GM results show a vertical change in position of the anterior margin of the condyle that is not seen in the EDMA results. Why these two methods disagree at this landmark is uncertain, though it may be tied to the far reduced sample size used in EDMA (32 individuals in two groups) compared to those used in the GM analysis (74 individuals in four groups).

Overall, both methods suggest an increase in size of the mandible in the anterior-posterior dimensions. Coupled with vertical changes in shape towards the anterior aspect of the mandible, these shape changes strongly suggest a superior rotation of the incisor. Previous orthodontic and animal model research predicts this sort of shape change in response to alterations in shape of the cranial base (Moss and Rankow 1968; Petrovich 1974)

4.1.3.3 25-day Sample Comparison

The shape changes seen in both the EDMA and GM analyses coincide with one another. Although not directly comparable, both methods demonstrate marked shape changes along the superior margin of the mandible and coronoid process, with a superior rotation of the incisor; this is particularly evident when comparing the EDMA results to those of PC1, PC3, PC5, and PC6 of the GM analyses. The changes seen in both methods in the mandibular angle, where the high dosage groups exhibit a more pronounced angle both posteriorly and inferiorly, are also mirrored. These results further demonstrate an overall change in shape in the 25-day sample that supports the overarching and secondary hypotheses: individuals exposed to maternal thyroxine demonstrate shape changes of the mandible in both an age- and dose-dependent manner, and these changes do affect the areas of muscle attachment.

Furthermore, the CVA analysis with GM can be compared to the overall shape changes seen with both EDMA and the PCA. The CVA results show a pronounced superior rotation of the anterior mandible in all three CV's (Figure 41). These results mirror those of the EDMA and PCA results, and are again suggestive of compensatory growth of the mandible in relation to shape changes of the cranial base. The CVA results regarding the mandibular angle also support those seen in the other methods, indicating that maternal thyroxine affects this area of the mandible, either through increased action of the masseter, changes in the bone itself, or a combination of both.

4.1.4 Overall Shape Changes and Existing Literature

Unfortunately, very little is known regarding shape changes of the craniofacial complex in regards to maternal thyroid levels; in light of this shortfall, orthodontic and dental research can be used as a predictive model for changes in mandibular shape as a result of shape changes elsewhere in the cranial base. The results described above demonstrate that thyroxine affects change on the mandible in both an age- and dose-dependent manner. As such, the 25-day high dose sample is a prime model for the overall effect of maternal thyroxine on the offspring mandible, as it displayed the most marked shape changes of any tested group. Preliminary studies of cranial base shape variation in the same samples 20-specimens suggest altered shape, especially in regard to the anterior aspect of the skull and maxilla (Cray, *unpublished*). These findings, particularly with individuals receiving higher doses of levothyroxine, should lead to a compensatory rotation of the anterior mandible to maintain occlusion (Moss and Rankow 1968; Enlow 1982).

The high dosage of thyroxine results in a pronounced superior rotation of the anterior aspect of the mandible, particularly the root of the incisor, towards the cranial base. Prior studies in orthodontics and dentistry have shown that rotation of this sort is primarily the result of response growth to maintain occlusion (Lavergne and Gasson 1976; Baumrind, Korn, and West 1984). The chin of the mouse is an area known to respond to changes elsewhere in the mandible (Atchley, Plummer, and Riska 1985). This rotation therefore suggests that the anterior aspect of the mandible is *responding* to growth elsewhere. The primary area of growth in the mandible is at the condyle and along the margin of the ramus (Petrovich 1974; Enlow 1982), so one would expect these areas to be changing as well. Indeed, there are demonstrable changes in the mediolateral position of the condyles, particularly in PC3 and PC7 of the 25-day sample; these two PC's showed a marked movement of the condyle *towards* the midline. Within the 20-day group, the location of the glenoid fossae narrowed, moving towards the midline of the cranial base, which would also affect the location of the mandibular condyles within the present study (Cray, *unpublished*).

Since no data exist regarding the role of thyroxine on areas of muscle attachment of the mandible, biomechanical research provides the only parallel with which to compare the present sample. The mandibular angle is formed in response to biomechanical stress placed upon it by the masseter and medial pterygoid muscles (Moss and Rankow 1968). As such, any alteration to this musculature would result in shape changes in this area. Reduced masseter function results in reduced mandibular angle, though it is also tied to reduced condylar formation and reduction of the posterior aspect of the ramus (Yonemitsu, Muramoto, and Soma 2007). Both the EDMA and GM results of the present study show an *increase* in size of the mandibular angle with increased dosage in younger ages, followed by a reduction in the 25-day sample (analogous to the early adult period in humans). The reduction in size of mandibular angle in the younger populations could be

tied to changes in masticatory habits or changes in biomechanical load, as these have been shown to reduce masseter size in animal models (Maeda et al. 1987; Widmer, Morris-Wiman, and Nekula 2002). The calvarial sample of the 20-day population of this group showed a narrowing of the zygomatic arch (Parsons et al. 2015), which may not necessarily alter the function of the masseter. The shape changes in the mandibular angle in this study thus remain an enigma, as little is known concerning alteration of zygomatic orientation on the function of the masseter muscle.

The final area of shape change seen in the mandibular sample is of the coronoid process. Both the EDMA and GM results demonstrated an overall reduction in size of the coronoid process as a function of dosage and age. This is assumed to be associated with a reduction in biomechanical load exerted by the temporalis (Moss 1997a; Enlow 1990). The cause of this reduction is not readily apparent, though the same sample (20-day, high dosage) exhibited a reduced vault height (Cray, *unpublished*). Should it be shown that the thyroxine is targeting calvarial bone growth, thus reducing either the attachment area of the temporalis or the area of the zygomatic arch, it would alter the size of the temporalis muscle, leading to corresponding reduction in the coronoid process. Further study on both the muscle attachment sites of the skull and muscle mass of the temporalis is needed to better describe the effect of maternal thyroxine, though an overall reduction in muscle area caused by a reduced cranial vault height remains a plausible explanation.

The shape changes observed in the present study, most pronounced in the 25-day high dosage sample, are suggestive of growth in response to shape changes in the cranial vault. Excess maternal thyroxine has been linked to changes in endochondral bone formation, including the cranial base (Hall 1973; Hanken and Summers 1988; Allan et al. 2000; Cray et al. 2013). The movement of the mandible towards the midline and superior rotation of the anterior mandible towards the cranial base are expected in light of mirror changes in the cranial base within the same

sample (Cray, *unpublished*). The shape changes in the mandibular angle are more difficult to explain, as the region is larger in size in the 15- and 20-day samples, and smaller in the 25-day sample. These changes could be tied to masticatory habits, shape changes of the zygomatic arch, or another unanticipated change in the sample, but cannot be easily explained in the thyroxine-exposed sample.

4.1.5 Strengths and Limitations

There are a number of strengths with the present study. First and foremost the overarching question of the role of maternal thyroxine levels on offspring craniofacial development. Despite a number of promising new studies, there is a paucity of literature regarding the role of maternal environment of mandibular development. Along these lines, this study also paves the way for future research further examining the nature of mandibular changes in direct response to cranial base shape changes, the role of thyroxine on masticatory muscles and the concomitant changes to occlusion and mastication, and other potential confounding factors affecting shape changes in the mandible. Finally, this research adds to existing literature regarding normal variation; with such a high prevalence of maternal thyroid issues, the resulting shape changes in the craniofacial complex of offspring (both mice and human) stands to account for part of the overall variation seen within a population.

This study was faced with multiple limitations commonly associated with biological and statistical projects. The primary limitation of this study is that of sample size. Large sample sizes in the 25-day sample allowed for adequate power to evaluate the proposed hypotheses. However, due to both data loss and sample damage amongst some groups, the sample sizes of the 15- and 20

day samples were smaller than anticipated. Limitations to the present study also exist regarding the nature of the sample images and the software used to evaluate landmark data. While Amira is designed to work with high-resolution micro-CT scans, both MorphoJ and EDMA require only landmark data in different formats. This requires careful manipulation of micro-CT images and their respective scaling, and second-hand review of these data can introduce errors to the software programs. This is the likeliest explanation of the EDMA errors encountered during this research; had these errors been systemic throughout the dataset, both the EDMA and GM samples would demonstrate extreme variance within the sample. However, the GM data *did not* show the same errors in the 15-day control group that precluded EDMA analysis of the sample.

The basic nature of geometric morphometrics, which scales data using Procrustes superimposition, means that it is capable of dealing with a number of different shapes and configurations of landmark data. However, GM does not adequately deal with *nuisance factors*, or variables in the sample that are not of interest yet still alter the overall shape of the sample (e.g., behavioral changes, environmental differences). Simply put, GM does not eliminate all nuisance factors within a dataset; rather, the fitting of data to a single coordinate system simply forces any nuisance parameters within the dataset in to a single shape (Lele and Richtsmeier 2001). This means that many factors that *could* be affecting the population may be omitted from analysis.

4.1.6 Future Directions

Geometric morphometric studies are on the rise in both the anthropological and clinical literature. The ability to evaluate shape changes are especially appealing for those interested in evolutionary comparisons both between and within species, both past and present (Viòarsdóttir,

O'Higgins, Paul, and Stringer 2002; Viòarsdóttir and O'Higgins 2003). In particular, studies of mandibular form shed light on form and functional changes in the past (Thayer and Dobson 2010; Pampush and Daegling 2016). Shape studies add a powerful lens with which to evaluate studies of paleoanthropological populations that have traditionally been analyzed using linear measurements alone (*see* Kesterke and Ahern 2007). The added tool of GM studies will no doubt continue to add to the understanding of past hominin population, and the added linear measurement methodology afforded by EDMA will help temper the shape-only results of the GM process.

Contemporary mandibular research still exists primarily in the dental and orthodontic literature, but its applicability to broader fields is readily apparent. Many studies have evaluated some of the proposed hypotheses regarding mandibular and chin formation in primate populations (Hylander 1979; Hylander 1984; Lieberman 2011), but the fact that the human chin is still a popular topic of both academic and popular debate highlights the enigma of its formation and function (Pampush and Daegling 2016). This project utilizes methods that may be used as a model for shape differences existing between different populations, be they extant primate or paleoanthropological, that have been proposed over the last decade (Schwartz and Tattersall 2000; Ichim, Swain, and Kieser 2006; Thayer and Dobson 2010; Garvin and Ruff 2012). A better understanding of both normal and abnormal mandibular development facilitates a fuller understanding of evolutionary and medical implications of craniofacial growth and development.

Future studies should continue to look at the role of maternal thyroid and its impact on osteoblasts, osteoclasts, and overall bone maintenance in offspring. With the high prevalence in thyroid dysfunction both in the U.S. and abroad, a better understanding of these hormones and their role on bone growth is certainly an avenue of research in need of further study; these studies need not apply solely to bone and/or craniofacial development, and continued research on *all*

aspects of thyroid function are needed. Research on the maternal environment, the *only* environment of a human for their first nine months post-conception, are in dire need of scientific scrutiny. Studies of teratogens are common, but the role of maternal environment on the offspring in regards to normal human variation carries implications beyond the realm of biomedicine and in to anthropology and elsewhere.

APPENDIX A: AMIRA PROTOCOL

Appendix A includes the entire landmarking protocol for Amira. This protocol was utilized for each skull to visualize the mandible, landmark the mandible, and export these landmarks for further analysis.

A.1 LANDMARKING

The following protocol manual was used for the above dissertation to evaluate the shape changes of mouse mandibles exposed to heightened maternal thyroxine during pregnancy. The processes described herein will be updated throughout the dissertation project as needed.

A.1.1 FILE LOCATIONS AND NAMING CONVENTIONS

All micro-CT scan files are stored on the shared research servers at the University of Pittsburgh's Craniofacial and Dental Genetics Laboratory.

/Volumes/ResearchStudies/Twist Mouse/Thyrox/Amira

Each individual has three associated files:

-one AmiraMesh file that has been cleaned and filtered (.am file)
-one Gaussian smoothing filter script file (.hx)
-one landmark file for cranial vault script studies (.hx)

The cleaned and filtered AmiraMesh files (.am files) will be used for the mandibular shape analyses. Prior to the start of this project, the files were named according to their specimen number and are indicated as filtered files due to their names and are all ~45Mb is size (examples below):

759-filtered.am
177_female-filtered.am

There is no indication in the file name as to the age or treatment group of the specimen.

A.1.2 IMPORT AND VISUALIZING AMIRAMESH FILES

The .am files for this project have already been trimmed and filtered, so very little additional filtering is necessary. To begin visualization of the file, use the 'Open Data…" button in the Pool Window and select the desired AmiraMesh file. This will place a green object with the file name within the Pool Window. Clicking on this object will populate the Properties Window, displaying the file size and voxel size for the skull. To visualize the skull, select the object with the Pool Window and click the "IsoSurface" button. This will add a yellow object to the Pool Window, and click on this object will populate the Properties Window allowing for various visualization options. The objects for this project will be compactified (default selection), and threshold will be adjusted to best visualize the mandibles. **Ideally, a threshold of 42.0 will be used for this project.** Thresholds below this introduce a lot of noise to the visualization, particularly around the alveolar border of the incisors, and thresholds above this introduce opacity in the rendering, particularly in the thinner aspects of the posterior ramus (Figure A1). Thresholds will be adjusted if needed for each file, though it is not expected.

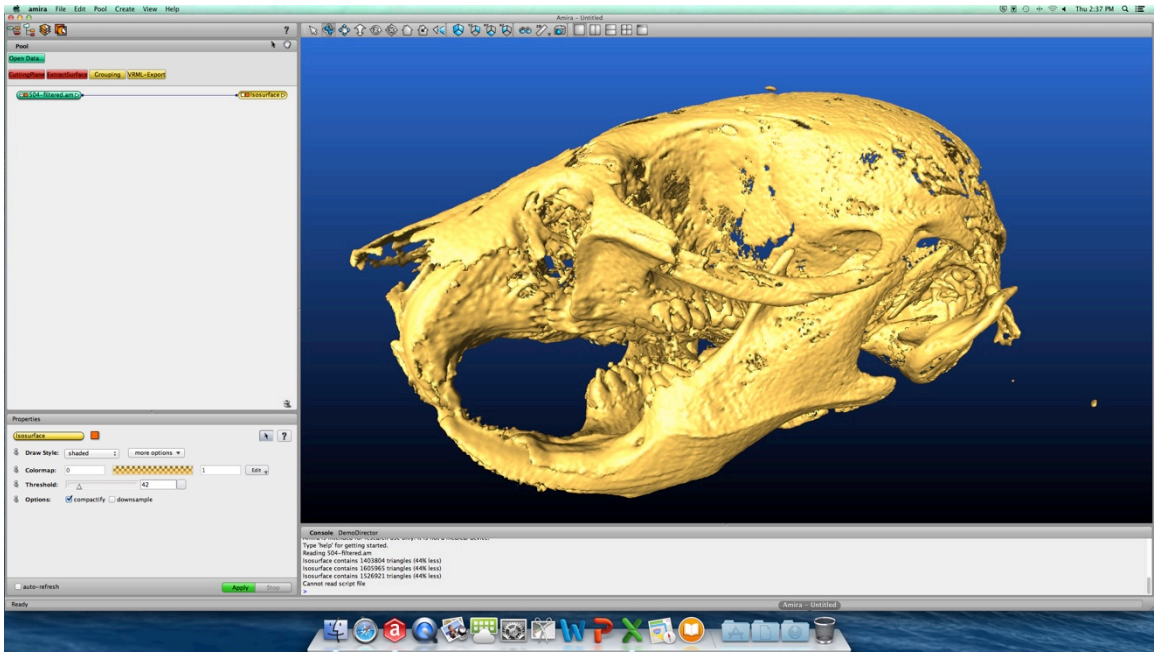

Figure A1. Setting a threshold and visualizing the AmiraMesh file.

Once a threshold has been entered, click on the green 'Apply' button in the Properties Window. The selected threshold for each mandible will be recorded on the master Excel file under the tab "Thresholds". If the thresholds are variable (e.g., one threshold for the alveolar landmarks and a different threshold for the condylar landmarks), it will be noted. The master Excel file for the thresholds is located in the directory:

/Volumes/ResearchStudies/Twist Mouse/Thyrox/Mandible Shape/Landmarking.xls

A.1.3 LANDMARKING THE MANDIBLE

Once the AmiraMesh file is loaded and an isosurface has been applied, landmarking can begin. To better visualize the location of each landmark, switch to 'Two Viewers' by clicking on the view change options above the rendering (Figure A2).

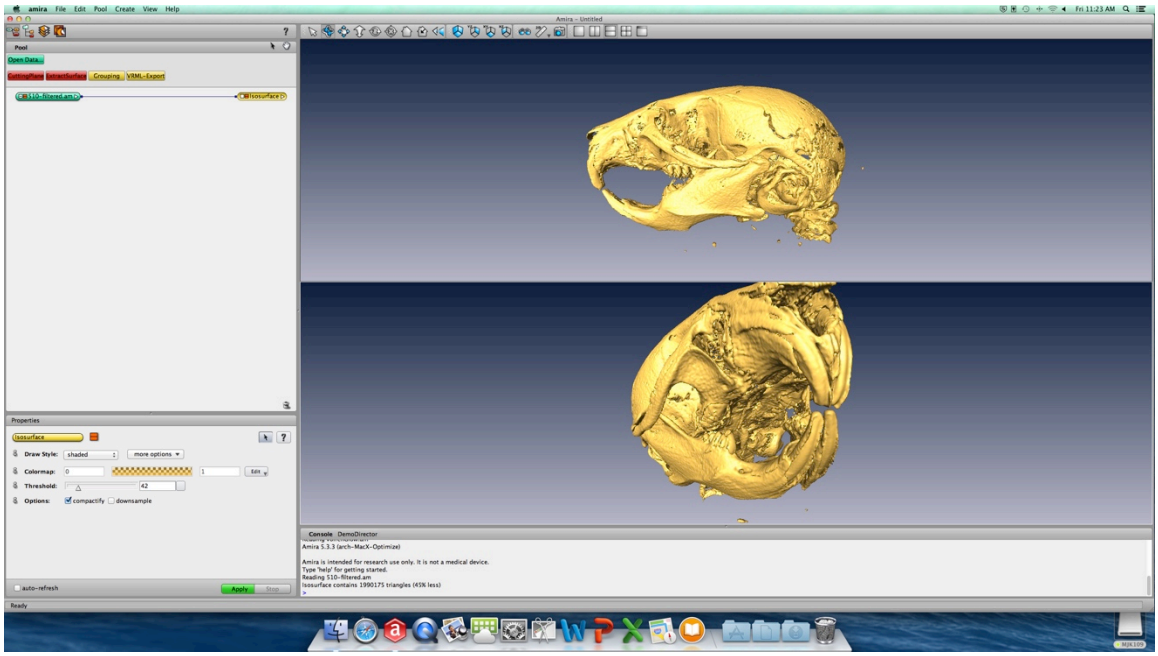

Figure A2. Views to Better Visualize the Data.

To begin landmarking, add a Landmarks object by right clicking in the Pool Window, highlighting ‘Create’, then ‘Data’, then click on ‘Landmarks’. This will add a green object called ‘Landmarks’ to the Pool Window. Within the Properties Window, click ‘Landmark Editor’ to create ’Landmark View’ object (Figure A3).

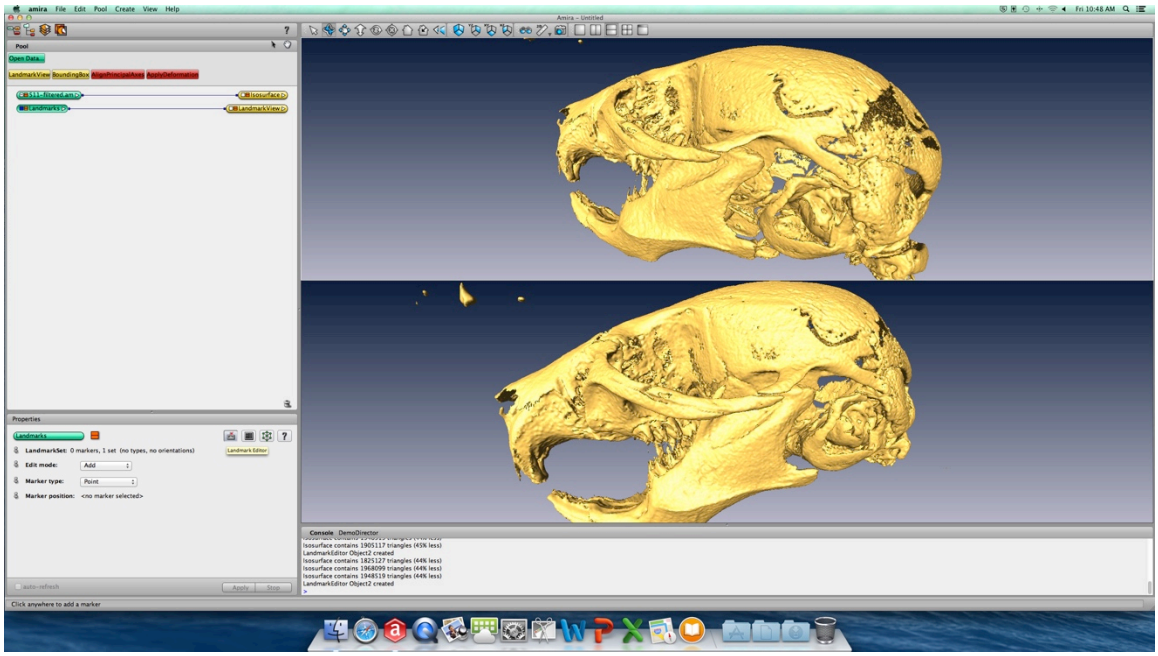

Figure A3. Creating a Landmark Object.

Within the Properties Window, be sure that Edit Mode is set to ‘Add’ and that the Interact cursor is selected in the Viewer. You can then begin to add landmarks to the mandible (Figure A4). You will need to alternate between the two viewers, the Interact cursor, and the Trackball cursor to accurately place the necessary landmarks. It may also be necessary to reduce the size of the landmarks in order to better visualize their placement; this can be done my clicking on the ‘Landmark View’ object and reducing the Size down to 0.5 within the Properties Window.

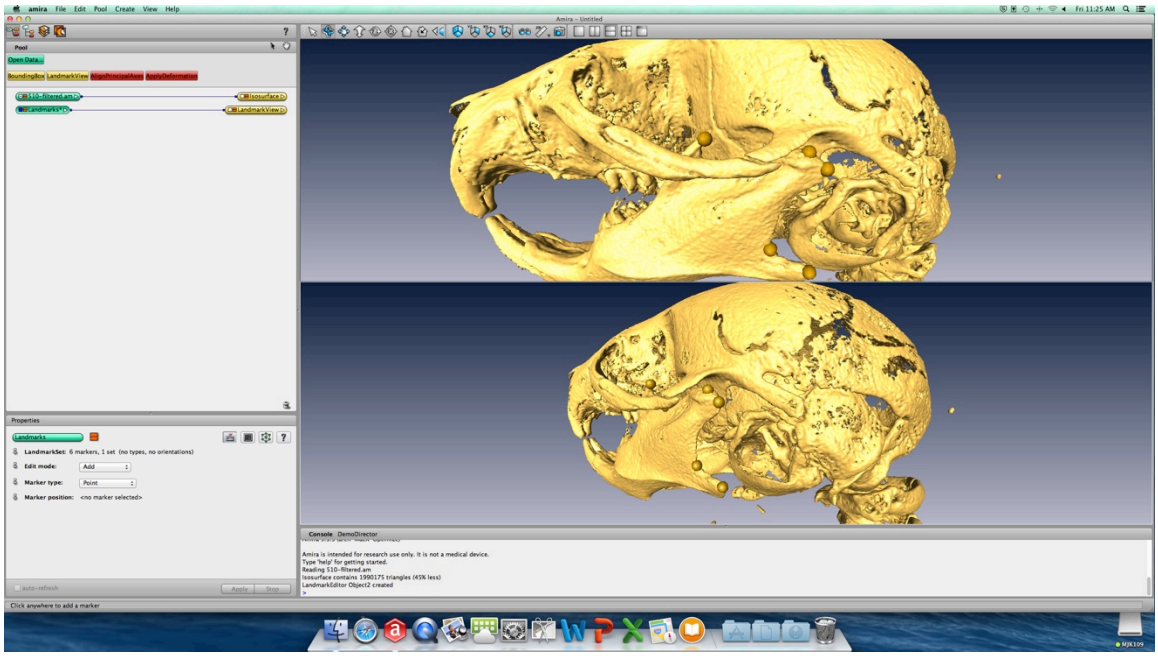

Figure A4. Placing Landmarks on the Mandible.

The order in which the landmarks are place is very important, and must be the same for each mandible. Placing the landmarks in the incorrect order will result in errors for both the EDMA and geometric morphometric analyses. For the purpose of this study, the left mandible will be landmarked first, and landmarks on the right mandible will be placed second (Table A1). **Multiple foramina:** in the event of multiple foramina, the anterior most foramen will be landmarked.

Table A1. Order of Mandibular Landmarks.

Side	Landmark Number	Landmark
Left	1	Anterior superior incisor alveolar rim (midline)
	2	Anterior edge of mental foramen
	3	Anterior edge molar alveolar rim (midline)
	4	Intersection molar alveolar rim and coronoid process
	5	Apex of coronoid process
	6	Posterior base of coronoid process (midline)
	7	Anterior edge of mandibular condyle (midline)
	8	Posterior edge mandibular condyle (midline)
	9	Most anterior point of subcondylar incisive
	10	Posterior tip of mandibular angle
	11	Most superior point of inferior border of mandibular angle
	12	Anterior edge of inferior border of masseteric ridge
	13	Most inferior point on mandibular symphysis
	14	Anterior inferior incisor alveolar rim (midline)
	15	Anterior edge of mandibular foramen
	16	Anterior edge ramal fossa foramen
	17	Most posterior point along molar alveolar border
Right	18	Anterior superior incisor alveolar rim (midline)
	19	Anterior edge of mental foramen
	20	Anterior edge molar alveolar rim (midline)
	21	Intersection molar alveolar rim and coronoid process
	22	Apex of coronoid process
	23	Posterior base of coronoid process (midline)
	24	Anterior edge of mandibular condyle (midline)
	25	Posterior edge mandibular condyle (midline)
	26	Most anterior point of subcondylar incisive
	27	Posterior tip of mandibular angle
	28	Most superior point of inferior border of mandibular angle
	29	Anterior edge of inferior border of masseteric ridge
	30	Most inferior point on mandibular symphysis
	31	Anterior inferior incisor alveolar rim (midline)
	32	Anterior edge of mandibular foramen
	33	Anterior edge ramal fossa foramen
	34	Most posterior point along molar alveolar border

A.1.4 EXPORTING LANDMARK DATA

Once the 34 landmarks are placed, they must be exported as an ASCII file for later import in to other software programs. To do so, right-click on the 'Landmarks', select 'Save Data As…" and save the landmark file in the following folder:

/Volumes/ResearchStudies/Twist Mouse/Thyrox/Mandible Shape/Mandible Landmarks

Files will be named according to their sample number, with underscores between identifiers:

511_mand_landmarks.ascii

This produces an Ascii file with coordinates that can be read by any text reader (Figure A5).

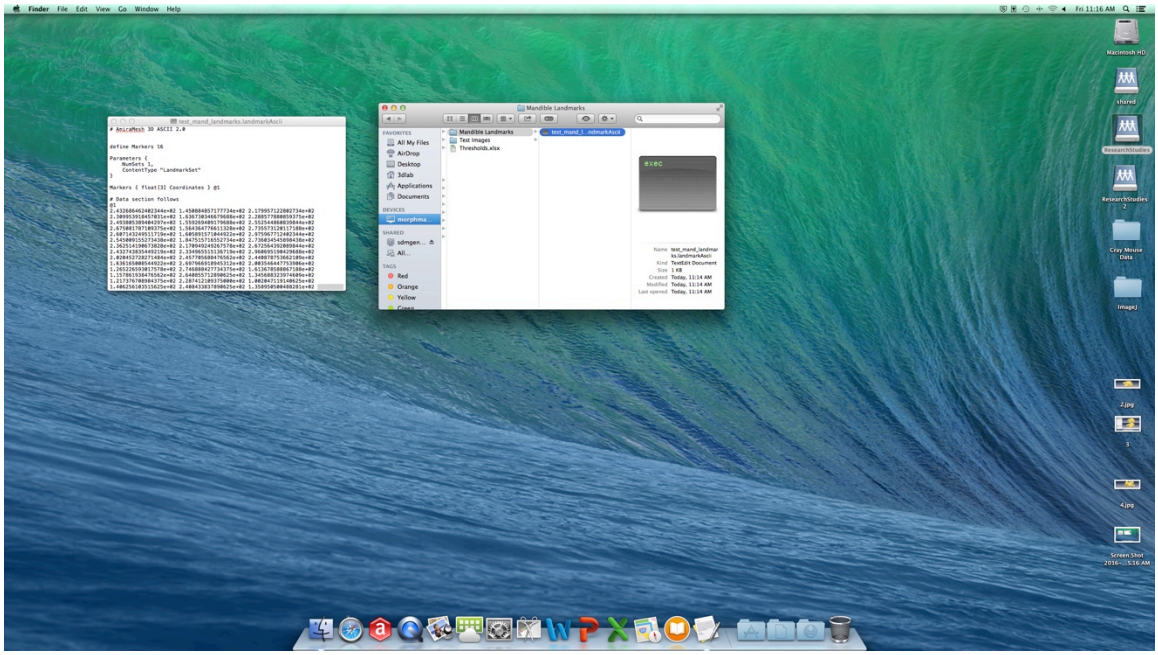

Figure A5. Example Ascii File.

The Amira network files (.hx files) will be saved in the same folder:

/Volumes/ResearchStudies/Twist Mouse/Thyrox/Mandible Shape/Mandible Landmarks

Files will be saved with the same filename as the associated landmark files (.ascii files):

511_mand_landmarks.hx

A.1.5 DEALING WITH MISSING DATA

In some instances, it may be necessary to omit a landmark from analysis. However, the exported landmarks in the Ascii file are only recorded in the order in which they are placed. Careful note must be taken when choosing to omit a landmark, and the output Ascii file must be updated accordingly. To do so, open the export file in a text editing program and insert ‘m m m’ in the place of the appropriate landmark (Figure A6). A space is necessary between each letter.

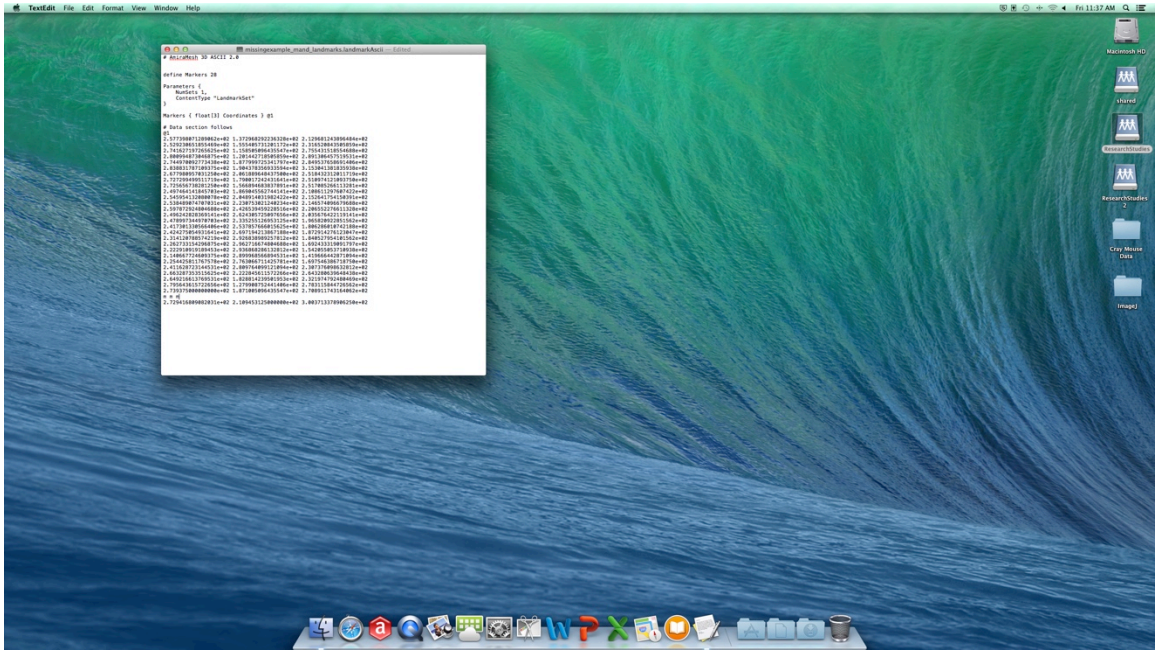

Figure A6. Dealing With Missing Data.

Any missing landmarks should also be noted on the master Excel file:

/Volumes/ResearchStudies/Twist Mouse/Thyrox/Mandible Shape/Landmarking.xls

Landmarks should only be omitted in cases where landmarks cannot be placed due to imaging issues due to threshold resolutions (e.g., alveolar border). In the event of damage to the mandible that alters overall shape in any way (e.g., fractures), or if imaging is unavailable, the entire mandible will be omitted from the study, though it will be noted in the master Excel file.

APPENDIX B: EDMA OUTPUTS

Appendix B consists of the complete EDMA output files. The following are the raw outputs used for the above dissertation to evaluate the shape changes of mouse mandibles exposed to heightened maternal thyroxine during pregnancy. The processes described herein will be updated throughout the dissertation project as needed. These results are discussed in detail in Chapter 3, Section 1.

Due to errors with the WINEDMA software, some of these files are incomplete, specifically many of the image outputs.

15-DAY SAMPLE

Mean shape-difference matrix for the 15-day samples: 15-day low dosage and 15-day high dosage.

	L1	*L2*	*L3*	*L4*	*L5*	*L6*	*L7*	*L8*	*L9*	*L10*	*L11*	*L12*	*L13*	*L14*	*L15*	*L16*
L1	0															
L2	0.3397	0														
L3	0.2517	0.0091	0													
L4	0.1028	-0.0051	-0.0210	0												
L5	-0.1120	0.0076	-0.0125	0.0070	0											
L6	-0.0628	0.0003	-0.0174	0.0029	0.0071	0										
L7	-0.1305	0.0375	0.0159	0.0349	0.0267	0.0269	0									
L8	-0.1628	0.0148	-0.0073	0.0102	0.0079	0.0013	-0.0181	0								
L9	0.0102	0.0213	-0.0011	0.0020	-0.0212	-0.0297	-0.0147	-0.0242	0							
L10	0.0164	0.0142	-0.0069	-0.0030	-0.0161	-0.0257	-0.0183	-0.0237	0.0001	0						
L11	0.1754	0.0393	0.0184	0.0066	-0.0133	-0.0252	-0.0055	-0.0280	-0.0072	-0.0238	0					
L12	0.3598	0.0183	-0.0047	-0.0307	-0.0205	-0.0346	0.0003	-0.0205	-0.0035	-0.0125	0.0071	0				
L13	0.4505	0.0099	0.0053	-0.0223	-0.0126	-0.0226	0.0091	-0.0139	0.0033	-0.0065	0.0163	0.0058	0			
L14	0.4150	-0.0281	-0.0122	-0.0331	-0.0213	-0.0284	0.0056	-0.0175	-0.0079	-0.0145	0.0101	-0.0023	0.0089	0		
L15	-0.0340	0.0208	0.0002	0.0135	-0.0109	-0.0164	0.0004	-0.0139	-0.0117	-0.0094	-0.0088	-0.0111	-0.0023	-0.0105	0	
L16	0.0833	0.0384	0.0230	0.0274	-0.0226	-0.0253	-0.0171	-0.0399	-0.0154	-0.0251	-0.0045	-0.0144	0.0011	0.0038	-0.0129	0

Z statistic: 0.45048

Confidence interval for Z with alpha = 0.100
Upper bound: 0.74987 Lower bound: -0.44808

Distribution of bootstrapped Z statistics

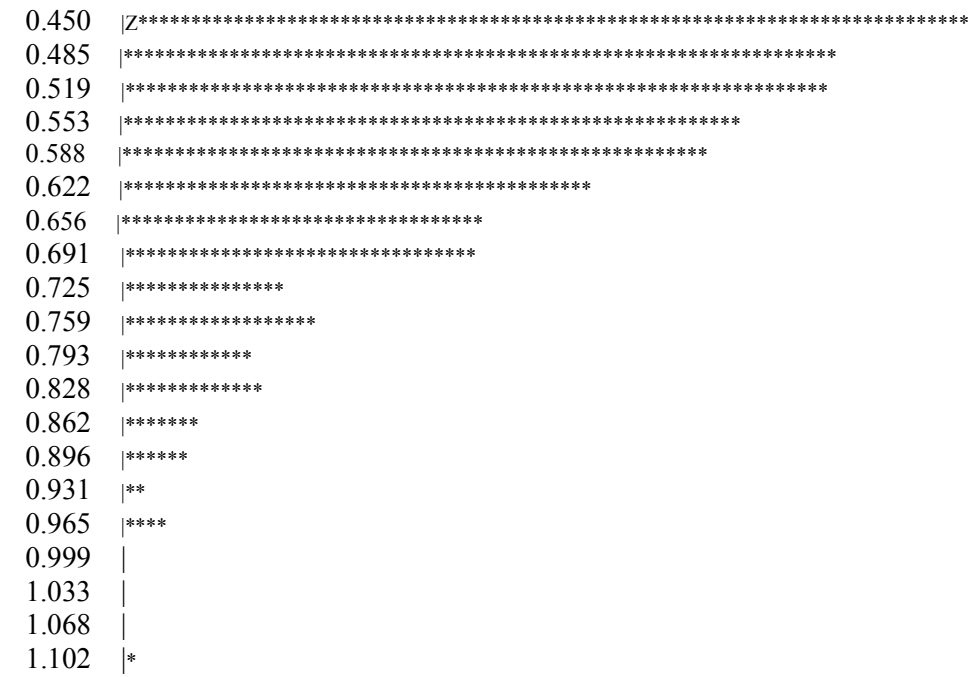

Confidence interval for scale difference with alpha = 0.100
Upper bound: 0.51477 Lower bound: -7.64195

Distribution of bootstrapped scale differences

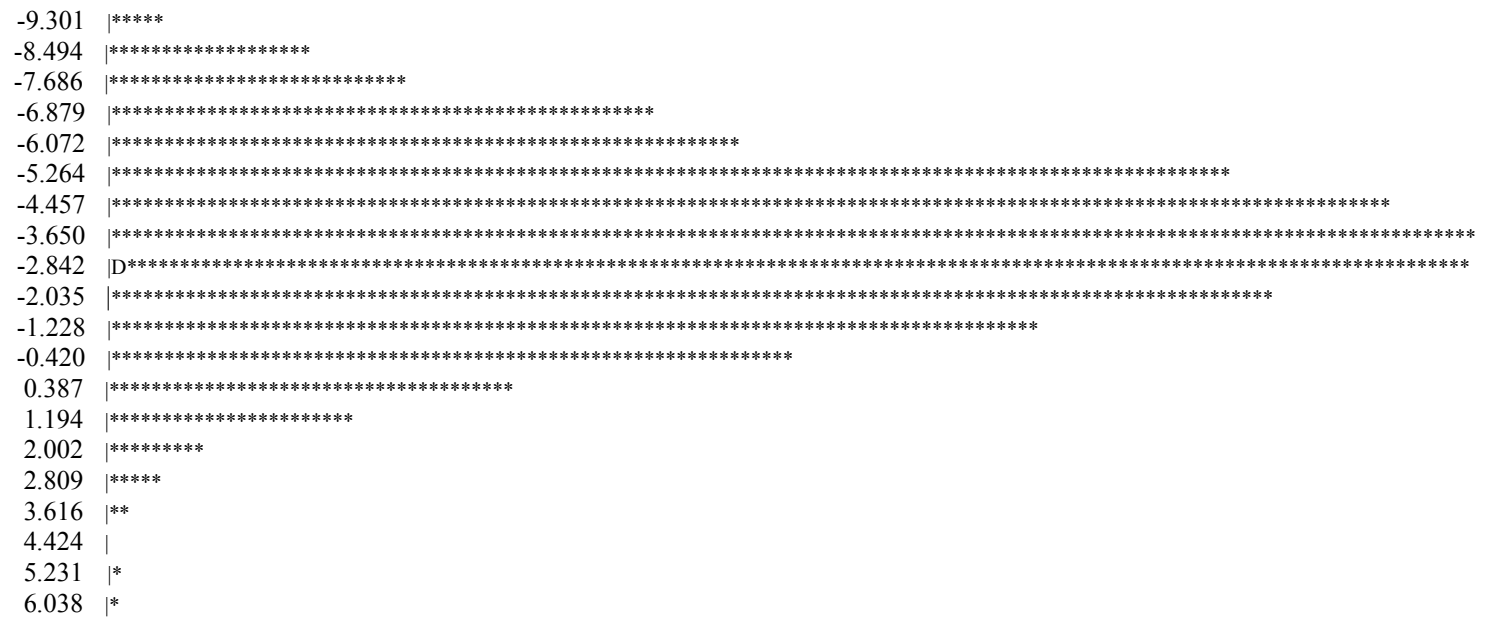

20-DAY SAMPLE

Mean shape-difference matrix for the 20-day samples: 20-day low dosage and 20-day high dosage.

	L1	*L2*	*L3*	*L4*	*L5*	*L6*	*L7*	*L8*	*L9*	*L10*	*L11*	*L12*	*L13*	*L14*	*L15*	*L16*
L1	0															
L2	0.2570	0														
L3	0.2819	0.0065	0													
L4	0.3003	0.0112	-0.0053	0												
L5	0.3335	0.0267	0.0113	0.0138	0											
L6	0.3365	0.0143	-0.0004	0.0020	0.0199	0										
L7	0.3270	0.0134	-0.0038	0.0016	-0.0162	-0.0129	0									
L8	0.3169	0.0128	-0.0056	0.0003	-0.0167	-0.0170	-0.0010	0								
L9	0.2704	0.0174	-0.0047	0.0003	-0.0082	-0.0273	-0.0074	-0.0084	0							
L10	0.2436	0.0059	-0.0167	-0.0115	-0.0188	-0.0369	-0.0137	-0.0117	-0.0105	0						
L11	0.2501	0.0047	-0.0157	-0.0067	0.0025	-0.0197	0.0015	0.0031	0.0105	0.0006	0					
L12	0.2298	0.0039	-0.0116	-0.0015	0.0111	-0.0077	0.0027	0.0027	0.0099	0.0003	-0.0019	0				
L13	0.2229	-0.0171	-0.0056	-0.0060	0.0068	-0.0080	-0.0039	-0.0048	-0.0009	-0.0110	-0.0119	-0.0142	0			
L14	0.2344	-0.0097	0.0073	0.0036	0.0182	0.0070	0.0054	0.0050	0.0105	0.0004	-0.0002	0.0019	0.0061	0		
L15	0.2974	0.0125	-0.0066	0.0012	0.0017	-0.0190	0.0053	0.0022	-0.0104	-0.0180	-0.0026	0.0000	-0.0075	0.0046	0	
L16	0.2991	-0.0036	-0.0169	-0.0229	-0.0071	-0.0285	-0.0065	-0.0066	-0.0251	-0.0319	-0.0369	-0.0221	-0.0095	-0.0018	-0.0237	0

Z statistic: 0.33652

Confidence interval for Z with alpha = 0.100
Upper bound: 0.56476 Lower bound: 0.14439

Distribution of bootstrapped Z statistics

Confidence interval for scale difference with alpha = 0.100
Upper bound: 2.23920 Lower bound: -4.37549

Distribution of bootstrapped scale differences

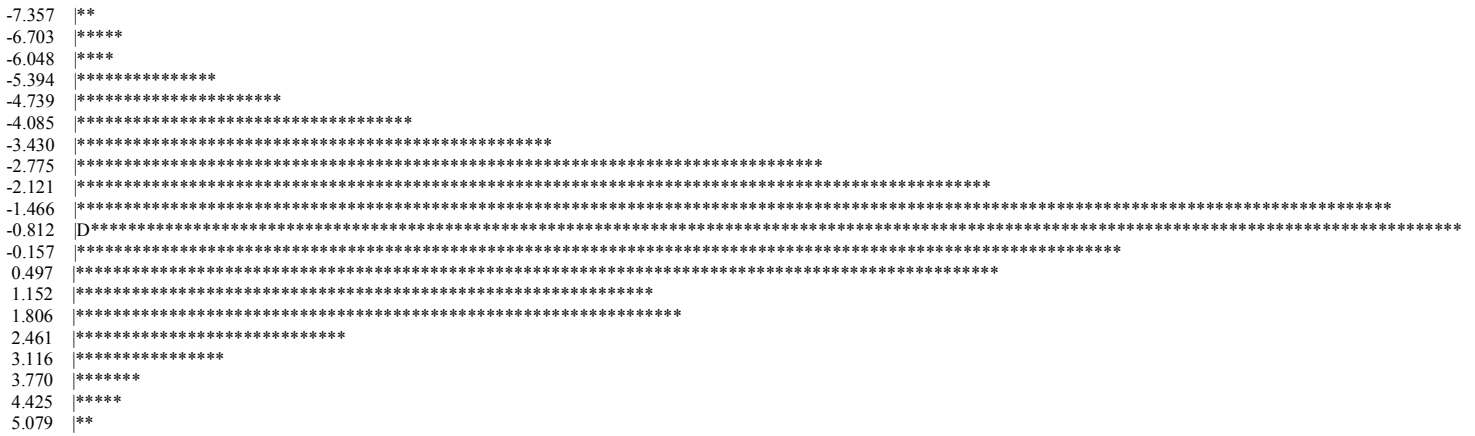

25-DAY SAMPLE

Mean shape-difference matrix for the 25-day samples: 25-day controls and 25-day high dosage.

	L1	*L2*	*L3*	*L4*	*L5*	*L6*	*L7*	*L8*	*L9*	*L10*	*L11*	*L12*	*L13*	*L14*	*L15*	*L16*
L1	0															
L2	0.1393	0														
L3	0.1514	-0.0079	0													
L4	0.2463	-0.0559	-0.0384	0												
L5	0.2631	-0.0575	-0.0466	0.0005	0											
L6	0.2768	-0.0469	-0.0334	0.0087	0.0004	0										
L7	0.3283	-0.0477	-0.0336	0.0049	0.0044	-0.0091	0									
L8	0.3896	-0.0502	-0.0341	-0.0021	0.0003	-0.0155	-0.0033	0								
L9	0.3612	-0.0085	0.0100	0.0178	-0.0040	-0.0100	-0.0129	-0.0305	0							
L10	0.4400	0.0058	0.0280	0.0363	0.0316	0.0222	0.0278	0.0102	0.0261	0						
L11	0.3287	-0.0600	-0.0316	-0.0239	0.0014	-0.0040	0.0179	0.0206	0.0602	0.0692	0					
L12	0.2418	-0.0198	0.0019	-0.0355	-0.0293	-0.0263	-0.0190	-0.0205	0.0202	0.0289	-0.0410	0				
L13	0.1730	0.0089	0.0078	-0.0407	-0.0406	-0.0329	-0.0305	-0.0312	0.0115	0.0217	-0.0474	-0.0069	0			
L14	0.1105	0.0122	0.0012	-0.0417	-0.0446	-0.0336	-0.0358	-0.0388	0.0006	0.0114	-0.0578	-0.0231	-0.0149	0		
L15	0.3624	-0.0366	-0.0148	0.0142	0.0227	0.0116	0.0177	-0.0040	-0.0250	0.0115	0.0089	-0.0203	-0.0237	-0.0265	0	
L16	0.3164	-0.0430	-0.0204	-0.0035	-0.0063	-0.0082	-0.0007	-0.0018	0.0303	0.0502	0.0043	-0.0191	-0.0313	-0.0352	0.0122	0

Z statistic: 0.43995

Confidence interval for Z with alpha = 0.100
Upper bound: 0.66977 Lower bound: 0.20294

Distribution of bootstrapped Z statistics

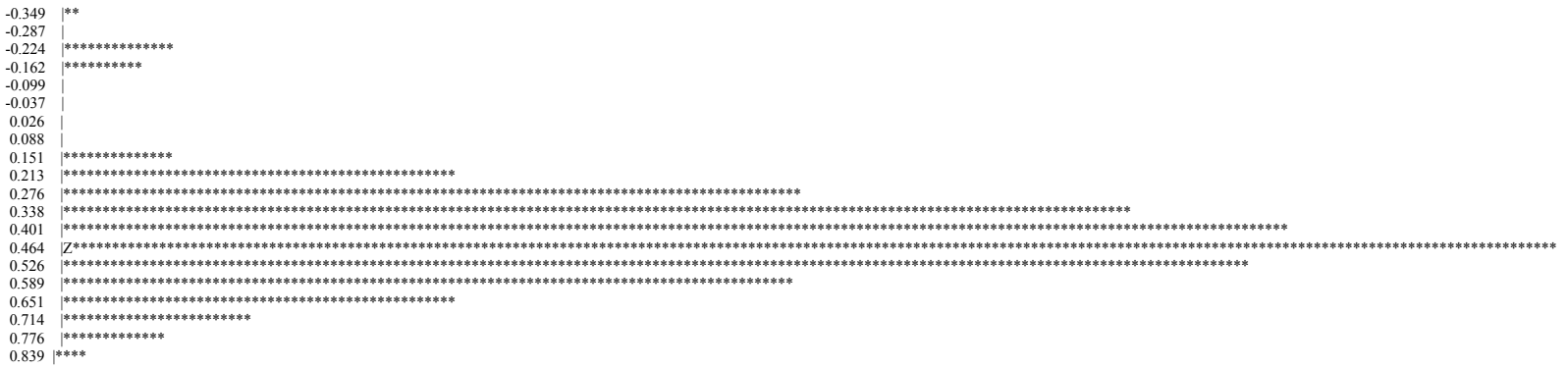

Confidence interval for scale difference with alpha = 0.100
Upper bound: 3.29279 Lower bound: -2.14588

Distribution of bootstrapped scale differences

APPENDIX C: GM OUTPUTS

Appendix C consists of the complete GM output files. These results are discussed in detail in Chapter 3, Section 2.

15-DAY SAMPLE

16 landmarks in 3 dimensions.
The dataset contains 49 observations, of which 49 are included for analyses.

Average shape:

Lmk.	Axis 1 (x)	Axis 2 (y)	Axis 3 (z)
1	-0.39043345	-0.00690972	-0.11172318
2	-0.23168044	0.02555497	-0.00866892
3	-0.18312336	0.00677576	-0.04896145
4	-0.02061470	0.00535360	-0.07405625
5	0.17362234	0.01130879	-0.16503202
6	0.13261984	0.00446730	-0.11688368
7	0.26664866	-0.00590003	-0.08863012
8	0.34874882	-0.00566006	-0.02559787
9	0.18525102	0.01546282	0.08613556
10	0.24061486	0.01065218	0.17256918
11	0.04976878	0.00375153	0.12953130
12	-0.13257365	0.01157993	0.13259618
13	-0.29533547	-0.02298626	0.09827937
14	-0.36023206	0.00859040	-0.00339237
15	0.17570233	0.00250008	0.00795654
16	0.04101648	-0.06454128	0.01587775

Procrustes sums of squares: 0.06789081012623971
Tangent sums of squares: 0.06778606133309208

PC	Eigenvalues	% Variance	Cumulative %
1.	0.00025826	18.288	18.288
2.	0.00022402	15.863	34.151
3.	0.00015834	11.212	45.363
4.	0.00011954	8.465	53.828
5.	0.00009445	6.688	60.516
6.	0.00008003	5.667	66.183
7.	0.00006953	4.923	71.106
8.	0.00006227	4.409	75.515
9.	0.00004930	3.491	79.007
10.	0.00004214	2.984	81.990
11.	0.00003031	2.146	84.137
12.	0.00002594	1.837	85.973
13.	0.00002201	1.558	87.532
14.	0.00002050	1.451	88.983
15.	0.00001897	1.343	90.326
16.	0.00001804	1.277	91.603
17.	0.00001508	1.068	92.671
18.	0.00001412	1.000	93.671
19.	0.00001254	0.888	94.559
20.	0.00001027	0.727	95.286
21.	0.00000903	0.640	95.925
22.	0.00000809	0.573	96.498
23.	0.00000774	0.548	97.046
24.	0.00000694	0.492	97.538
25.	0.00000593	0.420	97.957
26.	0.00000537	0.380	98.337
27.	0.00000427	0.303	98.640
28.	0.00000362	0.256	98.896
29.	0.00000308	0.218	99.115
30.	0.00000256	0.182	99.296
31.	0.00000201	0.142	99.438
32.	0.00000161	0.114	99.553
33.	0.00000147	0.104	99.656
34.	0.00000134	0.095	99.752
35.	0.00000119	0.085	99.836
36.	0.00000079	0.056	99.892
37.	0.00000065	0.046	99.938
38.	0.00000033	0.024	99.962
39.	0.00000030	0.021	99.983
40.	0.00000014	0.010	99.992
41.	0.00000011	0.008	100

Total variance: 0.00141221

20-DAY SAMPLE

16 landmarks in 3 dimensions.
The dataset contains 51 observations, of which 51 are included for analyses.

Average shape:

Lmk.	Axis 1 (x)	Axis 2 (y)	Axis 3 (z)
1	-0.38787621	0.10851161	-0.00379904
2	-0.22879119	0.00914619	0.02304849
3	-0.17667239	0.05116873	0.00500855
4	-0.01860061	0.07055633	0.00814633
5	0.17155322	0.16532403	0.01221474
6	0.13541255	0.11967449	0.00603246
7	0.26225086	0.08953251	-0.00740131
8	0.34953654	0.03319813	-0.00941033
9	0.19110534	-0.08984341	0.01411713
10	0.24538655	-0.18327864	0.01083837
11	0.03385534	-0.12832190	0.00502419
12	-0.13449114	-0.12829122	0.01072983
13	-0.29684765	-0.09230650	-0.02343650
14	-0.35990084	0.00105169	0.00691657
15	0.18081634	-0.01380278	0.00360562
16	0.03326328	-0.01231927	-0.06163512

Procrustes sums of squares: 0.06427403471189583
Tangent sums of squares: 0.06417702455186614

PC	Eigenvalues	% Variance	Cumulative %
1	0.0002016	15.706	15.706
2	0.00016911	13.176	28.882
3	0.00014799	11.53	40.412
4	0.00011177	8.708	49.12
5	0.00009384	7.311	56.431
6	0.00008296	6.464	62.894
7	0.00006438	5.016	67.91
8	0.00005346	4.165	72.075
9	0.00004964	3.867	75.943
10	0.00003753	2.924	78.867
11	0.00003412	2.658	81.525
12	0.00002999	2.337	83.862
13	0.00002567	2	85.862
14	0.00002454	1.912	87.774
15	0.00001957	1.525	89.299
16	0.00001932	1.505	90.804
17	0.00001586	1.236	92.039
18	0.00001309	1.02	93.059
19	0.00001165	0.908	93.967
20	0.00001126	0.877	94.844
21	0.0000087	0.678	95.522
22	0.00000827	0.644	96.167
23	0.00000765	0.596	96.763
24	0.000007	0.545	97.308
25	0.00000539	0.42	97.728
26	0.00000524	0.408	98.136
27	0.00000439	0.342	98.478
28	0.0000037	0.288	98.766
29	0.00000301	0.235	99.001
30	0.00000243	0.189	99.19
31	0.00000209	0.163	99.353
32	0.00000174	0.135	99.488
33	0.00000138	0.108	99.596
34	0.00000118	0.092	99.688
35	0.00000113	0.088	99.775
36	0.00000091	0.071	99.846
37	0.00000071	0.055	99.902
38	0.00000052	0.041	99.942
39	0.00000042	0.032	99.975
40	0.00000021	0.016	99.991
41	0.00000011	0.009	100

Total variance: 0.00128354

25-DAY SAMPLE

16 landmarks in 3 dimensions.
The dataset contains 118 observations, of which 118 are included for analyses.

Average shape:

Lmk.	Axis 1 (x)	Axis 2 (y)	Axis 3 (z)
1	-0.38248254	0.10649700	-0.00166561
2	-0.22857047	0.01141904	0.02182663
3	-0.17772298	0.05463452	0.00449788
4	-0.01881461	0.06839945	0.00791435
5	0.17330237	0.17174151	0.01200489
6	0.13515389	0.12191013	0.00505780
7	0.25836397	0.09364936	-0.00808090
8	0.34759856	0.02916161	-0.00928708
9	0.19534065	-0.09570148	0.01107281
10	0.25218099	-0.18499150	0.01364858
11	0.02760078	-0.12666285	0.00412673
12	-0.13514867	-0.12815150	0.01090576
13	-0.29477268	-0.09384553	-0.02445665
14	-0.36040843	-0.00129879	0.00717077
15	0.17739835	-0.01374064	0.00463199
16	0.03098081	-0.01302032	-0.05936795

Procrustes sums of squares: 0.1426041554143566
Tangent sums of squares: 0.14238834520171426

PC	Eigenvalues	% Variance	Cumulative %
1	0.00020352	16.724	16.724
2	0.00016926	13.908	30.631
3	0.00011288	9.275	39.907
4	0.00009083	7.464	47.37
5	0.000077	6.327	53.698
6	0.00006842	5.622	59.32
7	0.00006427	5.281	64.601
8	0.0000532	4.371	68.972
9	0.00004156	3.415	72.387
10	0.00003596	2.954	75.341
11	0.00003181	2.614	77.955
12	0.00002813	2.311	80.266
13	0.00002458	2.02	82.286
14	0.00002357	1.936	84.222
15	0.00002207	1.814	86.036
16	0.0000163	1.34	87.376
17	0.00001571	1.291	88.667
18	0.00001465	1.204	89.871
19	0.00001337	1.099	90.97
20	0.00001176	0.966	91.936
21	0.00001078	0.885	92.821
22	0.00000981	0.806	93.628
23	0.00000886	0.728	94.356
24	0.00000811	0.666	95.022
25	0.00000678	0.557	95.579
26	0.00000643	0.528	96.107
27	0.00000596	0.489	96.597
28	0.00000506	0.416	97.013
29	0.00000459	0.377	97.39
30	0.00000432	0.355	97.745
31	0.00000422	0.347	98.092
32	0.00000366	0.301	98.392
33	0.00000349	0.287	98.679
34	0.00000286	0.235	98.914
35	0.0000028	0.23	99.145
36	0.00000225	0.185	99.33
37	0.00000211	0.173	99.503
38	0.00000189	0.155	99.658
39	0.00000164	0.135	99.793
40	0.00000151	0.124	99.917
41	0.00000101	0.083	100

Total variance: 0.00121699

BIBLIOGRAPHY

Adams, Dean C., F. James Rohlf, and Dennis E. Slice
2013a Geometric Morphometrics: Ten Years of Progress Following the "revolution." Italian Journal of Zoology 71: 5–16.
2013b A Field Comes of Age: Geometric Morphometrics in the 21st Century. Hystrix, The Italian Journal of Mammalogy 24: 7–14.

Adler, Clause-Peter
2000 Bone Diseases: Macroscopic, Histological, and Radiological Diagnosis of Structural Changes in the Skeleton. Berlin: Springer.

Aldersey-Williams, Hugh
2013 Anatomies: A Cultural History of the Human Body. New York: W.W. Norton & Company.

Allan, W.C., J.E. Haddow, G.E. Palomaki, et al.
2000 Maternal Thyroid Deficiency and Pregnancy Complications: Implications for Population Screening. Journal of Medical Screening 7: 127–130.

Antón, Susan C.
2002 Evolutionary Significance of Cranial Variation in Asian Homo Erectus. American Journal of Physical Anthropology 118(4): 301–323.

Argiropoulos, B., and R.K. Humphries
2007 Hox Genes in Meatopoieses and Leukemogenesis. Oncogene 26: 6766–6776.

Atchley, William R., A. Alison Plummer, and Bruce Riska
1985 Genetics of Mandible Form in the Mouse. Genetics 111(3): 555–577.

Baker, Lawrence W.
1922 The Influence of the Forces of Occlusion on the Development of the Bones of the Skull. International Journal of Orthodontia, Oral Surgery and Radiography 8(5): 259–281.

Ballock, Tracy, and Regis J. O'Keefe
2003 The Biology of the Growth Plate. The Journal of Bone and Joint Surgery 85A: 715–726.

Bateson, William
1902 Variation and Differentiation in Parts and Brethren. Cambridge: Cambridge University Press.

Baumrind, Sheldon, Edward L. Korn, and Eugene E. West
1984 Prediction of Mandibular Rotation: An Empirical Test of Clinician Performance. American Journal of Orthodontics 86(5): 371–385.

Begg, P. Raymond
1954 Stone Age Man's Dentition: With Reference to Anatomically Correct Occlusion, the Etiology of Malocclusion, and a Technique for Its Treatment. American Journal of Orthodontics 40(4): 298–312.

Bejdová, S., V. Krajíček, J. Velemínská, M. Horák, and P. Velemínsky
2013 Changes in the Sexual Dimorphism of the Human Mandible during the Last 1200 Years in Central Europe. HOMO- Journal of Comparative Human Biology 64: 437–453.

Bhaskar, S.N., J.P. Weinmann, and I. Schour
1952 Role of Meckel's Cartilage in the Development and Growth of the Rat Mandible. Journal of Dental Research 32: 398–410.

Bjöek, Arne
1951 The Principle of the Andresen Method of Orthodontic Treatment, a Discussion Based on Cephalometric X-Ray Analysis of Treated Cases. American Journal of Orthodontics 37(6): 437–458.

Björk, Arne
1951 A Discussion on the Significance of Growth Changes in Facial Pattern and Their Relationship to Changes in Occlusion. The Dental Record 71: 197–208.
1953 Bite Development and Body Build. The Dental Record 75: 779–801.
1955 Facial Growth in Man, Studied with the Aid of Metallic Implants. Acta Odontologica Scandinavica 13: 9–34.
1963 Variations in the Growth Pattern of the Human Mandible: Longitudinal Radiographic Study by the ImplantMethod. Journal of Dental Research 42: 400–411.
1968 The Use of Metallic Implants in the Study of Facial Growth in Children: Method and Application. American Journal of Physical Anthropology 29: 243–254.

Björk, Arne, and Vibeke Skieller
1983 Normal and Abnormal Growth of the Mandible. A Synthesis of Longitudinal Cephalometric Implant Studies over a Period of 25 Years. The European Journal of Orthodontics 5: 1–46.

Bookstein, Fred L.
1991 Morphometric Tools for Landmark Data: Geometry and Biology. Cambridge: Cambridge University Press.

Boskey, Adele L.
1999 Mineralization, Structure, and Function of Bone. *In* Dynamics of Bone and Cartilage

Metabolism. Markus J. Seibel, Simon P. Robins, and John P. Bilezikian, eds. Pp. 153–164. San Diego: Academic Press.

Boyle, William J., W. Scott Simonet, and David L. Lacey
2003 Osteoclast Differentiation and Activation. Nature 423: 337–342.

Brickley, Megan, and Rachel Ives
2006 Skeletal Manifestations of Infantile Scurvy. American Journal of Physical Anthropology 129: 163–172.

Brixen, Kim, and Erik F. Eriksen
1999 Validation of Local and Systemic Markers of Bone Turnover. *In* Dynamics of Bone and Cartilage Metabolism. Markus J. Seibel, Simon P. Robins, and John P. Bilezikian, eds. Pp. 427–436. San Diego: Academic Press.

Browne, Marilyn L., Sonja A. Rasmussen, Adrienne T. Hoyt, et al.
2009 Maternal Thyroid Disease, Thyroid Medication Use, and Selected Birth Defects in the National Birth Defects Prevention Study. Birth Defects Research 85: 621–628.

Bruder, Scott P., David J. Fink, and Arnold I. Caplan
1994 Mesenchymal Stem Cells in Bone Development, Bone Repair, and Skeletal Regeneration Theory. Journal of Cellular Biochemistry 56: 283–294.

Burrow, G.N., D.A. Fisher, and P.R. Larsen
1994 Maternal and Fetal Thyroid Function. The New England Journal of Medicine 331: 1072–1078.

Canaris, Gay J., Neil R. Manowitz, Gilbert Mayor, and E. Chester Ridgway
2000 The Colorado Thyroid Disease Prevalence Study. Archives of Internal Medicine 160: 526–534.

Caplan, A.I., and B.D. Boyan
1994 Endochondral Bone Formation: The Lineage Cascade. Bone 8: 1–46.

Carlisle, R.C., and M.I. Siegel
1974 Some Problems in the Interpretation of Neanderthal Speech Capabilites: A Reply to Lieberman. American Anthropologist 76: 319–322.

Carlson, David S.
2005 Theories of Craniofacial Growth in the Postgenomic Era. Seminars in Orthodontics 11: 172–183.

Carter, D.R., M.C.H. van der Meulen, and G.S. Beaupré
1996 Mechanical Factors in Bone Growth and Development. Bone 18 (Supplement): 5S–10S.

Casey, Brian M., and Kenneth J. Leveno
2006 Thyroid Disease in Pregnancy. Obstetrics and Gynecology 108: 1283–1292.

Claude, Julien
2008 Morphometrics in R. New York: Springer.

Cole, David E.C., and M. Michael Cohen
1990 Mutations Affection Bone-Forming Cells. *In* Bone: The Osteoblast and Osteocyte. Brian K. Hall, ed. Pp. 431–487. Caldwell: The Telford Press.

Cole, T.M.
2003 WinEDMA: Software for Euclidean Distance Matrix Analysis. Kansas City: University of Missouri-Kansas City School of Medicine.

Cooper, David S.
1988 Thyroid Hormone and the Skeleton: A Bone of Contention. The Journal of the American Medical Association 259: 3175.

Corti, Marco
1993 Geometric Morphometrics: An Extension of the Revolution. Trends in Ecology and Evolution 8: 302–303.

Costanzo, Linda S.
2014 Physiology. 5th Edition. Philadelphia: Elsevier Press.

Crawley, Jacqueline N., John K. Belknap, Allan Collins, et al.
1997 Behavioral Phenotypes of Inbred Mouse Strains: Implications and Recommendations for Molecular Studies. Psychopharmacology 132: 107–124.

Cray, James J., Kameron Khaksarfard, Seth M. Weinberg, Mohammed Elsalanty, and Jack C. Yu
2013 Effects of Thyroxine Exposure on Osteogenesis in Mouse Calvarial Pre-Osteoblasts. PLoS ONE 8: e69067.

Croucher, Peter I., and Graham G. Russel
1999 Growth Factors. *In* Dynamics of Bone and Cartilage Metabolism. Markus J. Seibel, Simon P. Robins, and John P. Bilezikian, eds. Pp. 83–95. San Diego: Academic Press.

Daegling, David J.
2001 Biomechanical Scaling of the Hominoid Mandibular Symphysis. Journal of Morphology 250: 12–23.

Daneman, Denis, and Neville J Howard
1980 Neonatal Thyrotoxicosis: Intellectual Impairment and Craniosynostosis in Later Years. The Journal of Pediatrics 97: 257–259.

Delmas, P.D., and Pierre J. Meunier
1997 The Management of Paget's Disease of Bone. The New England Journal of Medicine 336: 558–566.

Deng, Chuxia, Anthony Wynshaw-Boris, Fen Zhou, Ann Kuo, and Philip Leder
1996 Fibroblast Growth Factor Receptor 3 Is a Negative Regulator of Bone Growth. Cell 84: 911–921.

Depew, Michael J., Abigail S. Tucker, and Paul T. Sharpe
2002 Craniofacial Development. *In* Mouse Development: Patterning, Morphogenesis, and Organogenesis. Janet Rossant and Patrick P.L. Tam, eds. Pp. 421–498. San Diego: Academic Press.

Dhanwal, Dinesh K.
2011 Thyroid Disorders and Bone Mineral Metabolism. Indian Journal of Endcrinology and Metabolism 15: S107–S112.

Dobson, Seth D., and Erik Trinkaus
2002 Cross-Sectional Geometry and Morphology of the Mandibular Symphysis in Middle and Late Pleistocene Homo. Journal of Human Evolution 43: 67–87.

Doll, Bruce
2005 Developmental Biology of the Skeletal System. *In* Bone Tissue Engineering. Bruce Doll, ed. Pp. 3–26. Boca Raton: CRC Press.

Doll, Bruce, and Hannjörg Koch
2005 Bone Physiology Dynamics. *In* Bone Tissue Engineering Pp. 27–42. Boca Raton: CRC Press.

Donahue, Henry J., Christopher A. Siedlecki, and Erwin Vogler
2005 Osteoblastic and Osteocytic Biology and Bone Tissue Engineering. *In* Bone Tissue Engineering. Boca Raton: CRC Press.

Drake, Richard L., A. Wayne Vogl, and Adam. W.M. Mitchell
2010 Gray's Anatomy for Students. 2nd edition. Philadelphia: Churchill Livingstone.

DuBrul, E.L., and H. Sicher
1954 The Adaptive Chin. Springfield: Charles C. Thomas.

Enlow, D.H.
1990 Facial Growth. Philadelphia: W.B. Saunders Company.

Enlow, Donald. H.
1968 The Human Face. New York: Hoeber Medical Division.

1982 Handbook of Facial Growth. 2nd Edition. Philadelphia: W.B. Saunders Company.

Enlow, Donald. H., and Mark G. Hans, eds.
1996 Essentials of Facial Growth. W.B. Saunders Company.

Ethier, C. Ross, and Craig A. Simmons
2007 Introductory Biomechanics: From Cells to Organisms. Cambridge: Cambridge University Press.

Fell, Honor B., and E. Mellanby
1955 The Biological Action of Thyroxine on Embryonic Bones Grown in Tissue Culture. Journal of Physiology 127: 427–447.
1956 The Effect of L-Triiodothyronine on the Growth and Development of Embryonic Chick Limb-Bones in Tissue Culture. Journal of Physiology 133: 89–100.

Feng, Weiguo, Sonia M. Leach, Hannah Tipney, et al.
2009 Spatial and Temporal Analysis of Gene Expression during Growth and Fusion of the Mouse Facial Prominences. PLoS One 4(12): e8066.

Frommer, Jack, and Michael R. Margolies
1970 Contribution of Meckel's Cartilage to Ossification of the Mandible in Mice. Journal of Dental Research 50: 1260–1267.

Frost, H.M.
1964 The Laws of Bone Structure. Springfield: Charles C. Thomas.
1983 The Skeletal Intermediary Organization. Metabolic Bone Disease and Related Research 4: 281–290.
1990 Skeletal Structureal Adaptations to Mechanical Usage (SATMU): 1. Redefining Wolff's Law: The Bone Modeling Problem. The Anatomical Record 226: 403–413.
1994 Wolff's Law of Bone's Structural Adaptations to Mechanical Usage: An Overview for Clinicians. The Angle Orthodontist 64: 175–188.
1998 Changing Concepts in Skeletal Physiology: Wolff's Law, the Mechanostat, and the "Utah Paradigm." American Journal of Human Biology 10: 599–605.
2000 The Utah Paradigm of Skeletal Physiology: An Overview of Its Insights for Bone, Cartilage, and Collagenous Tissue Organs. Journal of Bone Mineral Metabolism 18: 305–316.

Garvin, H.M., and C.B. Ruff
2012 Sexual Dimorphism in Skeletal Browridge and Chin Morphologies Determined Using a New Quantitative Method. American Journal of Physical Anthropology 147: 661–670.

Gerstenfeld, Louis C., Dennis M. Cullinane, George L. Barnes, Dana T. Graves, and Thomas A. Einhorn
2003 Fracture Healing as a Post-Natal Developmental Process: Molecular, Spatial, and Temporal Aspects of Its Regulation. Journal of Cellular Biochemistry 88: 873–884.

Goodman, F.R., and P.J. Scrambler
2001 Human HOX Gene Mutations. Clinical Genetics 59: 1–11.

Göthe, Sten, Zhendong Wang, Lily Ng, et al.
1999 Mice Devoid of All Known Thyroid Hormone Receptors Are Viable but Exhibit Disorders of the Pituitary–thyroid Axis, Growth, and Bone Maturation. Genes and Development 13: 1329–1341.

Graber, Thomas M.
1963 The "three M's": Muscles, Malformation, and Malocclusion. American Journal of Orthodontics 49(6): 418–450.

Gray, Henry
1918 Anatomy of the Human Body. 20th Edition. Philadelphia: Lea & Febiger. www.bartleby.com, accessed April 22, 2016.

Gregory, W.K.
1904 The Relations of the Anterior Visceral Arches to the Chondrocranium. The Biological Bulletin 7.1: 55–69.

Grob, Gerald N.
2014 Aging Bones: A Short History of Osteoporosis. Baltimore: Johns Hopkins University Press.

Gröning, F., M.J. Fagan, and P. O'Higgins
2011 The Effects of the Periodontal Ligament on Mandibular Stiffness: A Study Combining Finite Element Analysis and Geometric Morphometrics. Journal of Biomechanics 44: 1304–1312.

Gröning, F., M. Fagan, and P. O'Higgins
2012 Modeling the Human Mandible Under Masticatory Loads: Which Input Variables Are Important? The Anatomical Record 295: 853–863.

Haddow, James E., Glenn E. Palomaki, Walter C. Allan, et al.
1999 Maternal Thyroid Deficiency during Pregnancy and Subsequent Neuropsychological Development of the Child. New England Journal of Medicine 341(8): 549–555.

Hall, Brian K.
1973 Thyroxine and the Development of the Tibia in the Embryonic Chick. The Anatomical Record 176: 49–64.
1993 Immobilization and Cartilage Transformation into Bone in the Embryonic Chick. The Anatomical Record 173: 391–404.
2015 Bones and Cartilage: Developmental and Evolutionary Skeletal Biology. 2nd Edition. London: Academic Press.

Hallgrimsson, Benedikt, Christopher J. Percival, Rebecca Green, et al.
2015 Morphometrics, 3D Imaging, and Craniofacial Development. *In* Craniofacial Development. Yang Chai, ed. Pp. 561–597. Burlington: Academic Press.

Hanken, James, and Cliff H. Summers
1988 Skull Development During Anuran Metamorphosis: 111. Role of Thyroid Hormone in Chondrogenesis. The Journal of Experimental Zoology 246: 156–170.

Harvey, Clare B., Patrick J. O'Shea, Anthea J. Scott, et al.
2002 Molecular Mechanisms of Thyroid Hormone Effects on Bone Growth and Function. Molecular Genetics and Metabolism 75: 17–30.

Hennessy, Robin J., and Chris Stringer
2002 Geometric Morphometric Study of the Regional Variation of Modern Human Craniofacial Form. American Journal of Physical Anthropology 117: 37–48.

Hershman, Jerome M.
2009 Hypothyroidism and Hyperthyroidism. *In* Manual of Endocrinology and Metabolism. 4th Edition. Norman Lavin, ed. Philadelphia: Wolters Kluwer.

Hill, Cheryl A., Roger H. Reeves, and Joan T. Richtsmeier
2007 Effects of Aneuploidy on Skull Growth in a Mouse Model of Down Syndrome. Journal of Anatomy 210(4): 394–405.

Hollowell, Joseph G., Norman W. Staehling, W. Dana Flanders, et al.
2002 Serum TH, T4, and Thryoid Antibodies in the United States Population (1988 to 1994): National Health and Nutrition Examination Survey (NHANES III). The Journal of Clinical Endocrinoloy and Metabolism 87: 489–499.

Horton, William A., Judith G. Hall, and Jacqueline T. Hecht
2007 Achondroplasia. Lancet 370: 162–172.

Hotelling, Harold
1933 Analysis of a Complex of Statistical Variables into Principal Components. Journal of Educational Psychology 24(6): 417.

Hrdlička, A., and K. Pearson
1911 Human Dentition and Teeth from the Evolutionary and Racial Standpoint. Ontario Dental Association.

Huxley, Thomas H.
1859 The Croonian Lecture: On the Theory of the Vertebrate Skull. Proceedings of the Royal Society of London 9: 381–457.

Hylander, W.L.
1975 The Human Mandible: Lever or Link? American Journal of Physical Anthropology 43: 227–242.
1979 The Functional Significance of Primate Mandibular Form. Journal of Morphology 160: 223–240.
1984 Stress and Strain in the Mandibular Symphysis of Primates: A Test of Competing Hypotheses. American Journal of Physical Anthropology 64: 1–46.
1985 Mandibular Function and Biomechanical Stress and Scaling. American Zoologist 25: 315–330.

IBM SPSS Statistics for Macintosh
2015 Macintosh. Armonk, NY: IBM.

Ichim, I., M. Swain, and J.A. Kieser
2006 Mandibular Biomechanics and Development of the Human Chin. Journal of Dental Research 85: 638–642.

Jiang, Rulang, Jeffrey O. Bush, and Andrew C. Lidral
2006 Development of the Upper Lip: Morphogenetic and Molecular Mechanisms. Developmental Dynamics 235: 1152–1166.

Johnston, M.C., and P.T. Bronsky
1995 Prenatal Craniofacial Development: New Insights on Normal and Abnormal Mechanisms. Critical Reviews in Oral Biology & Medicine 6: 368–422.

Judd, Edward S.
1920 Results of Operations for Adenoma with Hyperthyroidism and Exophthalmic Goitre. Annals of Surgery 72: 145.

Kau, C.H., A. Zhurov, S. Richmond, et al.
2006 Facial Templates: A New Perspective in Three Dimensions. Orthodontics and Craniofacial Research 9: 10–17.

Keith, Arthur
1916 A Chapter of Conclusions. Englewood Cliffs.
1928 The Evolution of the Human Races. The Journal of the Royal Anthropological Institute of Great Britain and Ireland 58: 305–321.

Kemp, Norman E., and Judith A. Hoyt
1969a Sequence of Ossification in the Skeleton of Growing and Metamorphosing Tadpoles of Rana Pipiens. Journal of Morphology 129: 415–443.
1969b Ossification of the Femur in Thyroxine-Treated Tadpoles of Rana Pipiens. Developmental Biology 20: 387–410.

Kendall, D.G.
1977 The Diffusion of Shape. Advances in Applied Probability 9: 428–430.
1981 The Statistics of Shape. *In* Interpreting Multivariate Data. V. Barnett, ed. New York: Wiley.

Kesterke, Matthew J., and James C.M. Ahern
2007 Is the Later Neandertal Mandibular Sample from Vindija Cave (Croatia) Biased? Collegium Anthropologicum 31: 365–373.

Khoury, Muin J., José E. Becerra, and Philip J. D'Almada
1989 Maternal Thyroid Disease and Risk of Birth Defects in Offspring: A Population- based Case- control Study. Paediatric and Perinatal Epidemiology 3(4): 402–420.

Kingsbury, B.F.
1926 Branchiomerism and the Theory of Head Segmentation. Journal of Morphology 42: 83–109.

Klingenberg, C.P.
2011 MORPHOJ: An Integrated Software Package for Geometric Morphometrics. Molecular Ecology Resources 11: 353–357.

Klingenberg, C.P., and L.J. Leamy
2001 Qualitative Genetics of Geometric Shape in the Mouse Mandible. Evolution 55: 2342–2352.

Klingenberg, C.P., L.J. Leamy, and J.M. Cheverud
2004 Integration and Modularity of Quantitative Trait Locus Effects on Geometric Shape in the Mouse Mandible. Genetics(166): 1909–1921.

Klingenberg, C.P., L.J. Leamy, E.J. Routman, and J.M. Cheverud
2001 Genetic Architecture of Mandible Shape in Mice: Effects of Quantitative Trait Loci Analyzed by Geometric Morphometrics. Genetics 157: 785–802.

Krumlauf, Robb
1994 Hox Genes in Vertebrate Development. Cell 78: 191–201.

Landers, R.N.
2015 Computing Interclass Correlations (ICC) as Estimates of Interrated Reliability in SPSS. The Winnower.

Latham, R.A.
1970 Maxillary Development and Growth: The Septopremaxillary Ligament. Journal of Anatomy 107: 471–478.

Lavergne, Jean, and Nicole Gasson
1976 A Metal Implant Study of Mandibular Rotation. The Angle Orthodontist 46(2): 144–150.

Leboy, Phoebe
2006 Regulating Bone Growth and Development with Bone Morphogenic Proteins. Annals of the New York Academy of Sciences 1068: 14–18.

Lele, S, and T.M. Cole
1996 A New Test for Shape Differences When Variance-Covariance Matrices Are Unequal. Journal of Human Evolution 31: 193–212.

Lele, Subhash
1993 Euclidean Distance Matrix Analysis (EDMA) of Landmark Data: Estimation of Mean Form and Mean Form Difference. Math Geol 25: 574–602.

Lele, Subhash, and Joan T. Richtsmeier
1991 Euclidean Distance Matrix Analysis: A Coordinate-Free Approach for Comparing Biological Samples Using Landmark Data. American Journal of Physical Anthropology 86: 415–427.
1995 Euclidean Distance Matrix Analysis: Confidence Intervals for Form and Growth Differences. American Journal of Physical Anthropology 98: 73–86.
2001 An Invariant Approach to Statistical Analysis of Shapes. Boca Raton: Chapman & Hall.

Lieberman, Daniel E.
2011 The Evolution of the Human Head. Cambridge: The Belknap Press of Harvard University.

Lieberman, P., and E.S. Crelin
1971 On the Speech of Neanderthal Man. Linquistic Inquiry 2: 203–222.

Lifshitz, Jacobo
1976 Comparative Anatomic Study of Mandibular Growth in Rats after Bilateral Resections of Superficial Masseter, Posterior Temporal, and Anterior Digastic Muscles. Journal of Den 55: 854–858.

Linkhart, Thomas A., Subburaman Mohan, and David. J. Baylink
1996 Growth Factors for Bone Growth and Repair: IGF, TGFB, and BMP. Bone 19: 1S–12S.

Luewan, Suchaya, Patom Chakkabut, and Theera Tongsong
2011 Outcomes of Pregnancy Complicated with Hyperthyroidism: A Cohort Study. Archives of Gynecological Obstetrics 283: 243–237.

Maeda, N., T. Kawasaki, K. Osawa, et al.
1987 Effects of Long-Term Intake of a Fine-Grained Diet on the Mouse Masseter Muscle. Cells Tissues Organs 128(4): 326–333.

Marotti, Gastone
1990 The Original Contributions of the Scanning Electron Microscope to the Knowledge of Bone Structure. *In* The Ultrastructure of Skeletal Tissues: Bone and Cartilage in Health and Disease. E. Bonucci and P.M. Motta, eds. P. 1940. Boston: Kluwer Academic Publishers.

Massler, Maury, and John M. Frankel
1951 Prevalence of Malocclusion in Children Aged 14 to 18 Years. American Journal of Orthodontics 37(10): 751–768.

Mays, S., M. Brickley, and R. Ives
2007 Skeletal Evidence for Hyperparathyroidism in a 19th Century Child with Rickets. International Journal of Osteoarchaeology 17(1): 73–81.

Mays, Simon, Megan Brickley, and Rachel Ives
2006 Skeletal Manifestations of Rickets in Infants and Young Children in a Historic Population from England. American Journal of Physical Anthropology 129(3): 362–374.

McGinnis, William, and Robb Krumlauf
1992 Homeobox Genes and Axial Patterning. Cell 68: 283–302.

Mestman, Jorge H.
2009 Endocrine Diseases in Pregnancy. *In* Manual of Endocrinology and Metabolism. 4th Edition. Pp. 709–727. Philadelphia: Wolters Kluwer.

Microsoft Excel for Mac
2011 Macintosh. Microsoft.

Miettinen, Päivi J., Jennie R. Chin, Lillian Shum, et al.
1999 Epidermal Growth Factor Receptor Function Is Necessary for Normal Craniofacial Development and Palate Closure. Nature Genetics 22(1): 69–73.

Moore, Keith L., T.V.N. Persaud, and Mark G. Torchia
2013 Before We Are Born. 8th Edition. Philadelphia: Elsevier Press.

Morriss-Kay, Gillian M., and Andrew O.M. Wilkie
2005 Growth of the Normal Skull Vault and Its Alteration in Craniosynostosis: Insights from Human Genetics and Experimental Studies. Journal of Anatomy 207: 637–653.

Moss, Melvin M.
1968 A Theoretical Analysis of the Functional Matrix. Acta Biotheoretica 18: 195–202.

1997a The Functional Matrix Hypothesis Revisited. 1. The Role of Mechanotransduction. American Journal of Orthodontics and Dentofacial Orthopedics 112: 8–11.
1997b The Functional Matrix Hypothesis Revisited. 2. The Role of an Osseous Connected Cellular Network. American Journal of Orthodontics and Dentofacial Orthopedics 112: 221–226.

Moss, Melvin M., and Robin Rankow
1968 The Role of the Functional Matrix in Mandibular Growth. The Angle Orthodontist 38: 95–103.

Moss, Melvin M., and Letty Salentijn
1969a The Capsular Matrix. American Journal of Orthodontics November: 474–490.
1969b The Primary Role of Functional Matrices in Facial Growth. American Journal of Orthodontics June: 566–576.

Moss, Melvin M., and Richard W. Young
1960 A Functional Approach to Craniology. American Journal of Physical Anthropology 18: 281–292.

Murphy, Elaine, and Graham R. Williams
2004 The Thyroid and the Skeleton. Clinical Endocrinology 61: 285–298.

Murray, P.D.F.
1936 Bones: A Study of the Development and Structure of the Vertebrate Skeleton. Cambridge: Cambridge University Press.

Negro, Roberto, and Jorge H. Mestman
2011 Thryoid Disease in Pregnancy. Best Practice & Research Clinical Endocrinology & Metabolism 25: 927–943.

Nucera, Carmelo, Patrizia Muzzi, Cecilia Tiveron, et al.
2010 Maternal Thyroid Hormones Are Transcriptionally Active during Embryo–foetal Development: Results from a Novel Transgenic Mouse Model. Journal of Cellular and Molecular Medicine 14: 2417–2435.

O'Higgins, Paul, and Mark Collard
2002 Sexual Dimorphism and Facial Growth in Papionin Monkeys. Journal of Zoology 257: 255–272.

Ooi, C.G., and W.D. Fraser
1997 Paget's Disease of Bone. Postgraduate Medical Journal 73: 69–74.

Orliaguet, T., P. Dechelotte, T. Scheye, and G. Vanneuville
1993 The Relationship between Meckel's Cartilage and the Development of the Human Fetal Mandible. Surgical and Radiologic Anatomy 15: 113–118.

Ortner, D.J.
2003 Identification of Pathological Conditions in Human Skeletal Remains. 2nd edition. San Diego: Elsevier Press.

Ortner, Donald J., and Simon Mays
1998 Dry- bone Manifestations of Rickets in Infancy and Early Childhood. International Journal of Osteoarchaeology 8(1): 45–55.

Pampush, James D., and David J. Daegling
2016 The Enduring Puzzle of the Human Chin. Evolutionary Anthropology 25: 20–35.

Parsons, T.E., Seth M. Weinberg, Mohammed Elsalanty, et al.
2015 In Utero Exposure to Thyroxine Results in Altered Post-Natal Skull Shape in Mice. Poster presented at the 72nd Annual Meeting of the American Cleft Palate-Craniofacial Association, Palm Springs.

Parsons, T.E., S.M. Weinberg, Kameron Khaksarfard, et al.
2014 Craniofacial Shape Variation in Twist1 1/2 Mutant Mice. The Anatomical Record 297: 826–833.

Paul, Terri L., James Kerrigan, Marie Ane Kelly, Lewis A. Braverman, and Daniel T. Baran
1988 Long-Term L-Thyroxine Therapy Is Associated With Decreased Hip Bone Density in Premenopausal Women. The Journal of the American Medical Association 259: 3137–3141.

Pearson, Karl
1902 On the Fundamental Concepts of Biology. Biometrika 1: 320–344.

Petrovich, A.
1974 Control of Postnatal Growth of Secondary Cartilages of the Mandible by Mechanisms Regulating Occlusion. Cybernetic Model. Transactions of the European Orthodontic Society 64.

Prendergast, P.J., and R. Huiskes
1995 The Biomechanics of Wolff's Law: Recent Advances. Irist Journal of Medical Science 164: 152–154.

Quinonez, Shane C., and Jeffrey W. Innis
2014 Human HOX Gene Disorders. Molecular Genetics and Metabolism 111: 4–15.

Radlanski, Ralf J., and Herbert Renz
2006 Genes, Forces, and Forms: Mechanical Aspects of Prenatal Craniofacial Development. Developmental Dynamics 235: 1219–1229.

Radlanski, Ralf J., Herbert Renz, and Marie C. Klarkowski
2003 Prenatal Development of the Human Mandible 3D Reconstructions, Morphometry and Bone Remodelling Pattern, Sizes 12–117 Mm CRL. Anatomy and Embryology 207: 221–232.

Rasmussen, Sonja A., Mahsa M. Yazdy, Suzan L. Carmichael, et al.
2007 Maternal Thyroid Disease as a Risk Factor for Craniosynostosis. Obstetrics and Gynecology 110.

Von Recklinghausen, F.
1891 Die Fibrose Oder Deformierende Ostitis, Die Osteomalazie Und Die Osteoplastiche Carzinose in Ihren Gegenseitigen Beziehungen. Berlin: George Reimer.

Resnick, D., S.C. Manolagas, G. Niwayama, and M.D. Fallon
2002 Histogenesis, Anatomy, and Physiology of Bone. *In* Diagnosis of Bone and Joint Disorders. 4th Edition. D. Resnick, ed. Pp. 647–687. Philadelphia: W.B. Saunders Company.

Ricketts, Robert Murray
1960 A Foundation for Cephalometric Communication. American Journal of Orthodontics 46(5): 330–357.

Riesenfeld, A.
1969 The Adaptive Mandible: An Experimental Study. Cells Tissues Organs 72(2): 246–262.

Roberts, W. Eugene, Bruce N. Epker, David B. Burr, James K. Hartsfield Jr., and Jeffrey A. Roberts
2006 Remodeling of Mineralized Tissues, Part II: Control and Pathophysiology. Seminars in Orthodontics 12: 238–253.

Roberts, W. Eugene, Jeffrey A. Roberts, Bruce N. Epker, David B. Burr, and James K. Hartsfield Jr.
2006 Remodeling of Mineralized Tissues, Part I: The Frost Legacy. Seminars in Orthodontics 12: 216–237.

Robinson, L.
1913 The Story of the Chin. Knowledge 36: 410–420.

Rodríguez-Vázquez, J.F., J.R. Mérida-Velasco, J.A. Mérida-Velasco, et al.
1997 Development of Meckel's Cartilage in the Symphyseal Region in Man. The Anatomical Record 249: 249–254.

Rohlf, F. James, and Marco Corti
2000 Use of Two-Block Partial Least-Squares to Study Covariation in Shape. Society of Systematic Biologists 49: 740–753.

Rohlf, F. James, and Leslie F. Marcus
1993 A Revolution in Morphometrics. Trends in Ecology and Evolution 8: 129–132.

Sadler, T.W.
2012 Medical Embryology. 12th Edition. Baltimore: Lippincott Willams & Wilkins.

Schaefer, Maureen, Sue Black, and Louise Scheuer
2009 Juvenille Osteology. Burlington: Elsevier Press.

Schneider, C.A., W.S. Rasband, and K.W. Eliceiri
2012 NIH Image to ImageJ: 25 Years of Image Analysis. Nature Methods 9: 671–675.

Schoenwolf, Gary C., Steven B. Bleyl, Philip R. Brauer, and Philippa H. Francis-West
2009 Larsen's Human Embyology. 4th Edition. Philadelphia: Elsevier Press.

Schwartz, J.H., and I. Tattersall
2000 The Human Chin Revisited: What Is It and Who Has It? Journal of Human Evolution 38: 367–409.

Scott, Emmett J.
1938 An Experimental Study in Growth of the Mandible. American Journal of Orthodontics and Oral Surgery 24: 925–934.

Scott, J.H.
1956 Growth of Facial Sutures. American Journal of Orthodontics 42: 381–387.

Seeman, E., H.W. Wahner, K.P. Offord, et al.
1982 Differential Effects of Endocrine Dysfunction on the Axial and Appendicular Skeleton. Journal of Clinical Investigation 69: 1302–1309.

Šešelj, Maja, Dana D. Duren, and Richard J. Sherwood
2015 Heritability of the Human Craniofacial Complex. The Anatomical Record 298: 1535–1547.

Siegel, Michael M., and Mark P. Mooney
1990 Appropriate Animal Models for Craniofacial Biology. Celft Palate Journal 27: 18–25.

Siegel, Michael M., Mark P. Mooney, Jorg W. Eichberg, Thomas Gest, and D.Rick Lee
1990 Septopremaxillary Ligament Resection and Midfacial Growth in a Chimpanzee Animal Model. The Journal of Craniofacial Surgery 1: 182–186.

Singer, Peter A.
2009 Evaluation of Thyroid Function. *In* Manual of Endocrinology and Metabolism. 4th Edition. Norman Lavin, ed. Pp. 414–425. Philadelphia: Wolters Kluwer.

Smith, Fred, and James C.M. Ahern
2013 The Origins of Modern Humans: Biology Reconsidered. Hoboken: Wiley-Blackwell.

Sperber, G.
2001 Bone Development and Growth. *In* Craniofacial Developement. 2nd edition. G. Sperber, ed. Pp. 67–79. London: BC Decker, Inc.
2002 Craniofacial Embryogenesis: Normal Developmental Mechanisms. *In* Understanding Craniofacial Anomolies: The Etiopthogenesis of Craniosynostosis and Facial Clefting. Mark P. Mooney and Michael M. Siegel, eds. Pp. 31–59. New York: Wiley-Liss.

Stout, Sam, and Christian Crowder
2012 Bone Remodeling, Histomorphology, and Histomorphometry. *In* Bone Histology: An Anthropological Perspective. Christian Crowder and Sam Stout, eds. Pp. 1–22. Boca Raton: CRC Press.

Talaeipour, A.R., M. Shirazi, Y. Kheirandish, et al.
2005 Densitometric Evaluation of Skull and Jaw Bones after Administration of Thyroid Hormones in Rats. Dentomaxillofacial Radiology 34: 332–336.

Talbert, L.M., C.G. Thomas, W.A. Holt, and P. Rankin
1970 Hyperthyroidism During Pregnancy. Obstetrics and Gynecology 36.

Thayer, Zaneta M., and Seth D. Dobson
2010 Sexual Dimorphism in Chin Shape: Implications for Adaptive Hypotheses. American Journal of Physical Anthropology 143: 417–425.

Thoma, K.H.
1938 Principal Factors Controlling Development of Mandible and Maxilla. American Journal of Orthodontics and Dentofacial Orthopedics 24: 171–179.

Thompson, D' Arcy
1915 Morphology and Mathematics. Transactions of the Royal Society of Edinburgh 50: 857–895.
1917 On Growth and Form. Cambridge: Cambridge University Press.

Vanderoost, Jef, and G. Harry van Lenthe
2014 From Histology to Micro-CT: Measuring and Modeling Resorption Cavities and Their Relation to Bone Competence. World Journal of Radiology 6: 643–656.

Viòarsdóttir, Una Strand, and Paul O'Higgins
2003 Developmental Variation in the Facial Skeleton of Anatomically Modern Homo Sapiens. *In* Patterns of Growth and Development in the Genus Homo. Jennifer L. Thompson, Gail E. Krovitz, and Andrew J. Nelson, eds. Pp. 114–143. Cambridge: Cambridge University Press.

Viòarsdóttir, Una Strand, O'Higgins, Paul, and Chris Stringer
2002 A Geometric Morphometric Study of Regional Differences in the Ontogeny of the Modern Human Facial Skeleton. Journal of Anatomy 201: 211–229.

Vogl, Claus, William R. Atchley, David E. Cowley, et al.
1993 The Epigenetic Influence of Growth Hormone on Skeletal Development. Growth, Development, and Aging 57: 163–182.

Walkhoff, Dr Otto
1902 Der Unterkiefer Der Anthropomorphen Und Des Menschen in Seiner Funktionellen Entwickelung Und Gestalt, von Dr Otto Walkhoff,... CW Kreidel.

Wallis, W.D.
1917 The Development of the Human Chin. The Anatomical Record 12: 315.

Watt, David G., and Charles H.M. Williams
1951 The Effects of the Physical Consistency of Food on the Growth and Development of the Mandible and the Maxilla of the Rat. American Journal of Orthodontics 37: 895–928.

Webster, S.S. Lee
2005 The Past, Present, and Future of Bone Morphometry: Its Contribution to an Improved Understanding of Bone Biology. Journal of Bone Mineral Metabolism 23: 1–10.

Weinmann, J.P., and H. Sicher
1947 Bone and Bones: Fundamentals of Bone Biology. Saint Louis: CV Mosby.

Weiss, Robert M., and Charles R. Noback
1949 The Effects of Throxin and Thiouracil on the Time of Appearance of Ossification Cetners of Rat Fetuses. Endocrinology 45: 389–395.

White, Tim D., Michael T. Black, and Pieter A. Folkens
2012 Human Osteology. 3rd edition. Burlington: Elsevier Press.

Widmer, C. G., J. A. Morris-Wiman, and C. Nekula
2002 Spatial Distribution of Myosin Heavy-Chain Isoforms in Mouse Masseter. Journal of Dental Research 81(1): 33–38.

Wojcicka, Anna, J.H. Duncan Bassett, and Graham R. Williams
2013 Mechanisms of Action of Thyroid Hormone in the Skeleton. Biochimica et Biphysica Acta(1830): 3979–3986.

Wolff, J.
1892 Das Gesetz Der Transformation Der Knochen. P. Maquet and R. Furlong, trans. Translated in 1986. Berlin: A. Hirschwald.

Yonemitsu, Ikuo, Takeshi Muramoto, and Kunimichi Soma
2007 The Influence of Masseter Activity on Rat Mandibular Growth. Archives of Oral Biology 52(5): 487–493.

Zelditch, Miriam L., Donald L. Swinderski, H. David Sheets, and William L. Fink
2004 Geometric Morphometric Analysis for Biologists: A Primer. San Diego: Elsevier Press.